MOTILITY AND CHEMOTAXIS IN THE LYME DISEASE SPIROCHETE *BORRELIA BURGDORFERI*: ROLE IN PATHOGENESIS

By

Ki Hwan Moon

July, 2016

Director of Dissertation: MD A. MOTALEB, Ph.D.

Major Department: Department of Microbiology and Immunology

Abstract

Lyme disease is the most prevalent vector-borne disease in United States and is caused by the spirochete *Borrelia burgdorferi*. The disease is transmitted from an infected *Ixodes scapularis* tick to a mammalian host. *B. burgdorferi* is a highly motile organism and motility is provided by flagella that are enclosed by the outer membrane and thus are called periplasmic flagella. Chemotaxis, the cellular movement in response to a chemical gradient in external environments, empowers bacteria to approach and remain in beneficial environments or escape from noxious ones by modulating their swimming behaviors. Both motility and chemotaxis are reported to be crucial for migration of *B. burgdorferi* from the tick to the mammalian host, and persistent infection of mice. However, the knowledge of how the spirochete achieves complex swimming is limited. Moreover, the roles of most of the *B. burgdorferi* putative chemotaxis proteins are still elusive. *B. burgdorferi* contains multiple copies of chemotaxis genes (two *cheA*, three *cheW*, three *cheY*, two *cheB*, two *cheR*, *cheX*, and *cheD*), which make its

chemotaxis system more complex than other chemotactic bacteria. In the first project of this dissertation, we determined the role of a putative chemotaxis gene *cheD*. Our experimental evidence indicates that CheD enhances chemotaxis CheX phosphatase activity, and modulated its infectivity in the mammalian hosts. Although CheD is important for infection in mice, it is not required for acquisition or transmission of spirochetes during mouse-tick-mouse infection cycle experiments. However, it has an effect on the survivability of spirochetes in the arthropod vectors. This is the first report of the role of *cheD* in the host tissue colonization in any pathogenic bacterium. Delineating the role of *cheD* in *B. burgdorferi* will provide insights into not only the chemotaxis pathway of this spirochete, but also its asymmetric swimming and infectious life cycle of the spirochete.

Chemotaxis signal transduction systems control bacterial motility. Aside from the chemotaxis pathway, the architectural structure of the flagellar apparatus is also intimately intertwined with motility and the morphology of *B. burgdorferi*. Unlike other externally flagellated bacteria, spirochetes possess periplasmic flagella with a unique structural component called the collar. This unique component is located in the periplasmic space and is linked to the flagellar basal body. However, there are no reports regarding the gene(s) encoding for the collar or its function in any bacterium. In the second project of this dissertation, we have identified for the first time a gene, *flbB*, in any spirochete, and defined its function in motility, cell morphology, periplasmic flagella orientation, and assembly of other flagellar structures. We also demonstrated the mechanism shown as to how the organism tilts their periplasmic flagella toward the cell pole.

MOTILITY AND CHEMOTAXIS IN THE LYME DISEASE SPIROCHETE *BORRELIA BURGDORFERI*: ROLE IN PATHOGENESIS

A Dissertation Presented to

The Faculty of the Department of Microbiology and Immunology

Brody School of Medicine at East Carolina University

In Partial Fulfillment of the Requirements for the Degree

Doctor of Philosophy in Microbiology and Immunology

By

Ki Hwan Moon

July 29, 2016

Copyright Permission from Individual Journal

CHAPTER ONE: Fig. 1.4: Copyright Nature Publishing Group, Nature Reviews Microbiology, 2012 Jan 9; 10(2):87-99. doi: 10.1038/nrmicro2714. Copyright © 2012, Rights Managed by Nature Publishing Group. Fig. 1.5: Copyright Nature Publishing Group, Nature Reviews Microbiology, 2005 Feb; 3(2):129-43. Copyright © 2005, Rights Managed by Nature Publishing Group. Fig. 1.6: Copyright American Society for Microbiology, Clinical Microbiology Reviews, 1999 Oct; 12(4):633-53. Copyright © 1999, American Society for Microbiology. Fig. 1.8: Copyright Elsevier Inc., Plasmid, 2005 Jan; 53(1):1-13. Epub 2004 Dec 16. Copyright © 2005 Elsevier Inc. Figs. 1.9, 1.10: Copyright American Chemical Society, Biochemistry, 2014 Jul 15; 53(27):4323-33. doi: 10.1021/bi500059y. Epub 2014 Jul 1. Copyright © 2014 American Chemical Society. Fig. 1.12: Copyright Nature Publishing Group, Nature Reviews Microbiology, 2011 Mar; 9(3):153-65. doi: 10.1038/nrmicro2505. Epub 2011 Feb 1. Copyright © 2011, Rights Managed by Nature Publishing Group.

CHAPTER TWO: Copyright American Society for Microbiology, Infection and Immunity, 2016 May 24; 84(6):1743-52. doi: 10.1128/IAI.01347-15. Print 2016 Jun. Copyright © 2016, American Society for Microbiology

CHAPTER THREE: Copyright John Wiley & Sons Inc., Molecular Microbiology, 2016 July 15; In press. doi: 10.1111/mmi.13463. Copyright © 2016, John Wiley & Sons Inc.

Copyrighted materials were used with permission see **Appendix**

MOTILITY AND CHEMOTAXIS IN THE LYME DISEASE SPIROCHETE *BORRELIA BURGDORFERI*: ROLE IN PATHOGENESIS

by

Ki Hwan Moon

APPROVED BY:

DIRECTOR OF DISSERTATION

_____
MD A. Motaleb, Ph.D.

COMMITTEE MEMBER

_____
Everett C. Pesci, Ph.D.

COMMITTEE MEMBER

_____
R. Martin Roop, II, Ph.D.

COMMITTEE MEMBER

_____
Shaw M. Akula, Ph.D.

COMMITTEE MEMBER

_____
Stephanie L. Richards, Ph.D.

CHAIR OF THE DEPARTMENT OF
MICROBIOLOGY AND IMMUNOLOGY

_____
Everett C. Pesci, Ph.D.

INTERIM DEAN OF
THE GRADUATED SCHOOL

_____
Paul J. Gemperline, Ph.D.

ACKNOWLEDGEMENTS

First and foremost, I offer my sincerest gratitude to my advisor, Dr. MD A. Motaleb, who has supported and guided me throughout the years. The way he mentored me, the knowledge he shared, and the care he took has made me a better person both in the lab and in life. I really appreciate his effort and patience.

I would like to thank my collaborators, Drs. Jun Liu and Xiaowei Zhao, in University of Texas in Houston. Without them, these research projects would be incomplete, as they provided the cryo-electron tomogram data. I also thank my committee members, Drs. Everett C. Pesci, R. Martin Roop, II, Shaw M. Akula, and Stephanie L. Richards, who dedicated their time to guide and support me to graduate on time. Moreover, I am grateful to every faculty member in the Department of Microbiology and Immunology who gave me this great opportunity to work and study in the Brody School of Medicine at East Carolina University.

I also owe a great deal to my teammates in the Motaleb laboratory. I would like to thank the previous lab Postdocs, Drs. Syed Z. Sultan and Elizabeth A. Novak. Syed helped me with experimental training. His wonderful skills and advice always motivated me. Liz was always ready to lend a hand not only at the bench, but also with my writing. She has been the best Science and English teacher for me. I want to thank the previous lab technician Akarsh Manne and Master student Aaron M. Yerke for being great friends and roommates, who were always ready to help me, in or out of the laboratory. Their cheerful demeanor definitely helped make bench work more enjoyable. I also want to thank the current lab members, Postdoc Dr. Hui Xu, technician Zhou Yu, and Ph.D.

student Priyanka A.S. Theophilus for their exuberance and friendly atmosphere. Thanks also to all staff and students in the Biotechology building for providing a great learning environment, and the staff in the Department of Comparative Medicine who helped me with my animal experiments. Additionally, I would like to thank all my friends who I met in US for their friendship. A special thanks goes to Aaron's family who considered me a part of their own family, and my Brody admission siblings, who made this long journey with me.

I appreciate and thank my M.S. advisor and ECU alumnus Dr. Ho Young Kang, and his lab members (my old teammates) who always encouraged me. Dr. Kang initially brought me into the field of bacteriology and introduced me to ECU. Without his guidance and support, I even could not think about studying microbiology abroad. I also want to thank my best friends Deuk Jong Yoo, Kwang Hyun Jeon, Bong Seon Kim, and Young Tae Jeong for their encouragement and support. Thanks also to all my friends in South Korea for their friendship from the halfway across the world, and my friends in US for sharing the empathy as an international student.

Lastly, I am immensely grateful to my parents, Mr. Seong Yeor Moon and Mrs. Mi Hee Park who have always been there for me, to strengthen me, and cheering me up. Without their unconditional love, I could not have seen my way through to the completion of this Ph.D. program. I also want to thank my bother Ki Seop Moon, my sister-in-law Ju Myung Moon, and my first nephew Damkong who will be born in November for supporting and encouraging me in this endeavor. Additionally, I would like to thank my grandfather Mr. Byeong Jo Moon who gave tremendous love to his first grandson, and I deeply regret that I could not make to attend his funeral. RIP grandfa!

TABLE OF CONTENTS

LIST OF TABLES……ix

LIST OF FIGURES……x

CHAPTER ONE: INTRODUCTION……1

- LYME DISEASE……3

  History and discovery of Lyme disease……3

  Clinical manifestations of Lyme disease……4

  Infection rate and mortality of Lyme disease……7

  Diagnosis and treatment of Lyme disease……8

  Vaccine against of Lyme disease……17

  Epidemiology of Lyme disease……19

  Infectious life cycle (Mammalian and *Ixodes* tick hosts)……23

- *BORRELIA BURGDORFERI*……25

  Taxonomy of *B. burgdorferi*……25

  Biology of *B. burgdorferi*……28

  Genome of *B. burgdorferi*……30

  Periplasmic flagella of *B. burgdorferi*……32

  Motility and chemotaxis of *B. burgdorferi*……37

- STATEMENT OF THE PROBLEM, GOAL, SPECIFIC OBJECTIVES, AND HYPOTHESES……45

CHAPTER TWO: *BORRELIA BURGDORFERI* CHED PROMOTES VARIOUS FUNCTIONS IN CHEMOTAXIS AND THE PATHOGENIC LIFE CYCLE OF THE

SPIROCHETE……48

- Abstract……48
- Introduction……50
- Materials and methods……54
- Results……65
- Discussion……84

CHAPTER THREE: SPIROCHETES FLAGELLAR COLLAR PROTEIN FLBB HAS ASTOUNDING EFFECTS IN ORIENTATION OF PERIPLASMIC FLAGELLA, BACTERIAL SHAPE, MOTILITY, AND ASSEMBLY OF MOTORS IN *BORRELIA BURGDORFERI*……90

- Abstract……90
- Introduction……91
- Materials and methods……96
- Results……105
- Discussion……124

CHAPTER FOUR: SUMMARY AND FUTURE DIRECTIONS……128

REFERENCES……136

Appendix……161

LIST OF TABLES

Table 1.1. Differential diagnosis of erythema migrans……9

Table 1.2. Preferred antimicrobial therapies for Lyme disease……13

Table 2.1. Bacterial strains and plasmids used in this study……55

Table 2.2. Δ*cheD* mutant cells are able to establish infection in C3H/HeN mice but the infectivity is considerably reduced……77

Table 2.3. Δ*cheD* spirochete-infected nymphal ticks are able to transmit the organisms into naïve C3H/HeN mice……83

Table 2.4. Potential CheD modification substrate sites detected in *B. burgdorferi* chemoreceptors……85

Table 3.1. Bacterial strains and plasmids used in this study……97

Table 3.2. Δ*flbB* mutant cells periplasmic flagella are oriented abnormally toward the cell pole……113

LIST OF FIGURES

Figure 1.1. Signs and symptoms of untreated Lyme disease……5

Figure 1.2. Number of reported Lyme disease cases, United States, 1995 to 2014……21

Figure 1.3. Geographic distribution of confirmed Lyme disease cases, United States in 2014, *Ixodes scapularis* (Blacklegged tick), and *Ixodes pacificus* (Western blacklagged tick)……22

Figure 1.4. The enzootic life cycle of *B. burgdorferi*……24

Figure 1.5. Phylogeny of Spirochetes……26

Figure 1.6. Phylogeny of Lyme disease spirochete isolates as inferred from 16S rRNA gene sequence analysis……27

Figure 1.7. Dark-field microscopic image, and schematic diagram of *B. burgdorferi*……29

Figure 1.8. The segmented genome of *B. burgdorferi*……31

Figure 1.9. Comparative analysis of the intact motor between external flagella and periplasmic flagella……33

Figure 1.10. A model of flagellar assembly in *B. burgdorferi*……35

Figure 1.11. Swimming cells of *B. burgdorferi* as a function of the direction in which the periplasmic flagella rotate……39

Figure 1.12. The *Escherichia coli* chemotaxis pathway……40

Figure 1.13. Model of the *B. burgdorferi* chemotaxis system·····43

Figure 2.1. Affinity blot analysis indicate that CheD specifically interacts with CheX····66

Figure 2.2. CheD enhances phosphatase activity of CheX·····68

Figure 2.3. CheD specifically interacts with MCP3 and MCP4·····70

Figure 2.4. Schematic diagrams showing the construction of Δ*cheD* mutant and complemented strains·····72

Figure 2.5. Expression of *cheD* was abolished in the mutant but was restored in the *cheD*^{com} cells as determined by qRT-PCR·····73

Figure 2.6. Δ*cheD* mutant cells are deficient in chemotaxis·····75

Figure 2.7. Naïve ticks are able to acquire and transmit Δ*cheD* mutant spirochetes during mouse-tick-mouse infection studies·····79

Figure 2.8. Serology results of mice fed by the infected nymphs·····82

Figure 2.9. Role of chemotaxis in *B. burgdorferi*·····87

Figure 3.1. Unique collar structures are conserved in all spirochetes·····94

Figure 3.2. Construction of Δ*flbB* mutant and determination of polar effect on downstream genes expression·····106

Figure 3.3. Morphology and motility phenotype of the Δ*flbB* mutant cells·····109

Figure 3.4. Periplasmic flagellar orientation in wild-type and Δ*flbB* mutant……112

Figure 3.5. Comparative analysis of *in situ* flagellar motors from wild-type and Δ*flbB* reveals the 3D collar structure for the first time……114

Figure 3.6. FlbB directly interact with FliL……118

Figure 3.7. Transmembrane domain prediction of FlbB-GFP fusion protein……120

Figure 3.8. Expression and location of FlbB-GFP in *B. burgdorferi*……122

Figure 3.9. Location of FlbB-GFP as determined by cryo-ET……123

Figure 4.1. A model of CheD in the enzootic cycle of *B. burgdorferi*……131

Figure 4.2. Protein interaction network of *Treponema pallidum*……134

CHAPTER ONE: INTRODUCTION

Lyme disease is the most prevalent vector-borne disease in the United States and is caused by the spirochete *Borrelia burgdorferi* (1). The disease is transmitted from infected *Ixodes* ticks to mammalian hosts (2, 3). Early administration of select antibiotics can successfully eliminate these infections; however, similar treatment on established infections is less effective, and no commercial vaccine is currently available. The identification of novel targets for curative therapies is a significant need.

B. burgdorferi is a motile organism, and motility was reported to be critical for the infectious life cycle (tick-mouse) of the spirochete. Motility is controlled by chemotaxis, which allows bacteria to follow gradients of nutrients and other environmental stimuli. The components of the chemotaxis signal transduction systems that mediate these responses are highly conserved among prokaryotes. However, chemotaxis in *B. burgdorferi* is more complicated and differs from the other well-studied bacterial chemotaxis models such as *Escherichia coli* and *Bacillus subtilis*. The genome of *B. burgdorferi* encodes multiple homologs of several chemotaxis genes (e.g. two *cheA*, three *cheW*, three *cheY*, two *cheR*, and two *cheB* genes), making it much more complex than the model organisms. Most importantly, the roles of most of the *B. burgdorferi* putative chemotaxis proteins are still elusive. In this research project, we determined the role of a putative chemotaxis gene *cheD* in *B. burgdorferi*. The CheD homolog is relatively well-characterized in *B. subtilis*, where it plays an important role in chemotaxis by deamidation of methyl-accepting chemotaxis protein receptors (MCPs), by increasing the receptor-kinase activity or by enhancing CheC phosphatase activity, thereby regulating the levels of the CheY response regulator. We hypothesize that

CheD in *B. burgdorferi* would play a similar role as in other bacteria. Most importantly, we defined its role in mouse and tick-mouse models of Lyme disease. Delineating the role of CheD in *B. burgdorferi* will provide insights into not only the chemotaxis pathway of this spirochete but also its infectious life cycle.

B. burgdorferi has amphilophotrichous periplasmic flagella. The periplasmic flagella form a ribbon-like structure that wrap around the cell body or cylinder. When empowered by the motor rotation, the periplasmic flagella are rotated symmetrically or asymmetrically, resulting in complicated swimming behaviors (run, reverse or flexing swimming modes). The chemotaxis signal transduction system controls the rotation of flagella (see details below). Beside from the chemotaxis molecules, the flagellar motor components are also closely intertwined with the motility in this spirochete. Unlike other externally flagellated bacteria, the spirochetes periplasmic flagella contain a unique structure called the collar. However, nothing was known about the genes encoding the collar structure or their function in any spirochete. This novel component is conserved among spirochetes and located in the periplasmic space. Most interestingly, the collar is seen directly connected with the major component of the flagella leading to the hypothesis that the collar is important for flagellar assembly or providing proper rigidity and flexibility of flagella within the periplasmic space during rotation. In this research project, we identified and characterized a gene, *flbB*, that was found to be involved in the assembly of the collar structure. Understanding the intimate relationship between bacterial motility and the spirochetal unique collar structure in *B. burgdorferi* can provide ideas to comprehend an enigmatic spirochetes' asynchronous motility. In addition, this spirochete conserved collar structure could be a target for the new drug to disrupt

flagellar assembly. The structural information of the collar has provided new opprotunities for structure-based drug design, which would block motility and the spread of Lyme disease as well as other spirochete-borne diseases in the future.

LYME DISEASE

History and discovery of Lyme disease. Lyme disease was first recognized in the 1970s. In 1975, a tight geographic clustering of children in the area of Old Lyme, Connecticut displayed a mysterious syndrome which was initially thought to be juvenile rheumatoid arthritis. Dr. Allen Steere, a rheumatology resident at Yale University, investigated 51 residents who developed symptoms characterized by recurrent attacks of asymmetric swelling and pain in a few large joints, especially the knee, and suggested that this clinical manifestation was transmitted by an arthropod vector, and described it as Lyme arthritis in 1977 (4). He contacted Dr. Willy Burgdorfer, a medical entomologist at Rocky Mountain Laboratories of National Institute of Allergy and Infectious Diseases (NIAID), to investigate the Lyme arthritis. In 1982, Dr. Burgdorfer discovered a spirochete in the midgut of an *Ixodes scapularis* tick (5). The following year, he investigated the connection between this spirochete and Lyme disease (6), and in honor of its discoverer, the organism was named after him "*Borrelia burgdorferi*" (7). Even though the first recognized case of Lyme disease was reported only 40 years ago, the oldest human case of infection with *B. burgdorferi* was discovered by whole-genome sequencing in the Tyrolean Iceman which is a 5,300-year-old Copper Age individual, discovered in 1991 on the Tisenjoch Pass in the Italian part of the Ötztal Alps (8). In 2014, Dr. George Poinar Jr. in Oregon State University found spirochete-like cells (Spirochaetales: Spirochaetaceae) in the hemocoel and lumen of the alimentary tract of

a larva tick (*Amblyomma* sp. Arachnida: Ixodidae) which has similar size and shape of the present-day *Borrelia* species in 20-15 million year old Dominican amber fossil (9). This discovery of fossil spirochetes established a minimum time period of 20-15 million years when hard ticks were infected with *Borrelia*-type spirochetes.

Clinical manifestations of Lyme disease. The initial classification of Lyme disease was uncomplicated: erythema migrans (stage 1), meningitis or Bell's palsy (stage 2), and arthritis (stage 3) (10). However, the disease was re-classified in a system similar to that used to classify syphilis (11) due to the overlap of the clinical manifestations at different stages. Lyme disease is now subdivided into three different stages based on infection time (12-14).

Stage 1, early localized Lyme disease, occurs 3 to 30 days after an infected tick bite. The most common and clinical hallmark of this stage of Lyme disease is a skin rash known as erythema migrans (Fig. 1.1.A). This skin rash occurs in approximately 70 to 80 percent of patients, and typically appears at the site of the tick bite after a delay of about one week (ranging from 3 to 32 days), as a small red erythematous macule or papule due to the peripheral lymphocytic and eosinophilic infiltration of cutaneous vessels (3, 14, 15). The lesion subsequently enlarges, and may have vesicles or necrotic areas at the center. This lesion tends to have red outer borders with partial central clearing that can reach 61 cm (2 ft) in diameter or larger, for that reason the rash is also known as a "bull's-eye rash" (16-19). Erythema migrans lesions are able to occur anywhere on the body surface, although common sites are the back, legs, waist, groin, axilla, and in children the head and neck. The lesion itself is usually asymptomatic but may be pruritic or painful (10). Moreover, many patients have non-specific symptoms

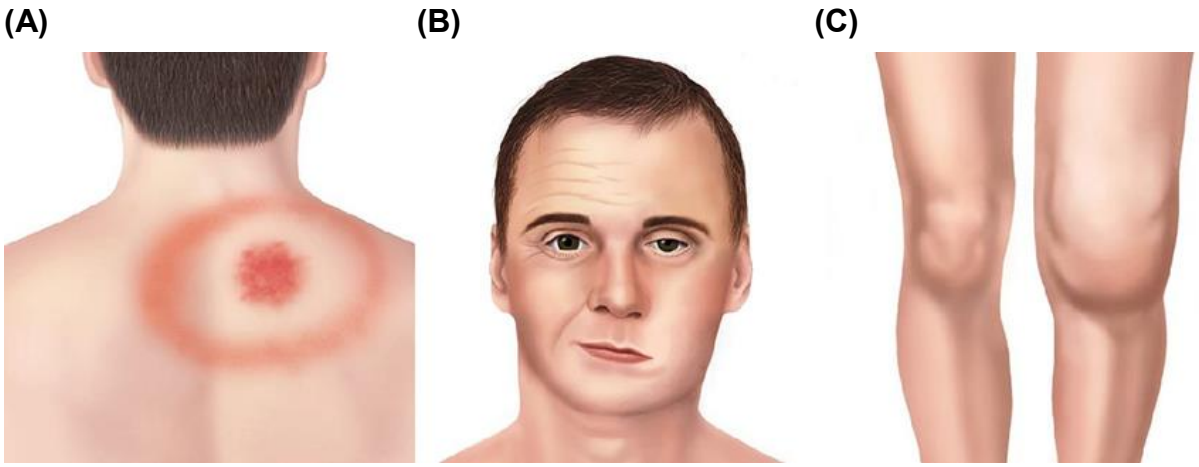

Figure 1.1. Signs and symptoms of untreated Lyme disease. From Lyme disease, Centers for Disease Control and Prevention. Available at: http://www.cdc.gov/lyme/signs_symptoms/index.html. Accessed August 17, 2015. **(A)** "Classic" erythema migrans rash. **(B)** Facial palsy. **(C)** Lyme arthritis.

such as fatigue, headache, cough, arthralgia, myalgia, stiff-neck, regional lymphadenopathy, and, less often, low-grade fever (10, 16-19).

Most patients with erythema migrans (70 to 80% of all patients) have a single lesion, but the bacteria are able to migrate out hematogeneously to other sites in the skin and to the extracutaneous sites. This disseminated infection is classified as stage 2, early-disseminated Lyme disease, and occurs in 2 to 8 weeks after the tick bite. The most common clinical manifestation of this stage is multiple erythema migrans. These secondary lesions appear 3 to 5 weeks after the tick bite and consist of multiple annular erythematous lesions similar to, but usually smaller than the primary lesion (3, 19). Extracutaneous manifestations of this stage of Lyme disease include neurologic conditions, such as cranial-nerve palsy (particularly facial-nerve palsy, also known as Bell's palsy) (Fig. 1.1.B), and meningitis that mimics aseptic meningitis. Neurological manifestations, such as peripheral and central nervous dysfunction, occur due to the lymphocytic infiltration (15). Rarely, carditis, which is most commonly manifested by various degrees of atrio-ventricular (A-V) blockage, may also occur at this stage (3, 20-22).

Stage 3, late persistent Lyme disease, occurs in 6 months after the tick bite. In the United States, the most common sign of late Lyme disease is arthritis, and it occurs in approximate 31% of all Lyme disease cases, and in less than 10% of all cases where patients were treated. Arthritis occurs weeks to months after the initial infection; it is usually monoarticular or oligoarticular (4, 23) and affects the large joints, particularly the knee (Fig. 1.1.C). Arthritis is believed to be not dependent on immune complex deposition, but rather a dysregulated cytokine and cell-mediated response. It is unclear

whether pathology is due solely to recognition of *Borrelia* spirochetes within the joint, or whether molecular mimicry is underlying an autoimmune based mechanism (15). Even though the joints are swollen and tender, the intense pain associated with septic arthritis is usually not present. Approximately 10% of patients are refractory to antimicrobial treatment at this stage of Lyme disease (24, 25).

The various clinical manifestations of chronic Lyme disease have been associated with different tissue tropisms of the three genospecies of *Borrelia*. In the United States, 31% of Lyme disease cases reported through national surveillance are associated with arthritis which is caused by a *B. burgdorferi* sensu stricto infection, whereas only 12% have neurologic symptoms (usually facial palsy) (26). Carditis is universally rare, generally accounting for less than 1% in most series (1, 27). Neurological and cutaneous manifestations such as neuroborreliosis and chronical skin rash (acrodermatitis chronica atrophicans) are often associated with *B. afzelii* and *B. garinii* infections, respectively (28, 29). These dermatologic and neurologic manifestations of Lyme disease are well known in Europe but are extremely rare in the United States (30).

Infection rate and mortality of Lyme disease. The cases of Lyme disease reported by the Centers for Disease Control and Prevention (CDC) increased approximately 260% between 1997 (12,801 cases) and 2014 (33,461 cases). Each year, approximately 30,000 cases of Lyme disease are reported, and the total cost of Lyme disease now tops two billion dollars annually in the United States (31-33). However, the CDC reported by its own investigation that the actual number of Lyme disease cases is underreported due to the lack of distinct disease symptoms and simple

diagnostic assays. The CDC estimates the actual cases of Lyme disease in the United States is approximately 300,000 each year with medical costs estimates over twenty billion dollars each year (34). Based on this report, the infection rate of Lyme disease in United States is ≥ 100 cases per 100,000 in the population, which is similar to the scale seen with gonorrhea—the second most-commonly reported infectious disease in United States (350,062 cases in 2014, 110.7 cases per 100,000 population) (35).

Although Lyme disease shows high infection rate, mortality rate of Lyme disease is very low. Based on systematic analysis of the medical literature, only a few cases of death caused by Lyme disease have been reported worldwide (36-42). From 1999 to 2003, 23 cases of death by Lyme disease were reported; however, 11 cases were improperly coded, and only one listed a consistent causal sequence (43). The potential for occult death caused by Lyme carditis was verified by a recent report of fatal Lyme carditis cases investigated through postmortem examination of donated tissues (44). Nonetheless, a follow-up study of more than 120,000 patients with Lyme disease during 1995 to 2013 found that only 0.6% died of any causes within a year of diagnosis, a rate less than the expected, age-adjusted, all-cause mortality for this population (27).

Diagnosis and treatment of Lyme disease. The CDC proposed that Lyme disease is diagnosed based on signs, symptoms, and a history of potential exposure to ticks in an area where Lyme disease is endemic (45). The clinical diagnosis of Lyme disease can be straightforward in patients with a history of infected tick exposure and physical findings (e.g., erythema migrans rash) (46). Although the erythema migrans rash is a distinctive sign for diagnosis of Lyme disease, a number of conditions resemble erythema migrans (Table 1.1) (47, 48); however, the rapid and prolonged

Table 1.1. Differential diagnosis of erythema migrans

Condition	Characteristics
Single erythema migrans lesion	Erythematous macule or papule at site of tick bite (although the tick is often not seen); enlarges relatively rapidly to 5–30 cm or more in diameter; typically flat and annular; usually uniformly erythematous or with heightened central erythema; may have central clearing; without treatment, persists for average of 3–4 weeks*
Cellulitis	Homogenous erythematous lesions associated with edema, tenderness, and warmth; enlarges rapidly; rarely circular; most commonly adjacent to an ulcer, laceration, or wound
Granuloma annulare	Small (2–5 cm in diameter), scaling erythematous lesions with central clearing; most commonly located on the feet and hands; develops over weeks; often on dorsum of extremities
Hypersensitivity reaction/dermatitis	Lesions of variable shape and size that may resemble certain objects (e.g., tape, nickel coins, necklaces); often pruritic
Methicillin-resistant *Staphylococcus aureus* infection	Erythematous lesions of variable size that may be associated with necrotic eschar; most commonly located on the extremities, but may involve the axilla, abdomen, chest, or back
Nummular eczema	Coin-shaped erythematous lesions that range in size from 2–10 cm; does not enlarge rapidly; pruritic; well demarcated; skin may be thickened or weepy; Most commonly located on the back and hands
Spider bite	Erythematous lesions of variable size that may be associated with necrotic eschar; often very painful; most commonly located on the extremities
Insect bite	Often raised papule with central punctum; pruritic; usually smaller than erythema migrans lesion; rarely continues to enlarge
Tinea (ringworm)	Annular or ring-form lesions of variable size with central clearing; variable region

Table 1.1. Differential diagnosis of erythema migrans (~continue)

Condition	Characteristics
Multiple erythema migrans lesions	Multiple ring like lesions; typically do not enlarge rapidly; a larger, primary lesion may be present; often associated with systemic symptoms
Erythema multiforme	Symmetric lesions (most are less than 2 cm in diameter) with central clearing; cause may be apparent (e.g., drug or infection); diffuse lesions with mucous membrane involvement
Urticaria	Raised erythematous lesions with an associated serpiginous border; may appear and disappear rapidly; variable region

*A similar lesion is found in southern tick-associated rash illness (STARI), which occurs primarily in southeastern and south central states. STARI does not have extracutaneous manifestations. The cause of STARI is unclear; no diagnostic test is available (49).

expansion of an erythematous lesion is unique to erythema migrans (16). Lesions most often occur at anatomic sites that are unusual for cellulitis and other conditions that mimic erythema migrans (e.g., back, groin, abdomen, axilla, popliteal fossa). Therefore, a complete skin examination should be performed before excluding erythema migrans (21).

Validated laboratory tests are generally of little use in patients with erythema migrans (48). The CDC and Infectious Diseases Society of America (IDSA) recommended serological tests as the most preferred initial diagnostic laboratory test (21, 50). Currently, the CDC recommends two-tier serology tests when analyzing blood for evidence of *B. burgdorferi*-specific antibodies in the patients with suspected Lyme disease. The first step uses a sensitive method such as enzyme linked immunosorbent assay (ELISA) or immunofluorescence assay (IFA). These tests should detect both immunoglobulin M (IgM) and IgG antibodies against *B. burgdorferi*. If the first-tier samples are positive or equivocal, a second step should be performed to confirm the results. The second step uses Western blot analysis, which detects separate IgM and IgG antibodies against borrelial specific antigens. The following criteria for a positive Western blot are adapted from the CDC; IgM should be reactive against 2 or 3 of 3 antigens [p21 (OspC), p39 (BmpA), and p41 (FlaB)], and IgG should be reactive against 5 or more of 10 antigens [p18, p21 (OspC), p28, p30, p39 (BmpA), p41 (FlaB), p45, p58, p66, and p93]. (50-53). Even though the two-tier test is used as a standardized method for Lyme disease diagnosis, it has low sensitivity in early infection, but is highly sensitive after 6 to 8 weeks of untreated infection (54).

In synovial fluid samples from patients with untreated late Lyme arthritis,

polymerase chain reaction (PCR) analysis has shown the highest sensitivity (47, 55, 56). However, borrelial DNA may persist after spirochetal killing, which limits its use as a test for active infection. Therefore, IDSA recommended that PCR testing be used as an optional test to further support the diagnosis for selected patients with late Lyme arthritis or neurological Lyme disease (21, 23). The urine borrelial antigen test is not recommended due to a high false-positive rate (57, 58).

Lyme disease usually can be treated with antibiotics. Lyme disease have various stages, and treatments differ according to the stage of infection. Both oral and intravenous (IV) antibiotics therapies are typically used in Lyme disease patients. The IDSA provided guidelines for the treatment of Lyme disease (Table 1.2) (21, 47, 54). Oral antibiotics administration (e.g. doxycycline, amoxicillin, or cefuroxime axetil for 14 days) is the recommended treatment for early localized or disseminated Lyme disease, in the absence of specific neurologic manifestations. Patients of Lyme disease with neurological manifestations are usually treated with IV antibiotics therapies. For instance, the IV antibiotic therapy (e.g. ceftriaxone for 14 days) is recommended for early Lyme disease adult patients with acute neurological manifestation such as meningitis or nerve root disorder (radiculopathy) (21). Patients of Lyme disease with cardiac symptoms, or, in a few cases, refractory Lyme arthritis are also treated with the IV regimens. Treatment of Lyme arthritis patients is more complex. Lyme arthritis patients are initially treated with an oral antimicrobials administration (e.g. doxycycline, amoxicillin, or cefuroxime axetil for 28 days). During and after the oral antibiotic therapy, non-steroidal anti-inflammatory drugs are commonly used to ameliorate symptoms. Lyme arthritis patients with neurological symptoms should receive IV ceftriaxone

Table 1.2. Preferred antimicrobial therapies for Lyme disease[*]

Manifestation	Treatment	Adult dosage	Pediatric dosage	Recommended duration (range)
Early disease (erythema migrans)	Doxycycline[+]	100 mg orally twice a day	<8 years: not recommended; ≥8 years: 4 mg/kg/day in 2 divided doses (maximum 100 mg/dose)	14 days (10–21 days)
	Amoxicillin	500 mg orally 3 times a day	50 mg/kg/day in 3 divided doses (maximum 500 mg/dose)	14 days (14–21 days)
	Cefuroxime axetil	500 mg orally twice a day	30 mg/kg/day in 2 divided doses (maximum 500 mg/dose)	14 days (14–21 days)
Early neurologic disease				
Cranial nerve palsy[#]	Same as for erythema migrans	Same as for erythema migrans	Same as for erythema migrans	14 days (14–21 days)
Meningitis or radiculopathy[##]	Ceftriaxone	2 gm IV per day	50–75 mg/kg IV per day in a single dose (maximum 2 gm/day)	14 days (10–28 days)

Table 1.2. Preferred antimicrobial therapies for Lyme disease[*] (~continue)

Manifestation	Treatment	Adult dosage	Pediatric dosage	Recommended duration (range)
Cardiac disease	Same as oral regimen for erythema migrans *or* use IV regimen as for neurologic disease[†]	2 gm IV per day	50–75 mg/kg IV per day in a single dose (maximum 2 gm/day)	14 days (14–21 days)
Late disease				
Arthritis without neurologic involvement	Same as for erythema migrans	Same as for erythema migrans	Same as for erythema migrans	28 days (28 days)
Recurrent arthritis after oral regimen	Repeat oral regimen *or* use IV regimen as for neurologic disease	Repeat oral regimen *or* use IV regimen as for neurologic disease	Repeat oral regimen *or* use IV regimen as for neurologic disease	28 days for oral regimens, 14–28 days for IV regimens
Central or peripheral nervous system disease	IV regimen as for early neurologic disease	IV regimen as for early neurologic disease	IV regimen as for early neurologic disease	14 days (14–28 days)

[*]Complete response to treatment may be delayed beyond the treatment period, regardless of the clinical manifestation, and relapse may recur. Patients with objective signs of relapse may need a second course of treatment. For a complete list of recommended and alternate therapies (21).

[+]Tetracyclines are relatively contraindicated in pregnant or lactating women and in children <8 years of age.

[#]Patients without clinical evidence of meningitis may be treated with an oral regimen. The recommendation is based on experience with seventh cranial nerve palsy. Whether oral therapy would be as effective for patients with other cranial neuropathies is unknown; the decision between oral and parenteral therapy should be individualized.

[##]For nonpregnant adult patients who are intolerant of β-lactam agents, doxycycline 200–400 mg/day orally [or intravenously (IV) if unable to take oral medications] in 2 divided doses may be adequate. For children ≥8 years of age, the dosage of doxycycline for this indication is 4–8 mg/kg/day in 2 divided doses (maximum 200–400 mg/day).

[†]A parenteral antibiotic regimen is recommended at the start of therapy for patients who have been hospitalized for cardiac monitoring; an oral regimen may be substituted to complete a course of therapy or to treat outpatients. A temporary pacemaker may be required for patients with advanced heart block.

treatment. If incomplete resolution of arthritis is observed with the patients after 4 weeks oral treatment, an additional course of oral or IV antibiotics treatment may be necessary (21).

About 10% of patients with Lyme arthritis develop antibiotic-refractory Lyme arthritis (or treatment-resistant Lyme arthritis) in the United States, and this joint inflammation persists for months to several years after antibiotic therapy (59). *B. burgdorferi* DNA is undetectable by PCR in synovial fluid from these chronic Lyme arthritis patients, but is detectable before antibiotic therapy. This suggests that antibiotic-refractory Lyme arthritis is not caused by chronic spirochete infection (60). Instead of a chronic infection, investigators suggest a link between the development of antibiotic-refractory Lyme arthritis and induction of autoimmunity.

The histologic lesion of this antibiotic-refractory Lyme arthritis mimics that of rheumatoid arthritis. Synovial tissue samples reveal hypertrophy, neovascularity, macrophage infiltration, and a mixed population of lymphocytes typically found in subsynovial areas (61). The majority of patients with antibiotic-refractory Lyme arthritis have human lymphocyte antigen (HLA)-DRB1*0401 or related alleles (62, 63), which are associated with the severity of rheumatoid arthritis (64). Moreover, the severity and duration of antibiotic-refractory Lyme arthritis correlates with cellular and humoral immune responses to outer surface protein A (OspA) of the spirochete. The $OspA_{165–173}$ epitope region has been shown to have sequence homology with human lymphocyte function associated antigen-1 (hLFA-1), and it has been predicted to bind to the DRB1*0401 molecule (61). In most antibiotic-refractory patients with Lyme arthritis, their T cells from synovial fluid responded to both OspA and hLFA-1, whereas those from

patients with other forms of chronic inflammatory arthritis did not (61). Although the pathogenesis of this antibiotic-refractory Lyme arthritis is still unclear, increasing the frequency of certain class II major histocompatibility complex (MHCII) molecules such as HLA-DR3 and HLA-DR4 alleles (61, 63), and molecular mimicry between a dominant T cell epitope of OspA and hLFA-1 (60, 61) may be an important factor in the persistence of joint inflammation in genetically susceptible patients with antibiotic-refractory Lyme arthritis.

Vaccine against Lyme disease. Although antibiotics therapies are effective treatment for Lyme disease, approximately 10% of patients still suffer from post-treatment Lyme disease syndromes such as treatment-resistant Lyme arthritis (65-67). In addition, the emergence rate of drug-resistant bacteria has been increasing in recent decades and cause serious problems not only in *B. bugdorferi* but also in other infectious bacteria (68-70). Based on pharmaco-economic studies, almost two billion dollars spent on medical claims for Lyme disease in the United States every year (32, 33). To prevent antibiotic overuse and reduce medical claims for Lyme disease, vaccines for Lyme disease are clearly needed (71, 72).

Currently, several licensed veterinary vaccines are available in the market; however, human Lyme disease vaccines are not commercially available at present (73). Previously, two pharmaceutical companies developed vaccines for Lyme disease in the early 1990s for human use. The US Food and Drug Administration (FDA) previously licensed a vaccine for Lyme disease on December 21, 1998, which was registered as LYMErix by SmithKline Beecham (now called GlaxoSmithKline). Another vaccine was registered as ImuLyme by PasteurMe´rieux-Connaught. However, the company did not

go forward with a biologic license application for the vaccine, despite efficacy in their phase III clinical trial (74-77). Both vaccines were designed against the *B. burgdorferi* outer surface protein A (OspA). The vaccine inoculator developed circulating bactericidal antibodies against the OspA that would be ingested by the tick during a blood meal. These antibodies would then be sufficient to bind and neutralize viable *B. burgdorferi* present in the tick gut, such that, during a blood meal, infectious spirochetes could not be regurgitated through the dermis, effectively preventing infection. However, the tenure of LYMErix was short, purportedly due to poor sales. In the 2001, sales of LYMERix had decreased to five million dollars annually with the purchase of only 93,000 doses of vaccine. In the first 2 months of 2002, sales had dwindled to 10,000 doses (78). Due to the low public demand for the vaccine, the manufacturer voluntarily withdrew the vaccine production and marketing of LYMERix in February 2002. The decline in sales could be traced to concerns, real or perceived, of possible adverse effects, including a chronic inflammatory arthritis that could theoretically develop in HLA-DR4 positive patients (i.e. vaccine associated auto-immune arthritis) (79). The outer surface protein A, OspA-based vaccines have another concern that is the frequency of boosts required to maintain long-term protection. *B. burgdorferi* upregulated the expression level of OspA in the larval tick host after first blood meal. OspA is expressed in the tick midgut to tether with a tick midgut protein TROSPA (80). After larvae molted into the nymphs, the nymphal ticks feeding on a mammalian host. During this second blood meals, *B. burgdorferi* OspA is rapidly downregulated, resulting in spirochetes no longer being tethered to the tick midgut and migrating out to salivary gland and

subsequently to the dermis of the host. In the mammalian host, OspA is poorly expressed (81, 82).

These problems associated with OspA-based vaccines can be avoided by using different antigens, which are expressed at high levels during mammalian infection, such as outer surface protein C, OspC (83). OspC is immunodominant during early infection in the mammalian host and can elicit bactericidal antibodies, however, the protective range is narrow (84, 85). Because OspC is one of the most highly diverse proteins of *B. burgdorferi*; OspC sequences form at least 38 distinct phyletic *ospC* clusters or types (86-88), and its inherent diversity has hampered OspC vaccine development. Identification of protective epitopes of each OspC type will allow for construction of recombinant, polyvalent, chimeric vaccines that will elicit broad protection. Thus, a tetravalent and an octavalent vaccine based on OspC types have been developed. These constructs elicited an antibody response against each of the components epitopes, and those antibodies show a complement-dependent bactericidal activity (89, 90). A DNA-vaccine encoding an *ospC* gene was also shown to be suitable for inducing protection against Lyme borreliosis (91). However, a limited number of studies for Lyme disease vaccine are being investigated since 2002, and there has been no active, sustained interest in developing or licensing a new Lyme disease vaccine in the United States.

Epidemiology of Lyme disease. According to the CDC, Lyme disease has been the most common vector-borne disease in United States since 1985 (26), and has been a nationally notifiable condition since 1991 (1). In 2014, Lyme disease was the fifth most common nationally notifiable disease. From 1992 to 2014, the United States and its

territories reported 455,899 confirmed cases of Lyme disease to the CDC (26, 35, 92-94). During this period, annual case counts continuously increased approximate 3-fold, from 9,908 cases in 1992 to 33,459 cases in 2014 (Fig. 1.2) (26, 35, 92-94). Within North America, the incidence of Lyme disease is highest in the Northeastern, Mid-Atlantic, and North Central United States. In 2014, more than 96% of confirmed Lyme disease cases in the United States were reported from 14 states; Connecticut, Delaware, Maine, Maryland, Massachusetts, Minnesota, New Hampshire, New Jersey, New York, Pennsylvania, Rhode Island, Vermont, Virginia, and Wisconsin (Fig. 1.3.A). The genus *Ixodes* ticks are well-known vectors for transmitting Lyme disease. In the Eastern and North Central United States, the *Ixodes scapularis* tick (also known as the black-legged tick) is the main vector (infection rate >50%) (Fig. 1.3.B), whereas in the Pacific States transmission occurred mainly by the *I. pacificus* (also known as the Western black-legged tick, infection rate 1-6%) (Fig. 1.3.C). The white-footed mouse (*Peromyscus leucopus*) is the primary reservoir of *B. burgdorferi* in the Northeastern United States (95). Mice are generally infected when fed upon by primarily nymphal stage *Ixodes* ticks, which acquired *B. burgdorferi* during the larvae stage blood feeding on small mammalian hosts (96). The white-tailed deer (*Odocoileus virginianus*) serves as the primary host for adult ticks.

Interestingly, lizards rarely serve as competent reservoir hosts in the United States. The western fence lizard (*Sceloporus occidentalis*) is naturally and experimentally refractory to *B. burgdorferi* infection. The alternative complement pathway of *S. occidentalis* typically destroys *B. burgdorferi* present in the tissues of attached and feeding nymphal stage ticks, thus potentially reducing the probability of

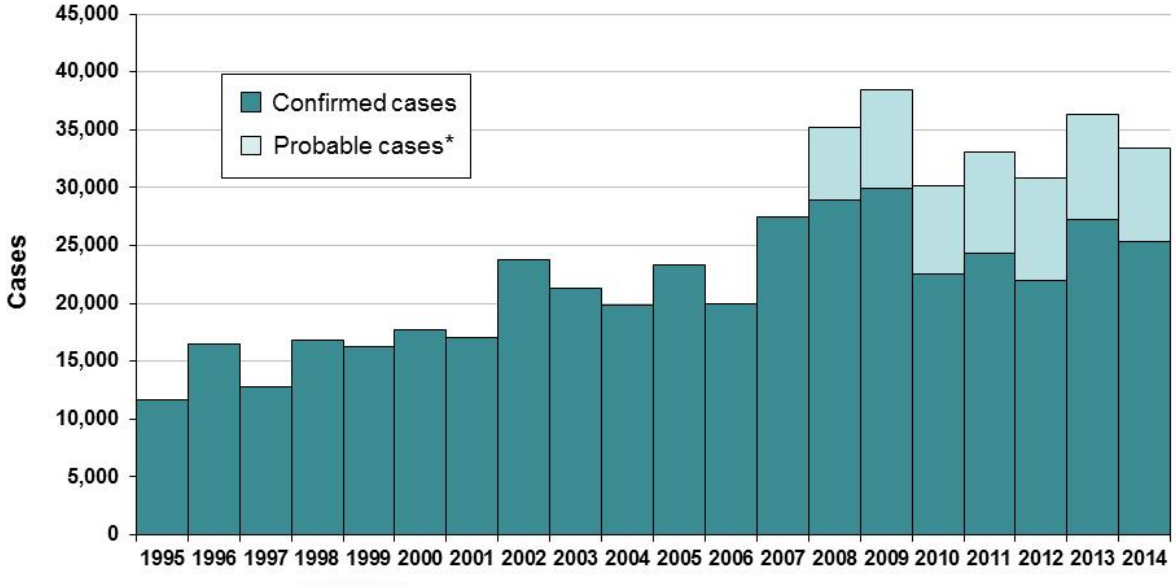

*National surveillance case definition revised in 2008 to include probable cases.

Figure 1.2. Number of reported Lyme disease cases, United States, 1995 to 2014. From Lyme disease, Centers for Disease Control and Prevention. Available at: http://www.cdc.gov/lyme/stats/graphs.html. Accessed November 5, 2015.

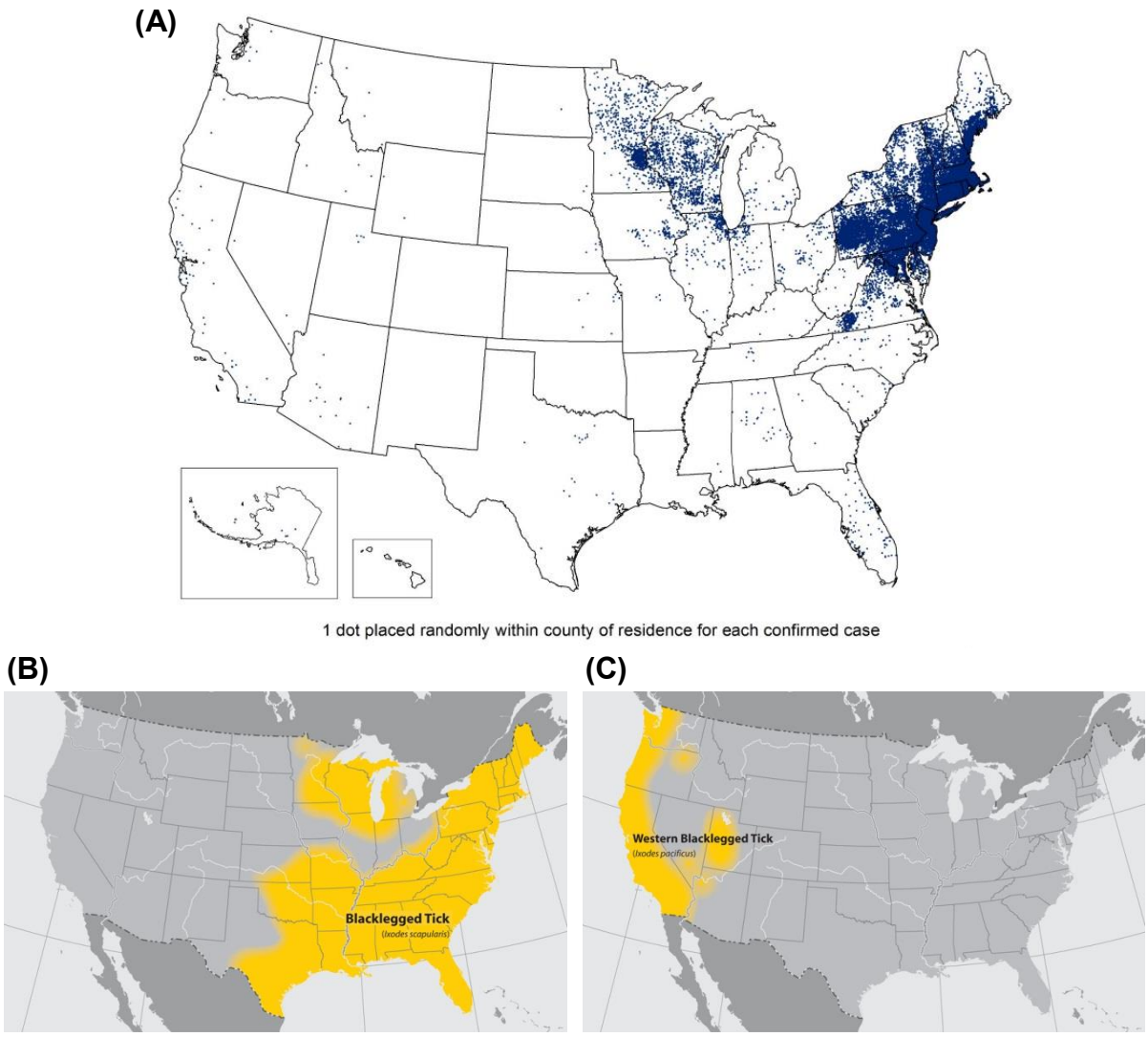

Figure 1.3. Geographic distribution of confirmed Lyme disease cases, United States in 2014 (A), *Ixodes scapularis* (Blacklegged tick) (B), and *Ixodes pacificus* (Western blacklagged tick) (C). (A) From Lyme disease, Centers for Disease Control and Prevention. Available at: http://www.cdc.gov/lyme/stats/maps.html. Accessed November 5, 2015. **(B, C)** From Geographic distribution of ticks that bite humans, Centers for Disease Control and Prevention. Available at: http://www.cdc.gov/ticks/geographic_distribution.html. Accessed June 1, 2015.

transmission of spirochetes to humans and other animals by the resulting adult ticks (97, 98). Based on this consequence, ecologists have proposed the hypothesis that the reason for lower Lyme disease incidence in California and the Southern part of United States is based on the population of lizards between epidemic and non-epidemic region of Lyme disease (99-101).

Infectious life cycle (Mammalian and *Ixodes* tick hosts). *Ixodes* ticks undergo a four-stage life cycle: the egg, larva, nymph, and adult stages (Fig. 1.4). The larvae are uninfected when they are hatched from eggs. These naïve larvae can acquire the spirochetes from an infected small-mammal or avian reservoir hosts during their first blood meal. After molt into nymphal stage, the nymphs transmit the spirochetes (if acquired during the larval stage) into the mammalian host during the tick's second blood meal. The number of *B. burgdorferi* transmitted varies from 10 to 10,000, with an average of approximately 1,500 (102). Fed nymphs molt into adult ticks, and the adults feed predominantly on larger vertebrate hosts such as a white tailed deer (*O. virginianus*). Although deer are incompetent hosts for persistence of *B. burgdorferi*, they are important for maintenance of the tick population because adult ticks mate on this large mammalian host. After mating, the male tick dies and the female lays eggs on the forest floor before dying (1, 2).

Transovarial (eg. mother-to-egg) transmission of *B. burgdorferi* in *Ixodes* ticks has been reported to possibly occur in 1–5% of ticks (103-105). However, the number of transovarially infected ticks are rare and inadequate to maintain the infected populations of either the tick vector or vertebrate hosts (106). In addition, recent experimental evidence has failed to demonstrate transovarial transmission (105, 107). Larvae,

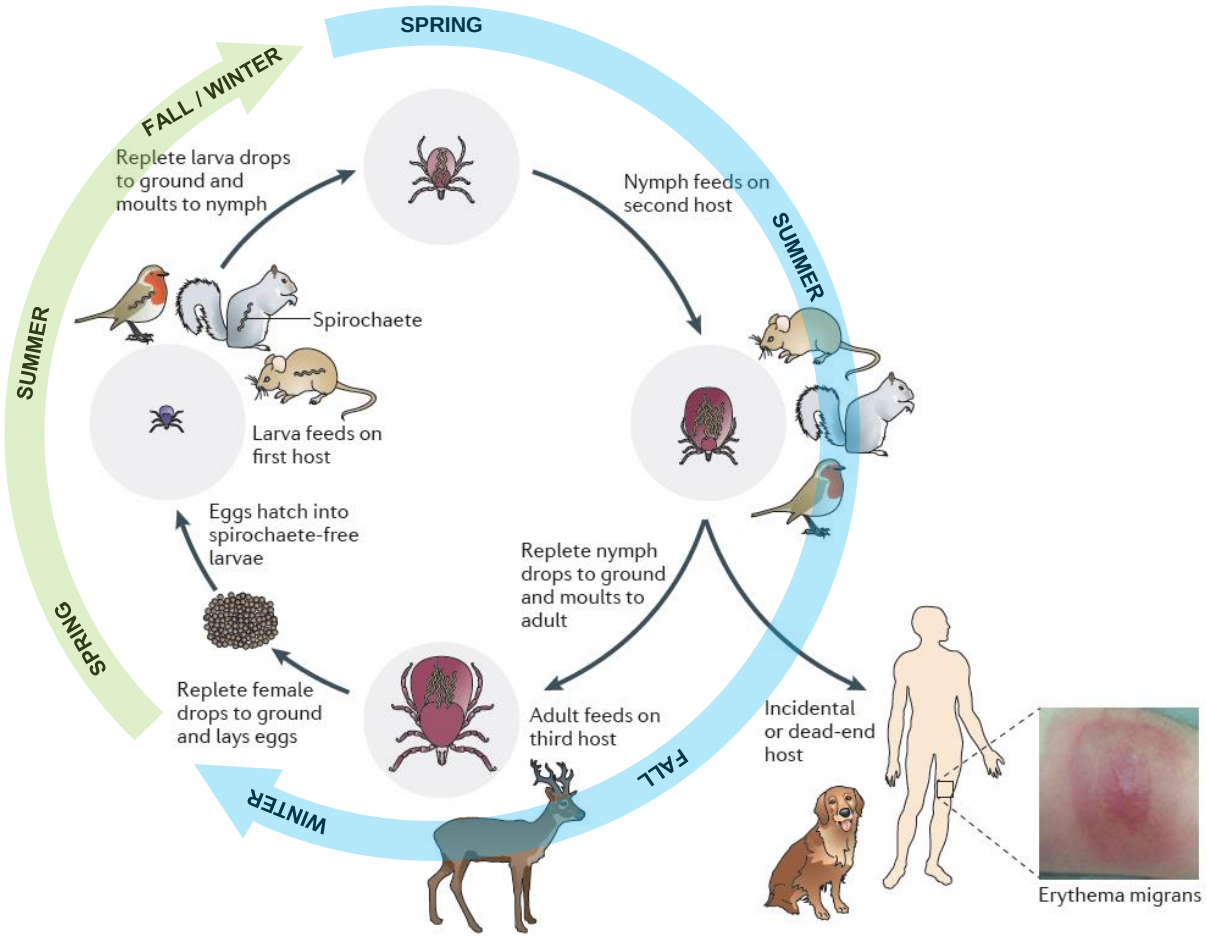

Figure 1.4. The enzootic life cycle of *B. burgdorferi*. *Ixodes scapularis* (also known as the blacklegged tick) is the main vector of *B. burgdorferi* in the United States, and has a two-year life cycle with four life stages: the eggs, and three differential develpemental stages: the larva, nymph, and adult stages.

therefore, are most likely born uninfected.

Until now, Lyme disease is believed to be only transmitted by the bite of infected arthropod vectors. Recently, few intriguing studies have suggested the clinical, epidemiological, and experimental evidence for sexual transmission of Lyme disease in animal models (108-111) and humans (112-115). This hypothesis of sexual transmission of the *B. burgdorferi* remains speculative, it might create a paradigm shift that would transform Lyme disease from a tick-borne illness into a sexually transmitted infection (116).

There is no cases of Lyme disease have been reported by blood transfusion (117, 118). However, investigators have found that *Borrelia* species can live in blood that is stored for donation (119, 120). For that reason, CDC and Red Cross restricted the blood donation from individuals being treated for Lyme disease with an antibiotic.

BORRELIA BURGDORFERI

Taxonomy of *B. burgdorferi*. Spirochetes are a group of phylogenetically-distinct eubacteria (121). The phylum Spirochetes is composed of a single class (Spirochetes) and order (Spirochetales). The order is divided into three families: Brachyspiraceae, Leptospiraceae, Spirochaetaceae (122). Within the family Spirochaetaceae is the genus *Borrelia*. Of the 37 known *Borrelia* species, 12 can cause Lyme disease (123) (Fig. 1.5). Since the discovery of *B. burgdorferi* in 1982, 10 different tick-borne *Borrelia* species have been identified; *B. burgdorferi* sensu stricto (124), *B. garinii* (124), *B. afzelii* (124, 125), *B. japonica* (126), *B. valaisiana* (127), *B. lusitaniae* (128), *B. andersonii* (129), *B. tanukii* (130), *B. turdi* (130) [the name has been corrected from *B. turdae* (131)], and *B. bissettii* (132, 133) (Fig. 1.6). The term "*Borrelia*

Figure 1.5. Phylogeny of Spirochetes. Members of the phylum *Spirochaetes* are easily identified by their unique coiled morphology and periplasmic flagella. The phylum is composed of a single class (*Spirochaetes*) and order (*Spirochaetales*), divided into three families; *Brachyspiraceae*, *Leptospiraceae*, and *Spirochaetaceae*.

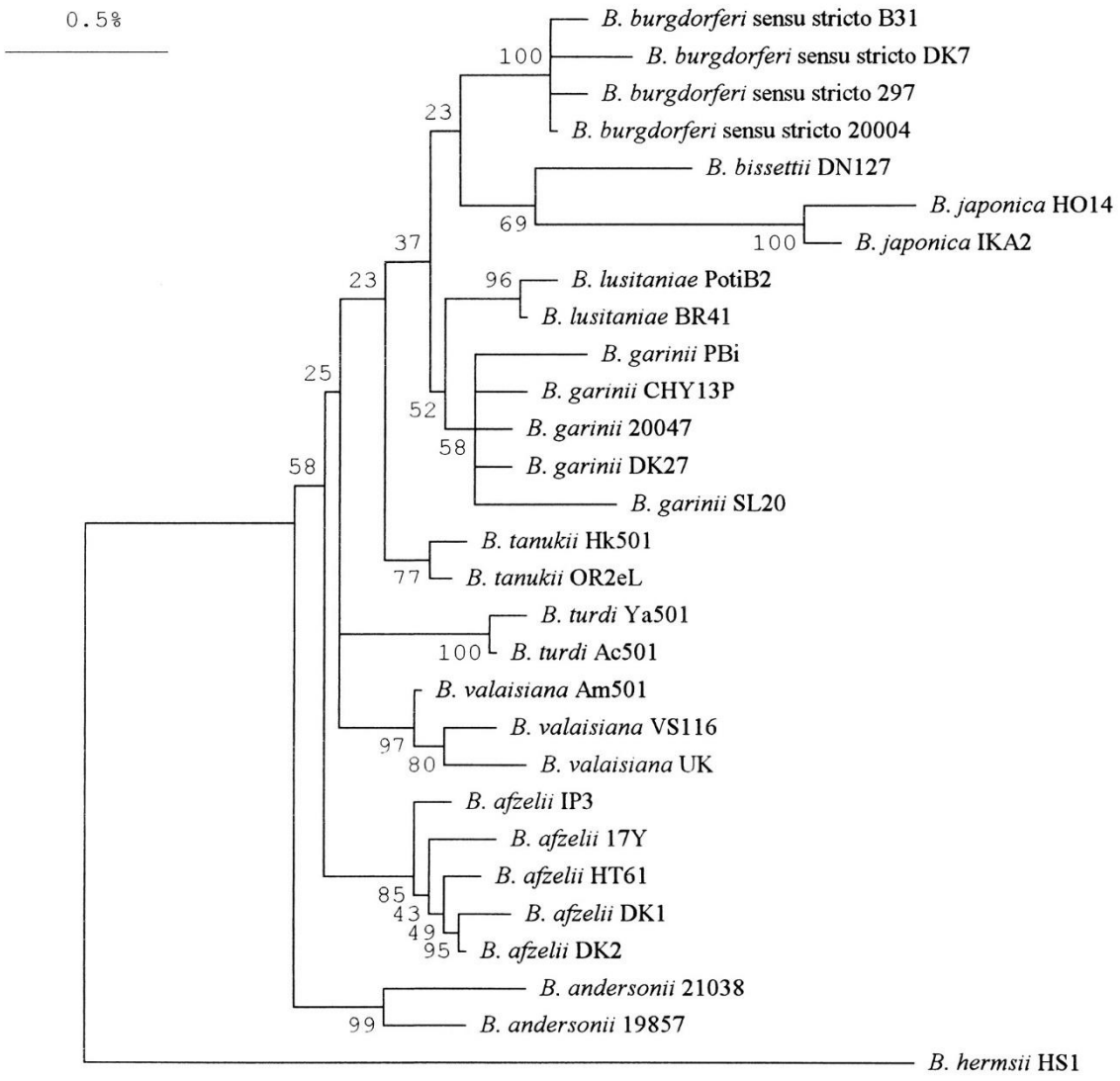

Figure 1.6. Phylogeny of Lyme disease spirochete isolates as inferred from 16S rRNA gene sequence analysis. The phylogenetic tree was constructed by using the neighbor-joining method in the MEGA program. A total of 28 *B. burgdorferi* sensu lato isolates representing 10 different *Borrelia* species were included in this analysis. *B. hermsii* HS1 was used as the outgroup. Numbers at the branch nodes indicate the results of bootstrap analysis. The bar represents 0.5% sequence divergence.

burgdorferi sensu lato" is collectively used for all *Borrelia* isolates within this cluster and to distinguish it from the species "*Borrelia burgdorferi* sensu stricto" (strict sense of *Borrelia burgdorferi*) (124).

Biology of *B. burgdorferi*. Spirochetes, including *B. burgdorferi*, have unique and distinctive structural features: 1) helical or flat-wave morphology and four swimming modes; 2) a double-membrane: an outer membrane without the lipopolysaccharide (LPS) and phosphatidylethanolamine that surrounds the protoplasmic cylinder complex, consisting of the cytoplasm, the peptidoglycan complex, and the inner membrane; and 3) periplasmic flagella instead of external flagella seen in most motile bacteria. Spirochetes flagellar filaments are located in the periplasmic space between the outer membrane and the peptidoglycan layer with the flagellar basal body embedded in the inner membrane (Fig. 1.7) (134-136). *B. burgdorferi* is a long and thin bacterium, 10–20 μm in length and 0.33 μm in diameter (137). The shape of this spirochete is characterized as a planar, regular, with periodic undulation of the cell body of an amplitude of 0.78 μm and a wavelength of 2.83 μm (called the flat-wave morphology) (138). *B. burgdorferi* is a fastidious bacterium, which means it requires a rich growth medium. These bacteria can be cultured *in vitro* with Barbour-Stoenner-Kelly (BSK) II medium, which constitutes CMRL-1066 without L-glutamine, neopeptone, yeastolate, 4-(2- hydroxyethyl)-1-piperazineethanesulfonic acid (HEPES), glucose, sodium citrate, sodium pyruvate, sodium bicarbonate, *N*-acetylglucosamin, bovin serum albumin, and rabbit serum (139), at 30–37°C in microaerophilic conditions (5, 140, 141). Even under optimal laboratory conditions, the generation time for *B. burgdorferi* is long, dividing every 5–12 hours during exponential phase growth and culture adapted strains achieve

(A)

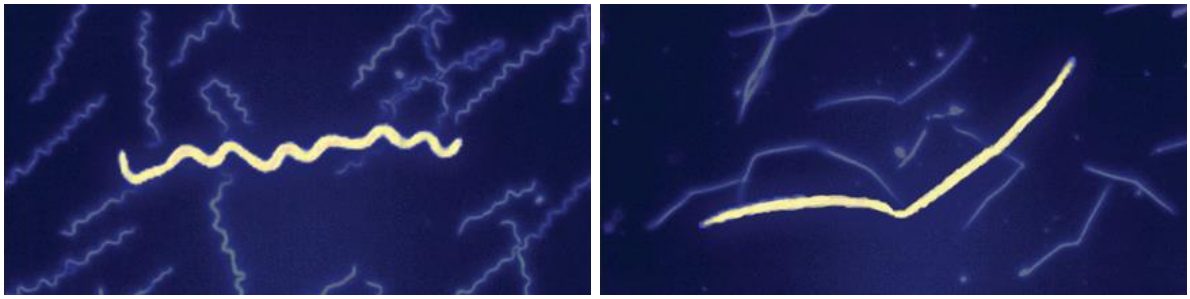

(B)

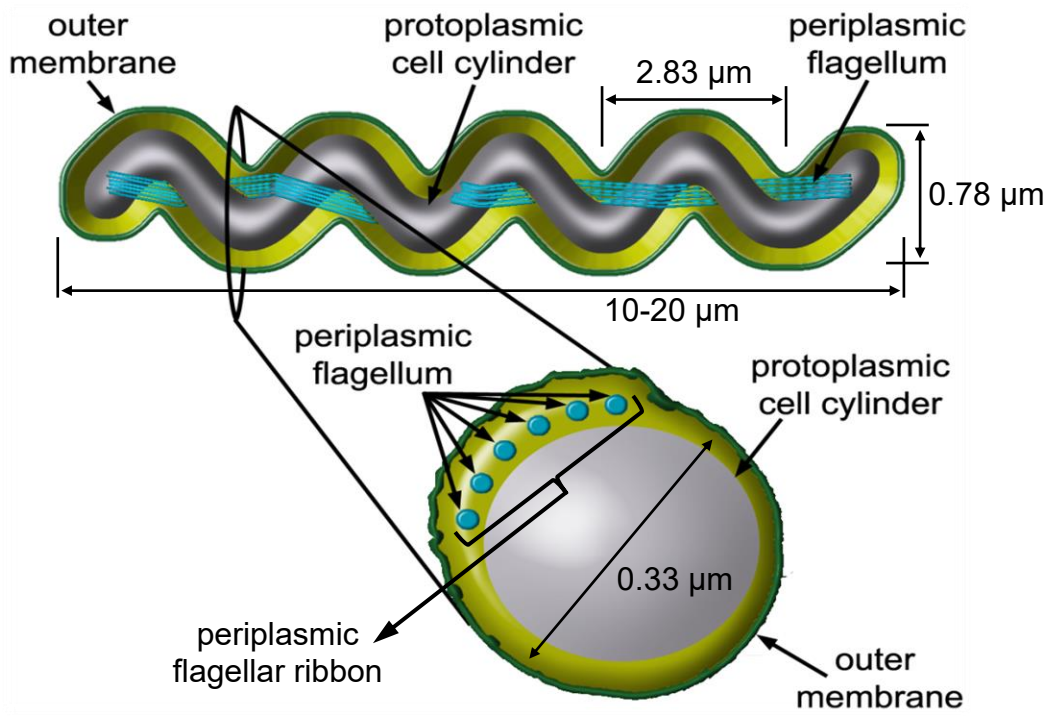

Figure 1.7. Dark-field microscopic image, and schematic diagram of *B. burgdorferi*. (A) Wild-type *B. burgdorferi* possesses a distinctive flat-wave morphology (left), while *B. burgdorferi* Δ*flaB* mutant cell form a straight rod shape (right). One enlarged cell from microscopic field is shown in yellow. **(B)** Longitudinal diagram (top) and cross-section diagram (bottom) of *B. burgdorferi*. Note that periplasmic flagella overlap in the cell center, and form a tightly packed ribbon that causes the outer membrane to bulge.

cell densities of about 10^8/ml (141-143).

Although, *B. burgdorferi* possesses a double membrane similar to other Gram-negative bacteria, the LPS and phosphatidylethanolamine, which typically are found in Gram-negative bacteria, are absent in this organism (145, 146). Instead, *B. burgdorferi* possesses an extraordinary abundance of lipoproteins and glycolipids on its membrane (145, 147-149). In addition, the outer membrane contains a relatively low density of transmembrane proteins (150).

Genome of *B. burgdorferi*. The genome of *B. burgdorferi* sensu stricto strain B31 was completely sequenced in 1997 (151), and found to be unique. The B31 genome is composed of a small linear chromosome of 910,725 base pairs (bp) with an average G+C content of 28.6%. In addition to this linear chrosome, *B. burgdorferi* possesses extremely high numbers of endogenous plasmids—12 linear and 9 circular plasmids that total 610 kilobase pairs (kb), which is the largest number known for any bacterium (Fig. 1.8). The linear plasmids (lp) and circular plasmids (cp) are numbered according to their sizes in kb. The isolate B31 contains the following linear plasmids: lp5, lp17, lp21, lp25, four different homologous plasmids of 28 kb (lp28-1, lp28-2, lp28-3, and lp28-4), lp36, lp38, lp54, and lp56; and the following circular plasmids: cp9, cp26, and seven homologous plasmids of 32 kb (cp32-1, cp32-3, cp32-4, cp32-6, cp32-7, cp32-8, and cp32-9) (151, 152). However, comparisons with other B31 cultures suggest that this isolate may have lost one linear plasmid (lp21) and one or two 32 kb circular plasmids during growth in culture since its original isolation from the midgut of an *Ixodes* tick (151, 153-158). Among these 21 endogenous plasmids, eight plasmids (lp5, lp21, lp28-1, lp28-2, lp28-4, lp56, cp9 and cp32-3) tend to show a plasmid curing event

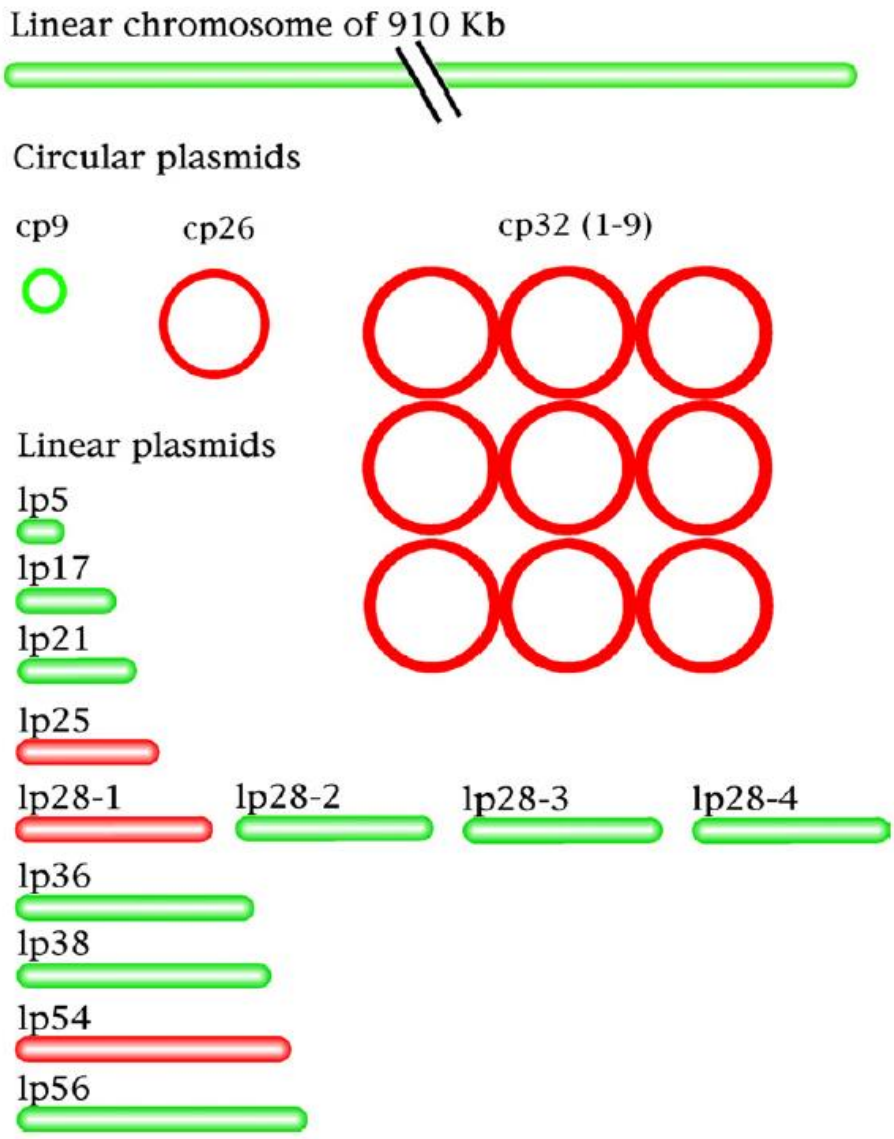

Figure 1.8. The segmented genome of *B. burgdorferi*. Linear plasmids are abbreviated lp and circular plasmids cp, the number represents the approximate size of the plasmid in kilobase pairs. Evidence supports that plasmids shown in red are required for infectivity or persistence in the tick or vertebrate hosts. Sizes are not drawn to scale.

(spontaneously lost) during the *in vitro* propagation (159). Because these plasmids could not maintained in *B. burgdorferi* without *in vivo* environmental pressure, those are believed to be important for infectious life cycle of *B. burgdorferi*. For this reason, investigators use a low-passage strain and verify retention of endogenous plasmids before conducting an *in vivo* experiment with *B. burgdorferi*. The overall G+C content of the plasmids varies from 20.7% to 31.6% (160).

Periplasmic flagella of *B. burgdorferi*. A bacterial flagellum consists of three basic parts; basal body, hook, and filament. Unlike other externally flagellated bacteria—where flagella are in the ambient environment—the flagella of spirochetes are located in the periplasmic space (161). Cryo-electron tomography (cryo-ET) of bacterial flagellar motors suggests that the architectural structure of flagellar motors between external flagella and periplasmic flagella are very similar, consisting of the MS-ring, C-ring, P-ring, stator, hook, export apparatus, and the filaments (compare Fig. 1.9.A, B with 1.9.C, D) (162-164). However, some structures are absent in the periplasmic flagellar motor which observed in the extermal flagellar motor (e.g., L-ring). On the contrary, the periplasmic flagellar motor possess some features that are absent in all externally flagellated bacterial motors studied to-date. One of them is a structure called the collar (Fig. 1.9.D) (162, 164). The collar structure is a spirochete-specific novel component, located in the periplasm, that is linked to the major components of the flagella (162-164).

The intact flagellar motor of *B. burgdorferi* consists of the C-ring, the MS-ring, the rod, the export apparatus, and the stator (Fig. 1.9.D). The C-ring of *B. burgdorferi* is approximate 57 nm in diameter composed of multiple copies of proteins FliG, FliM, and

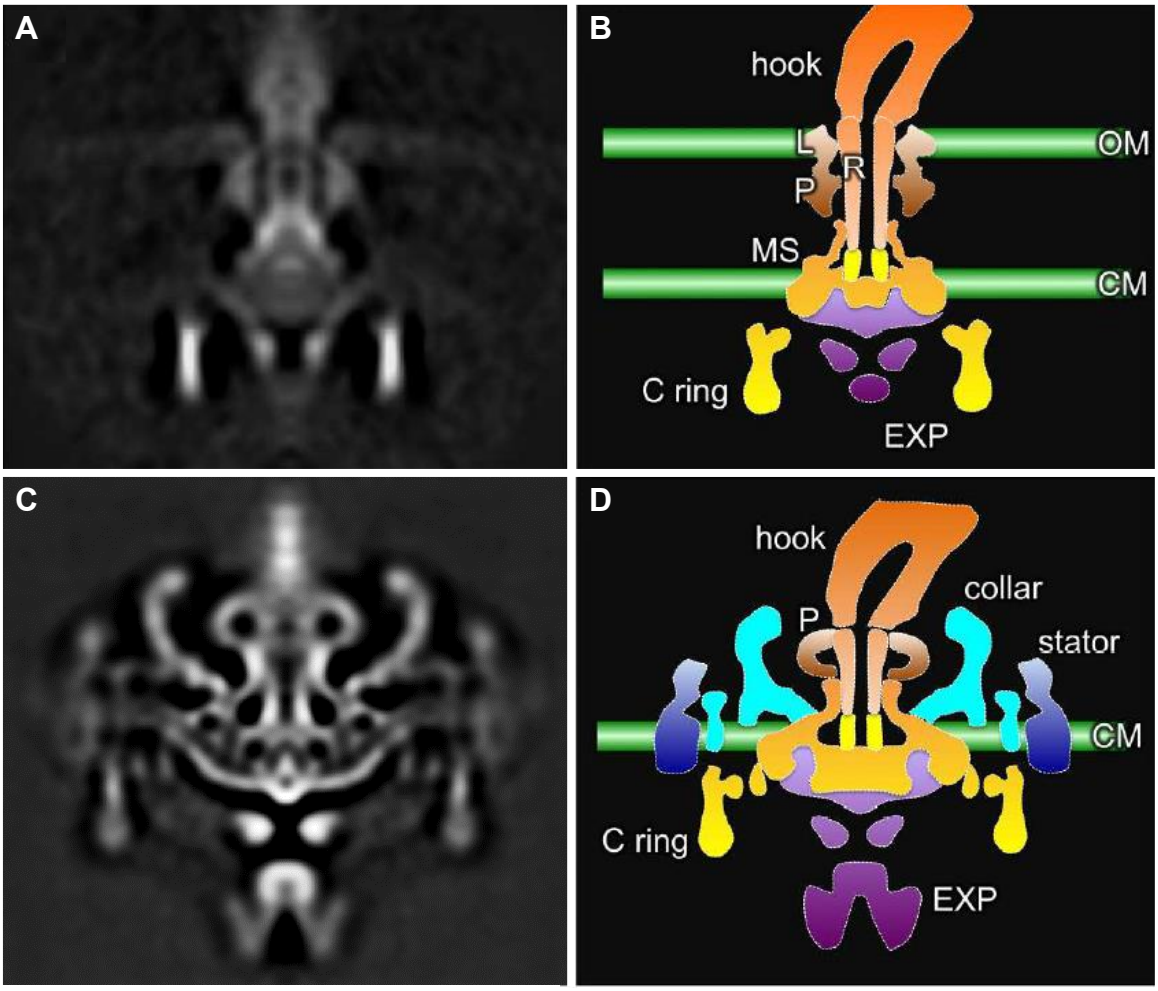

Figure 1.9. Comparative analysis of the intact motor between external flagella and periplasmic flagella. (A) *In situ Salmonella enterica* motor structure reconstructed by cryo-ET. **(B)** A cartoon model of *S. enterica* flagellar motor. **(C)** Intact motor structure of *B. burgdorferi*. The basal body portion is outlined in the intact motor. **(D)** A cartoon model of *B. burgdorferi* flagellar motor. OM, outermembrane; CM, cytoplasmic membrane; L, L-ring; R, rod; P, P-ring; MS, MS-ring; EXP. export apparatus.

FliN. The C-ring or switch complex is important for switching motor rotation from clockwise (CW) to counter-clockwise (CCW) or vice versa. Motor switching occurs when chemotaxis response regulator CheY binds to FliM and FliN (below). The MS-ring is composed of FliF. The MS-ring acts as a platform for assembly of the C-ring, the stator, and the flagellum-specific type III secretion apparatus (Fig. 1.10, 1st panel). The rod is a multiprotein complex that assembles in the order FliE-FlgB-FlgC-FlhO-FlhG (Fig. 1.10, 2nd and 3rd panels) (163). This flagellar rod functions as an export channel of hook and flagellin proteins, and drive shaft. The stator is composed of the MotA and MotB proteins, and generated flagellar mechanical movement by proton gradients across the membrane. *B. burgdorferi* contains 16 stator units around the C-ring rotor. The cytoplasmic domain of the stator is adjactent to the C-terminal domain of the FliG switch protein. This stator-rotor interaction induces a conformational change of FliG, which is likely to be a fundamental mechanism for flagellar rotation (163). FliL is localized between the stator and the rotor, which is partially involved in the proper orientation of periplasmic flagella in *B. burgdorferi* (165).

The flagellar hook of *B. burgdorferi* is 61 nm long hollow tube structure consisting of FlgE polymer (approximately 133 units) (166). The hook serves as a universial joint connecting the flagellar filament to the basal body (167), however, the FlgE subunits in *B. burgdorferi* are covalently cross-linked to form a stable high-molecular weight complex (over 250 kDa; FlgE monomer ~50 kDa). This covalent cross-linked FlgE hook in spirochetes may be important for providing structural strength during rotation within the periplasm (168). Hook assembly is mediated by the hook-cap FlgD (Fig. 1.10, 3rd and 4th panels) (163).

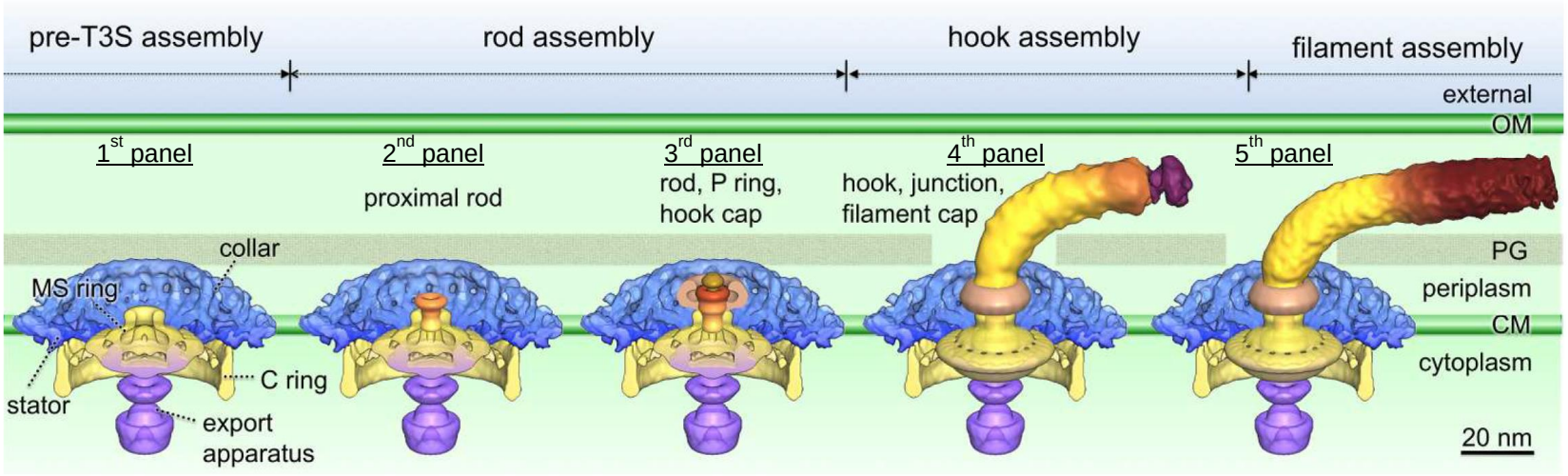

Figure 1.10. A model of flagellar assembly in *B. burgdorferi*. In the pre-type III secretion (T3S) assembly state, many flagellar components assemble, including the MS-ring, the C-ring, the stators, the export apparatus, and the collar. The secretion channel in the MS-ring is closed (first panel). In the presence of FliE and FlgB, rod substrates can be secreted but are unable to form a stable structure until all of the proximal rod substrates (FliE, FlgB, FlgC, and FlhO) are present (second panel). The distal rod protein FlgG adds onto the proximal rod and polymerizes until it reaches a determined length (third panel). A hook cap composed of FlgD forms at the distal end of the rod (third panel) and promotes hook assembly (forth panel). Assembly of the filament (FlaA and FlaB) is promoted by the filament cap (FliD) (fifth panel). OM, outer membrane; PG, peptidoglycan layer; CM, cytoplasmic membrane.

The flagellar filaments are assembled on top of the hook and are composed of a major filament protein FlaB (41 kDa) and a minor filament protein FlaA (38 kDa) (169-171). Filament assembly is mediated by the filament-cap protein FliD (Fig. 1.10, 4th and 5th panels) (163). FlaB monomers are secreted into the periplasmic space by the flagellar-specific type III secretion pathway, and form the flagellar filament core. The periplasmic flagella have a major role in not only motility, but also in morphology of *B. burgdorferi*. Previous studies revealed that the major periplasmic flagellin, encoded by *flaB*, is essential for the motility and wave-like morphology of the cells. Without the periplasmic flagella (in a *flaB* mutant), spirochetes show a non-motile, rod-shaped morphology, instead of being a motile and wave-like shaped as the wild-type (Fig. 1.7.A. right) (143, 172). In contrast to FlaB, FlaA excretes using the Sec-mediated pathway. FlaA forms the sheath surrounding the FlaB core near the hook (171). The role of FlaA is unknown, but recent unpublished data with a Δ*flaA* mutant indicates that the mutant displays reduced motility compared to the wild-type cells (Motaleb *et al*., unpublished).

In other bacteria, such as *E. coli* or *Salmonella*, the motility and chemotaxis genes are tightly regulated by a transcriptional hierarchy (regulatory cascade class I, II, and III) (173). In contrast, *B. burgdorferi* does not employ a transcription cascade to regulate its motility and chemotaxis genes. It is noteworthy to mention that all the motility and chemotaxis genes of *B. burgdorferi* identified thus far fall under the regulation of the housekeeping sigma factor (σ^{70}) (138). However, our understanding of the regulation of motility and chemotaxis gene expression in *B. burgdorferi* is still very limited.

Recent studies indicated that the borrelial carbon storage regulator A (CsrA) is a

regulator of transcriptional control of the major flagellin *flaB* gene expression in *B. burgdorferi* (174). The two-component regulatory system called HK2/Rrp2 and its downstream transcriptional factors RpoN and RpoS (the Rrp2-RpoN-RpoS pathway) are involved in motility and chemotaxis gene expression in *B. burgdorferi* (175-179). The second messenger, 3', 5'-cyclic-diguanosine monophosphate (c-di-GMP), also controls motility and chemotaxis (180-183). Translational control of motility gene expression appears to be important, with CsrA and c-di-GMP emerging as major regulator of motility and chemotaxis. However, many questions, such as what is the interplay between the identified regulatory elements in modulating gene expression and how do environmental signals play a role in differential gene expression within the different hosts, remain unanswered.

Motility and chemotaxis of *B. burgdorferi*. Chemotaxis and motility genes comprise approximately 5-6% of the genome of *B. burgdorferi*, suggesting the importance of these functions in its life cycle (138, 151). Indeed, motility and chemotaxis are found to be esential for host tissue colonization or disease production by many bacteria, including the spirochetes (138, 143, 184-194). While motility and chemotaxis has been extensively studied in other bacteria such as *E. coli* (195-197), the chemotaxis system of *B. burgdorferi* and the motility, which is generated by rotation of the periplasmic flagella are poorly understood. *B. burgdorferi* contains 7–11 periplasmic flagella inserted at each pole of the cell, and those periplasmic flagella form a tight packed ribbon that causes the outer membrane to bulge (Fig. 1.7.B). Periplasmic flagellar filaments wrap around the cell cylinder as they extend toward the other pole of the cell (137, 138, 198). *B. burgdorferi* has four different motility modes based on the

direction of flagellar rotation: two translational modes and two non-translational modes (Fig. 1.11). The periplasmic flagella of the two ribbons rotate asymmetrically during translational mode. In this mode, the periplasmic flagella of the anterior ribbon rotate counter-clockwise (CCW), and those of the posterior ribbon rotate clockwise (CW) (Fig. 1.11.A, top). Reversals occur when the periplasmic flagella of both ribbons change the direction of rotation (Fig. 1.11.A, bottom). In contrast, both periplasmic flagella ribbons rotate in the same direction (both rotate either CW or CCW) in the non-translational modes (Fig. 1.11.B). This asymmetric mode of motility is unique to the spirochetes (138, 169). When the flagellar motors are engaged at each end of the bacteria, they impart a wave-like morphology and an unusual “corkscrew-like” locomotion. This unusual motility pattern is believed to be important for efficient motility within the dense tissues through which these spirochetes preferentially disseminate in both vertebrate and arthropod hosts (186). Interestingly, swimming speed of *B. burgdorferi* increases substantially as the concentration of viscous material such as methylcellulose or hyaluronate is increased in the *in vitro* viscoelastic medium (199). The increasing swimming speed in a higher viscosity environment suggests that *B. burgdorferi* motility may be optimized for migration through host tissues.

Chemotaxis allows bacteria to follow gradients of nutrients and other environmental stimuli. The components of the chemotaxis signal transduction systems that mediate these responses are highly conserved among prokaryotes. The best-studied system is that found in *E. coli* (200) (Fig. 1.12). In this model bacterium, membrane-spanning methyl-accepting chemotaxis protein receptors (MCPs) are coupled to a histidine kinase (CheA) and a linker protein CheW. The catalytic activity of

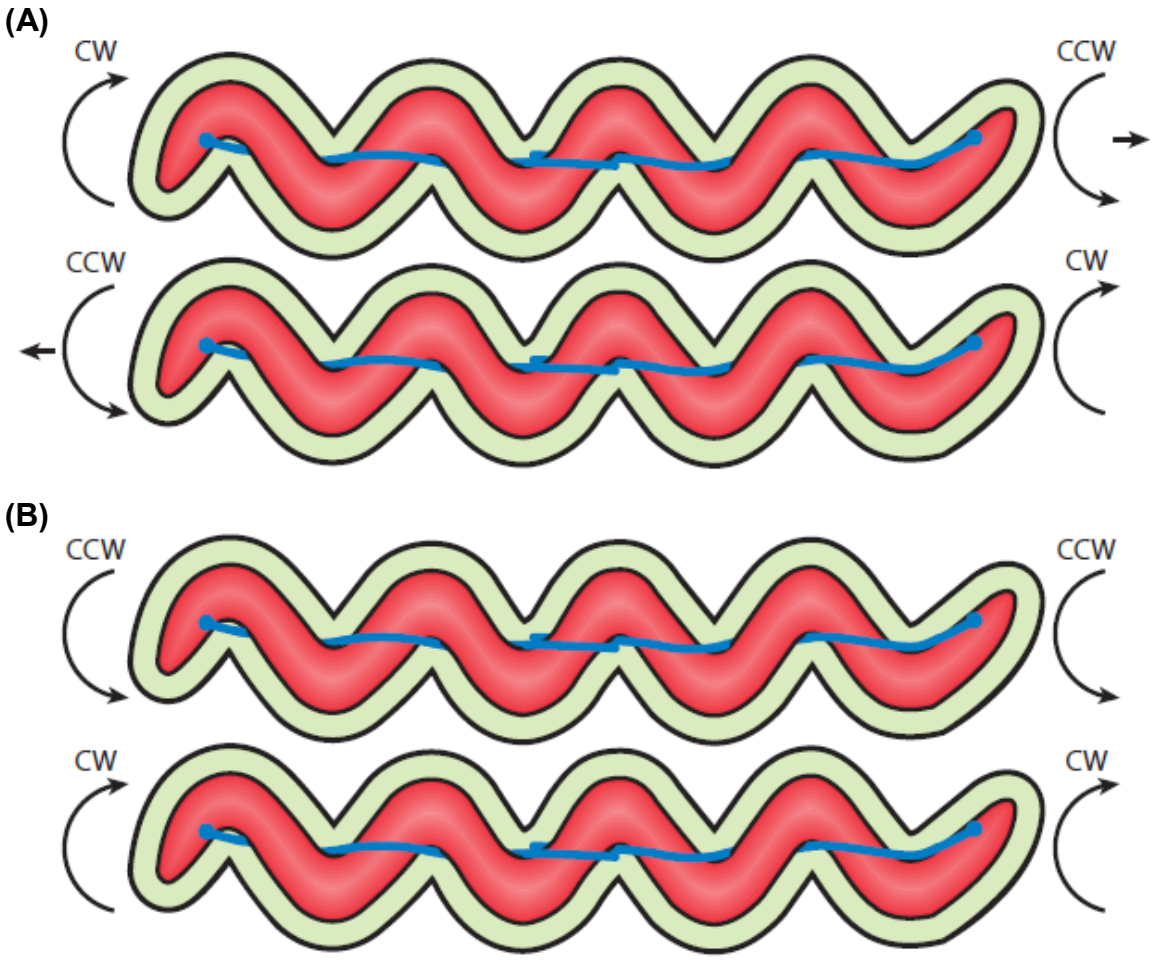

Figure 1.11. Swimming cells of *B. burgdorferi* as a function of the direction in which the periplasmic flagella rotate. Straight arrows at cell ends indicate direction of swimming. Curved arrows indicate the direction in which the periplasmic flagella rotate. For simplification, only one periplasmic flagella is shown attached at each end of protoplasmic cell cylinder. Panel **(A)** shows translational forms, and panel **(B)** shows non-translational forms. CW, clockwise; CCW, counter-clockwise.

Figure 1.12. The *Escherichia coli* chemotaxis pathway. (A) Changes in chemoeffector levels are detected by transmembrane chemoreceptors. These signal through CheW to the chemotaxis histidine protein kinase, CheA. In response to decreased attractant concentration, the chemoreceptors activate CheA autophosphorylation. Phosphorylated CheA (CheA-P) phosphorylates either of its cognate response regulators, CheB and CheY. CheY-P binds to the flagellar motor and promotes a switch in the direction of rotation from counter-clockwise to clockwise. CheB-P is a methylesterase that mediates adaptation in conjunction with the chemotaxis methyltransferase, CheR. CheZ is a specific phosphatase that dephosphorylates CheY-P, allowing rapid signal termination. **(B)** Switching of the bidirectional *Escherichia coli* flagellar motor. The counter-clockwise and clockwise conformations of the motor exist in equilibrium. In the absence of CheY-P, counter-clockwise rotation is strongly favoured. CheY-P binding to FliM and FliN (components of the switch complex) shifts the equilibrium in favour of clockwise rotation. There are believed to be ~34 binding sites for CheY-P, and as more of these sites become occupied, the probability of clockwise rotation increases cooperatively.

(A)

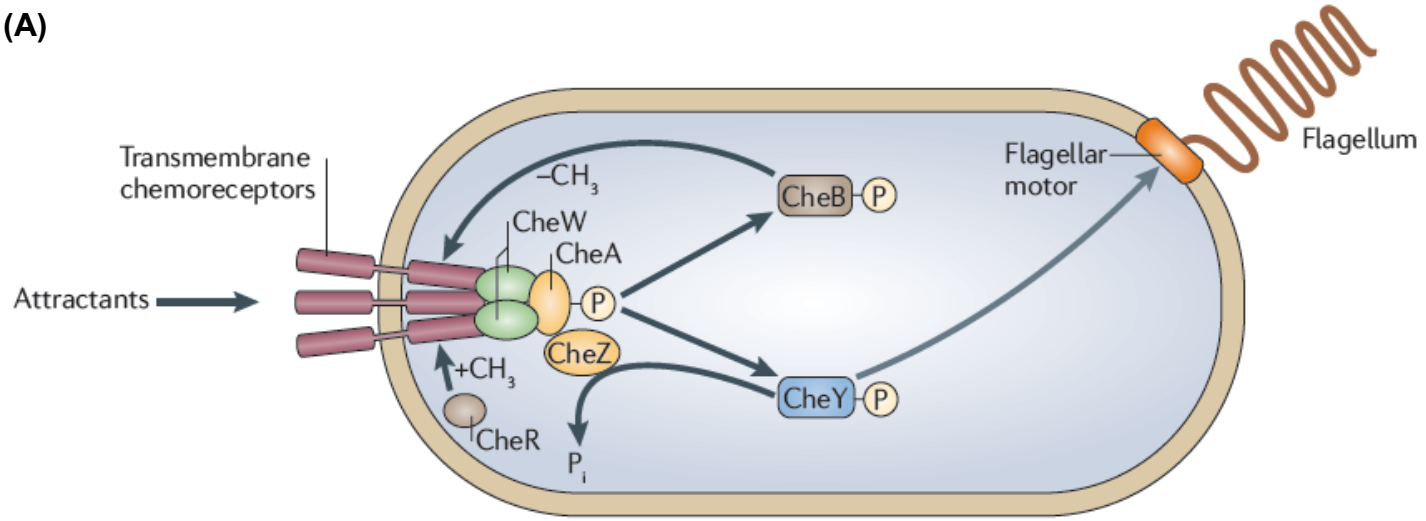
Transmembrane
chemoreceptors
Attractants
–CH3
CheW
CheA
P
CheZ
+CH3
CheR
Pi
CheB
P
CheY
P
Flagellar
motor
Flagellum

(B)

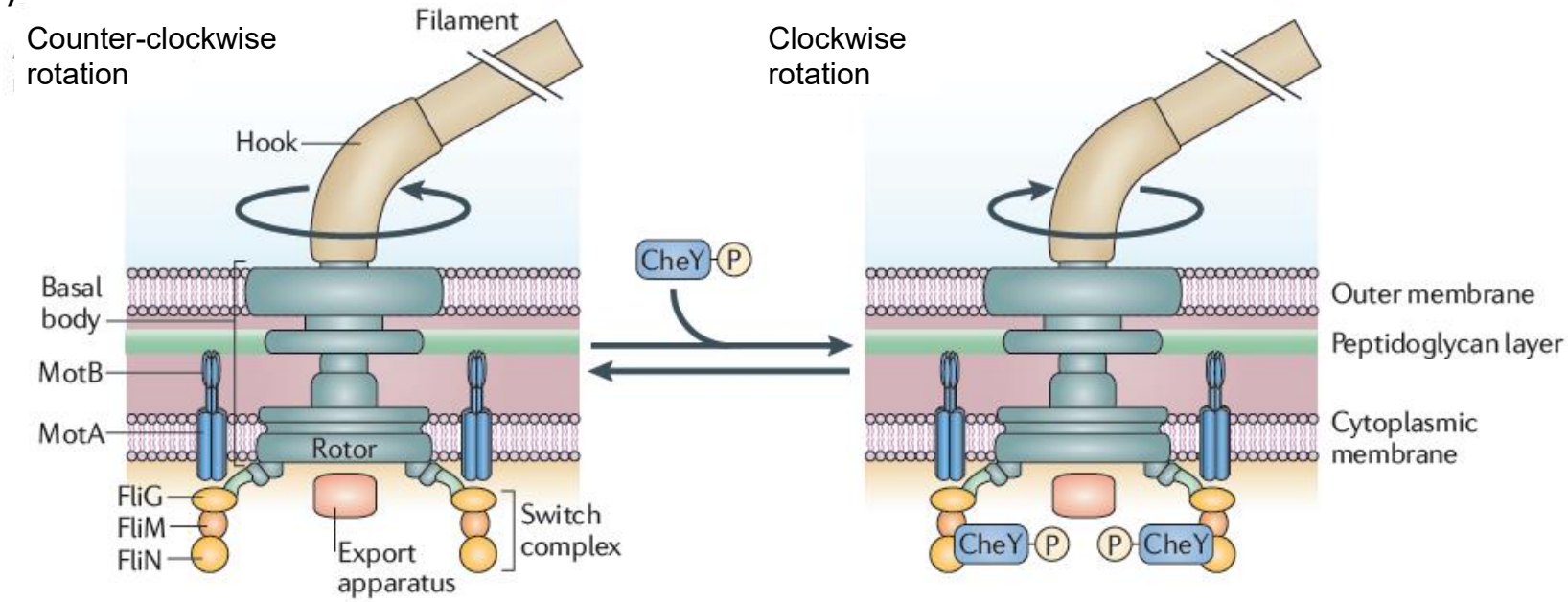
Counter-clockwise
rotation
Filament
Hook
Basal
body
MotB
MotA
Rotor
FliG
FliM
FliN
Export
apparatus
Switch
complex
CheY
P
Clockwise
rotation
Outer membrane
Peptidoglycan layer
Cytoplasmic
membrane
CheY
P
P
CheY

CheA is regulated by occupancy of these MCPs with a ligand (e.g., an attractant or repellent). CheA uses ATP to autophosphorylate, and the phosphate group is then transferred to the response regulator CheY. The phosphorylated CheY (CheY-P) binds to the flagella motor switch protein FliM and FliN (201, 202). This binding results in the change of direction of the flagella from the default counter-clockwise (running motility) to clockwise rotation, resulting in tumbling motility (no net movement of bacteria). Binding of attractant to the MCPs decreases the kinase activity of CheA, resulting in reduced CheY-P and tumbling frequency. The concentration of CheY-P determines whether a cell runs (requiring high CheY-P) or tumbles (low CheY-P). The chemotaxis system adapts to persistent modification via receptor methylation by methyltransferase CheR (positive stimuli) and demethylation by methylesterase CheB (negative stimuli). CheR and CheB are the only known chemoreceptor modification enzymes in this model (203). Even though the components of the chemotaxis signal transduction system are highly conserved among prokaryotes, the chemotaxis pathway in *B. burgdorferi* differs from other well-studied bacterial models and is more complicated due to the presence of multiple copies of chemotaxis genes, including six *mcp*, two *cheA*, three *cheY*, two *cheB*, two *cheR*, and three *cheW* (Fig. 1.13). It has only one CheY-P phosphatase (CheX) which is commonly found in bacteria. *B. burgdorferi* also has a putative gene encoding CheD, which is not found in *E. coli* (151). CheD is relatively well-characterized in *Bacillus subtilis* and *Thermotoga maritima*, where it plays an important role in chemotaxis by modification of MCPs by deamidation or by enhancing CheC phosphatase activity, thereby regulating the levels of the CheY-P response regulator (204-207). Phosphotransfer analyses revealed that chemotaxis response regulators of

Figure 1.13. Model of the *B. burgdorferi* chemotaxis system. A simplistic chemotaxis signaling pathway of *B. burgdorferi*. The genome of *B. burgdorferi* encodes multiple homologs of several chemotaxis genes (e.g. six *mcp*, two *cheA*, three *cheW*, three *cheY*, two *cheB*, and two *cheR* genes), making it more complex than other bacteria. The role of most borrelial chemotaxis proteins are still unknown. To date, only two studies have shown that chemotaxis—specifically involving the histidine kinase *cheA2* (**box 1**) and chemotaxis response regulator *cheY3* (**box 2**)—are essential for the infectious life cycle of *B. burgdorferi* (189, 209). CheY2 may serve as a regulator for a virulence determinant in *B. burgdorferi* (**box 3**) (Xu *et al*., manuscript in progress). The role of *cheY1* and other putative chemotaxis genes in the infectious life cycle of *B. burgdorferi* has not been studied until now.

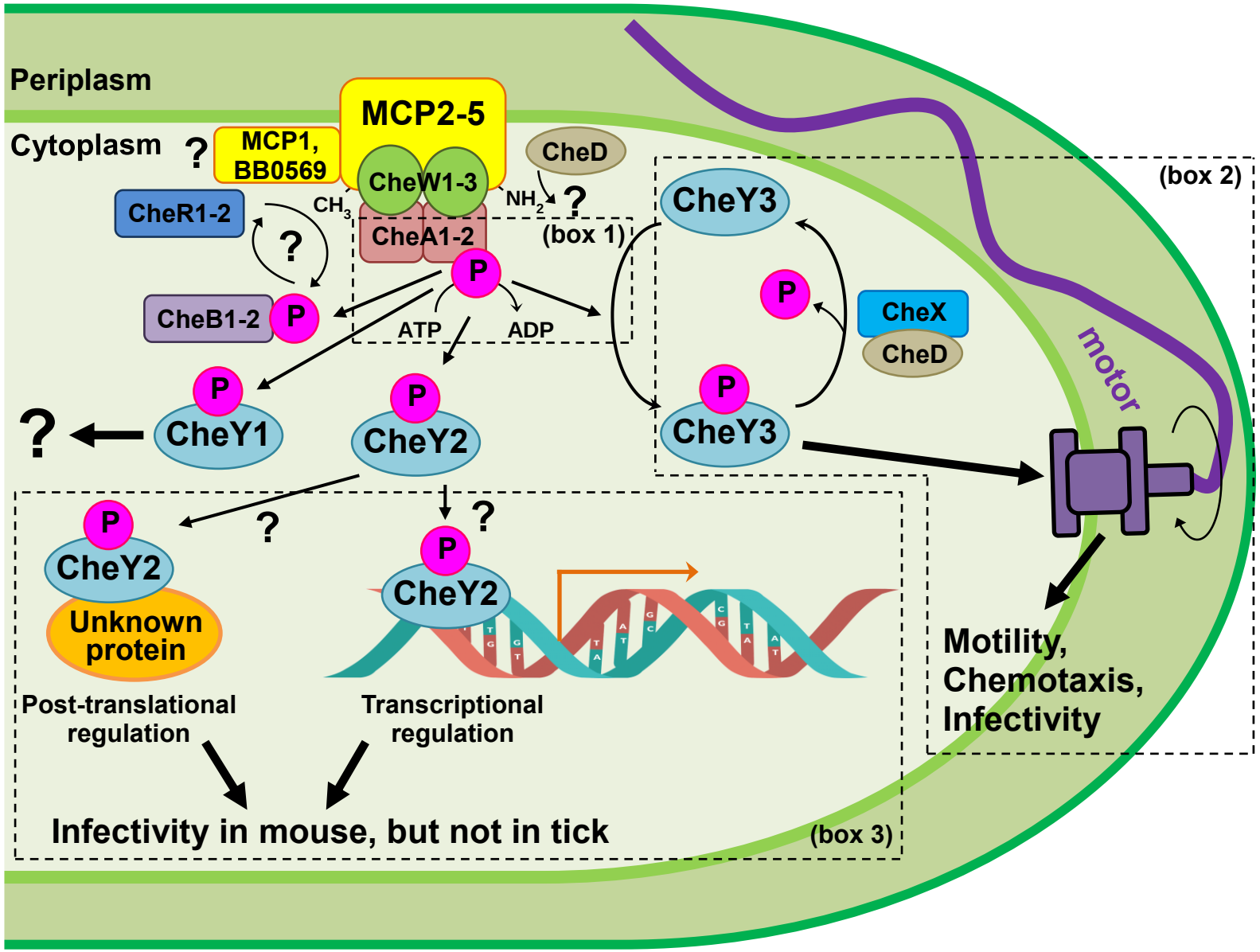
Periplasm
Cytoplasm
MCP2-5
MCP1, BB0569
CheW1-3
CheA1-2
CheD
CheR1-2
CheB1-2
CH3
NH2
ATP
ADP
(box 1)
(box 2)
CheY3
CheX
CheD
motor
CheY1
CheY2
Unknown protein
Post-translational regulation
Transcriptional regulation
Motility, Chemotaxis, Infectivity
Infectivity in mouse, but not in tick
(box 3)

B. burgdorferi are phosphorylated by both the histidine kinases, CheA1 and CheA2 (208). However, only *cheY3* was found to be essential for motility and chemotaxis *in vitro* (208). Recently, *cheY3*-mediated chemotaxis is also found to be crucial for motility *in vivo*, dissemination, and viability of *B. burgdorferi* in mice and ticks (Fig. 1.13, dotted lined box 2) (209). Interestingly, the CheY proteins do not functionally overlap with each other (208). The *cheY2* mutant cell was not defective in motility or chemotaxis *in vitro*, survived normally in ticks, and those mutant-infected ticks transmitted the spirochetes into mice (208, Xu *et al*., manuscript in progress). However, the *cheY2* mutant spirochetes are considerably attenuated in murine infection via both needle injection and tick transmission (Xu *et al*., manuscript in progress). It is unclear as to why the *cheY2* mutant spirochetes show attenuation in mouse infection, but not in the tick hosts. We assume that CheY2 may function distinctively from most other typical chemotaxis signaling systems such as either binding to an operon promoter or a protein to modulate the expression or activity of some virulence determinants in *B. burgdorferi* (Fig. 1.13, dotted lined box 3). Intensive studies are required to identify the role of *B. burgdorferi* putative chemotaxis proteins.

STATEMENT OF THE PROBLEM, GOAL,

SPECIFIC OBJECTIVES, AND HYPOTHESES

This dissertation research mainly focused on motility and chemotaxis of *B. burgdorferi*, and the research goal was divided into two sections: **1)** Determining the role of *B. burgdorferi* CheD in motility, chemotaxis, and mouse/tick-mouse models of *B.*

burgdorferi; and **2)** Discovery and characterization of the novel spirochete flagellar proteins in *B. burgdorferi*.

Motility and chemotaxis are reported to be crucial for the infectious life cycle of *B. burgdorferi* (143, 186, 188, 190, 191, 194). After transmission from tick to mammalian host, *B. burgdorferi* must quickly perceive its new local environment and make the appropriate adaptations, rapidly disseminating through skin tissues to evade the cellular immune response and migrating to appropriate target tissues that allow for persistence and evasion of the expanding adaptive immune response. After residing in this mammalian host for weeks to years, *B. burgdorferi* must then be able to detect that a new tick vector has attached to host skin, and then rapidly migrate to the bite site, and enter the vector via the blood meal before the tick feeds to repletion and detaches. Until now, only two chemotaxis genes [*cheA2* (189), and *cheY3* (209)] have been studied in the *B. burgdorferi* infectious life cycle. A rigorous study is needed in order to understand the function of other putative chemotaxis genes.

Chapter 2 of this dissertation focuses on the putative genes encoding CheD. We hypothesize that *cheD* plays an important role in *B. burgdorferi* motility, chemotaxis, and in the mouse-tick-mouse life cycle of the spirochete. In chapter 2, we have characterized the *cheD* mutant in detail. Moreover, we have shown the role of *cheD* in *B. burgdorferi*. This study is the first investigation of CheD in the disease process. Our studies provide more information in understanding the chemotaxis signaling pathway of the spirochete. Dissecting the roles of *cheD* may provide clues as to how the spirochete achieves asymmetric modes of motility.

Motility and chemotaxis are intimately interlaced as the chemotaxis response regulator, CheY, binds to the periplasmic flagellar switch proteins to control motor rotation. In addition to chemotaxis, this dissertation research project also focuses on demonstrating the roles of unique periplasmic flagellar proteins in motility in *B. burgdorferi*. Unlike externally flagellated bacteria, *B. burgdorferi* possesses periplasmic flagella that contain a novel structural component called the collar (162, 164). Recent cryo-ET analyses revealed that the collar structure is conserved among the spirochetes but is absent from all other flagellated bacteria (162-164). However, nothing is known about the proteins encoding the collar or their function in any spirochete. The collar proteins are hypothesized to play an important role in motility, flagellar assembly as well as for providing proper rigidity and flexibility of flagella within the periplasmic space during rotation.

Chapter 3 focuses on the *B. burgdorferi* gene *flbB*, which we identified to be involved in collar assembly through an exhaustive search. This chapter describes the role of *flbB* in motility, cell morphology, periplasmic flagellar orientation, and assembly of other motor structures. Moreover, using various comprehensive approaches, several additional proteins are identified. These proteins are potential candidates for the spirochete-specific collar structure. Our studies clearly indicate that the *B. burgdorferi* genome possesses additional genes encoding the periplasmic flagella. However, these newly identified genes were annotated as hypothetical or “function unknown” in the *B. burgdorferi* genome (151).

CHAPTER TWO: *BORRELIA BURGDORFERI* CHED PROMOTES VARIOUS FUNCTIONS IN CHEMOTAXIS AND THE PATHOGENIC LIFE CYCLE OF THE SPIROCHETE

ABSTRACT

Borrelia burgdorferi possesses a sophisticated chemotaxis signaling system, however, the role of the majority of the chemotaxis proteins in the infectious life cycle has not yet been demonstrated. Specifically, the role of CheD during host colonization has not been demonstrated in any bacterium. Here, we systematically characterized the *B. burgdorferi* CheD homolog using genetics, biochemical, and mouse-tick-mouse infection cycle studies. *Bacillus subtilis* CheD plays an important role in chemotaxis by deamidation of methyl-accepting chemotaxis protein receptors (MCPs) and by increasing the receptor-kinase activity or enhancing CheC phosphatase activity, thereby regulating the levels of CheY response regulator. Our biochemical analysis indicates that *B. burgdorferi* CheD significantly enhances CheX phosphatase activity by specifically interacting with the phosphatase. Moreover, CheD specifically binds two of the six MCPs, indicating that CheD may also modulate the receptor proteins. Although the motility of the *cheD* mutant cells was indistinguishable from the wild-type cells, the mutant did exhibit reduced chemotaxis. Importantly, the mutant showed significantly reduced infectivity in C3H/HeN mice via needle inoculation. Mouse-tick-mouse infection assays indicate that CheD is dispensable for acquisition or transmission of spirochetes, however, the viability of *cheD* mutants in ticks is marginally reduced compared to the wild-type or complemented *cheD* spirochetes. These data suggest that CheD plays an

important role in chemotaxis and pathogenesis of *B. burgdorferi.* We propose potential connections between CheD, CheX, and MCPs, and discuss how these interactions play critical roles during the infectious life cycle of the spirochete.

INTRODUCTION

Borrelia burgdorferi, the causative agent of Lyme disease cycles between *Ixodes* ticks and a mammalian host. Motility and chemotaxis are known to be required for host tissue colonization or disease production by many bacteria, including the spirochetes; however, these processes have not been rigorously characterized in any spirochete (138, 143, 184-194). *B. burgdorferi* is a spirochetal motile bacterium that contains a sophisticated and complicated chemotaxis signal transduction system. This spirochete is a long (10-20 μm) and thin (0.33 μm) organism with flat-wave morphology, and its motility is provided by flagella that are located within the periplasm. There are 7-11 periplasmic flagella inserted at each pole of the cell forming a ribbon-like structure that wraps around the cell cylinder as they extend toward the other pole of the cell (138, 188, 190). When the periplasmic flagellar motors rotate asymmetrically [i.e., flagella at one pole rotate in clockwise (CW) and the flagella in other pole rotate in counter-clockwise (CCW)] the spirochete runs. When the flagellar motors at both poles of the cell rotate in the same direction (both in CW or CCW), *B. burgdorferi* cells flex with no net translocation (210). This manner of swimming also produces an unusual "corkscrew-like" locomotion. This distinctive motility pattern is believed to be important for efficient migration within the dense tissues through which these spirochetes preferentially disseminate in both vertebrate and arthropod hosts (138, 211). Interestingly, where most externally flagellated bacteria either slow down or stop within viscous material (212, 213), the velocities of spirochetes actually increase within viscous media (214-216), thus empowering the spirochetes to penetrate into tissues that other bacteria fail to invade.

Chemotaxis is also believed to be very important for the complex vector-host life cycle utilized by *B. burgdorferi*. After transmission from tick to mammalian host, *B. burgdorferi* must quickly perceive its new local environment and make the appropriate adaptations, rapidly disseminating through skin tissues to evade the cellular immune response and migrating to appropriate target tissues, which allows for evasion of the expanding adaptive immune response and survival. After residing in this mammalian host for weeks to years, *B. burgdorferi* must then be able to detect that a new tick vector has attached to host skin, and then rapidly migrate to the bite site and enter the vector (54).

Chemotaxis allows bacteria to follow gradients of nutrients and other environmental stimuli by governing their motility. The components of the chemotaxis signal transduction systems that mediate these responses are highly conserved among prokaryotes. The best studied system is found in *Escherichia coli* (or *Salmonella enterica* serovar Typhimurium) (203, 217, 218). In this model organism, membrane-spanning methyl-accepting chemotaxis protein receptors (MCPs) detect environmental signals. These MCP proteins are coupled to a histidine kinase (CheA) and a linker protein CheW. The catalytic activity of CheA is regulated by occupancy of these MCPs with a ligand (e.g. an attractant or repellent). CheA uses ATP to autophosphorylate, and the phosphate group is then transferred to the response regulator CheY. The phosphorylated CheY (CheY-P) then binds to the flagella motor switch proteins FliM and FliN (201). This binding results in the change of direction of the flagella from the default CCW (running motility) to CW rotation, resulting in tumbling motility. Binding of attractant to the MCPs decreases the kinase activity of CheA, resulting in reduced

CheY-P as well as tumbling frequency. The concentration of CheY-P determines whether a cell runs (requires low CheY-P) or tumbles (high CheY-P). CheY-P is able to be autodephosphorylate, however, the phosphatase CheZ efficiently dephosphorylate the levels of CheY-P in *E. coli* (219). This phosphorylation-dephosphorylation is crucial for the bacterial cells to respond appropriately to the environmental stimuli. The chemotaxis system adapts to persistent modification via receptor methylation by methyltransferase CheR (positive stimuli) and demethylation by methylesterase CheB (negative stimuli). CheR and CheB are the only known chemoreceptor modification enzymes in this *E. coli* model (203).

Even though the components of the chemotaxis signal transduction system are conserved among prokaryotes, the chemotaxis pathway in *B. burgdorferi* differs from the other well-studied bacterial models and is much more complicated due to the presence of multiple copies of chemotaxis genes, including six *mcp*, two *cheA*, three *cheY*, two *cheB*, two *cheR*, and three *cheW* genes—which may contribute to the asymmetric motility of the spirochete. Moreover, *B. burgdorferi* has a putative gene encoding CheD, which is not found in *E. coli* (138). CheD is relatively well characterized in *Bacillus subtilis* and *Thermotoga maritima* (204-207). In *B. subtilis*, CheD plays an important role in motility and chemotaxis. A *cheD* mutant displays a distinctive motility pattern: wild-type cells exhibit running and tumbling motility, whereas the Δ*cheD* constantly tumbles. At the molecular level, CheD interacts with the receptor MCPs. MCP proteins contain the well-conserved substrate-binding site of CheD, A/S-X-X-Q/E-Q/E-X-X-A/S (A, alanine; S, serine; Q, glutamine; E, glutamate; X, any amino acid). CheD modifies the MCPs by deamidating glutamine to glutamate residues. The

deamidation by CheD is required for the *B. subtilis* chemoreceptors to effectively transduce signals to the CheA kinase (206, 220). Additionally, CheD interacts with the phosphatase CheC, enhancing its enzymatic activity and fine-tuning the intracellular concentration of CheY-P (204, 206) *B. burgdorferi* possesses a phosphatase, CheX, that has been previously reported to possess CheY-P dephosphorylating activity, and that the *cheX* mutant cells constantly flexes (221-223). It is noteworthy to mention that the “flex” of *B. burgdorferi* is considered to be equivalent to the tumbling phenotype seen in *E. coli*. Moreover, the MCPs of *B. burgdorferi* contain the well-conserved potential substrate-binding sites of CheD (183, 206, 220). These observations lead us to hypothesize that CheD in *B. burgdorferi* plays a role similar to its counterpart in *B. subtilis*. Most importantly, even though the role of CheD in motility and chemotaxis has been demonstrated in other bacteria, its role in pathogenesis has not been reported in any organism. To-date, only one chemotaxis (*cheA2*) gene has been investigated in the *B. burgdorferi* infectious life cycle (i.e., tick to mouse transmission) (189). A rigorous study is therefore warranted in order to understand the function of other putative chemotaxis genes.

In this study, we determine the requirement of *cheD* in motility and chemotaxis in *B. burgdorferi* by inactivating the *cheD* gene as well as by demonstrating its enzymatic role in chemotaxis signaling system. Moreover, we define the role of *cheD* in the disease process (mouse-tick-mouse infection cycles) for the first time. We show that CheD is important in not only chemotaxis as it enhances the CheX phosphatase activity, but also is essential for the infectious life cycle of *B. burgdorferi*.

MATERIALS AND METHODS

Ethics statement. East Carolina University is accredited by the International Association for Assessment and Accreditation of Laboratory Animal Care. Protocols for tick and animal experimentations were approved by the East Carolina University animal care and use committee.

Bacterial strains, plasmids, and growth conditions. The bacterial strains and plasmids used in this study are listed in Table 2.1. Low-passage, virulent *B. burgdorferi* strain B31-A3 was used as a wild-type clone throughout the study (224, 225). The genome of the virulent B31 strain was found to contain a total of 21 plasmids, with 12 linear and 9 circular plasmids, in addition to its 960-kb linear chromosome (151, 152). Clone B31-A3 lacks circular plasmid 9 (cp9) but remains infectious in tick-mouse cycle studies (225, 226). Constructions of *cheD* mutants and its complemented strains are described below. *B. burgdorferi* cells were cultured in liquid Barbour-Stoenner-Kelly (BSK-II) medium, and plating BSK was prepared using 0.5% agarose (143, 227, 228). Cells were grown at 35°C in a 2.5% CO_2 humidified incubator as described previously (143, 225, 227). Antibiotics, when required, were included in the *B. burgdorferi* culture medium with the following concentrations: 200 µg/ml kanamycin, 40 µg/ml gentamicin, 100 µg/ml streptomycin. *Escherichia coli* cells were grown at 37°C in Luria-Bertani (LB) broth or LB agar (229). Antibiotics, when required, were included in the *E. coli* culture medium with the following concentrations: 100 µg/ml ampicillin, 35 µg/ml chloramphenicol, 100 µg/ml spectinomycin.

Construction and complementation of the *cheD* mutant. Construction of the *cheD* inactivation plasmids, electroporation, and plating conditions were described

Table 2.1. Bacterial strains and plasmids used in this study

Strains or Plasmids	Relevant characteristics*	Reference or Source
Borrelia burgdorferi		
B. burgdorferi B31-A3	B31 (ATCC 35210), the prototype strain of *B. burgdorferi* sensu stricto, originally isolated from a tick collected on Shelter Island, NY, A low-passage infectious clone	(224, 225)
B. burgdorferi B31-A3 Δ*cheD*	B31-A3 derived, Δ*cheD*, Kan^R	This study
B. burgdorferi B31-A3 $cheD^{com}$	B31-A3 Δ*cheD* derived, integrated P_{cheD}-*cheD* within the intergenic region of *bb0445* and *bb0446*, Kan^R $Gent^R$	This study
B. burgdorferi B31-A3 Δ*cheY3*	B31-A3 derived, Δ*cheY3*, Kan^R	Lab collection (209)
Escherichia coli		
E. coli DH5α	Transformation host for cloning vector, F^- *Φ*80d*lacZ*ΔM15, Δ(*lacZYA-argF*) U169 *recA*1 *endA*1 *hsdR*17(r_k^-,m_k^+) *phoA*, *supE*44 *thi*-1 *gyrA*96 *relA*1	Promega Inc.
E. coli BL21 (DE3)	Host for overexpression, F^- *ompT* $hsdS_B$ (r_B^-,m_B^-) *gal dcm* (DE3)	Promega Inc.
E. coli M15	Host for overexpression, F^- *Φ*80Δ*lac*M15 *thi* lac^- mtl^- $recA^+$, Kan^R	Qiagen Inc.
Plasmids		
pGEM-T Easy	Cloning vector for PCR product, ColE1 ori, Amp^R	Promega Inc.
pXLF14301	Suicide vector, pUC ori, Amp^R	(183, 230, 231)
pASK-IBA7$^+$	Overexpression vector, Strep-tag, ColE1 ori, Amp^R	IBA Inc.

Table 2.1. Bacterial strains and plasmids used in this study (~continue)

Strains or Plasmids	Relevant characteristics*	Reference or Source
Plasmids		
pMAL c2x	Overexpression vector, MBP-tag, pBR322 ori, *Amp^R*	NEB Inc.
pQE30	Overexpression vector, 6xHis-tag, ColE1 ori, *Amp^R*	Qiagen Inc.
Teasy::*cheD*_KO	*cheD-P$_{flgB}$-aph1* in pGEM-T Easy for *cheD* knockout, *Amp^R*	This study
pXLFCheD	*P$_{cheD}$-cheD* in pXLF 14301 for *cheD* complementation, *Amp^R*	This study
IBA7$^+$::CheD	*cheD* orf in pASK-IBA7$^+$ for CheD overexpression, *Amp^R*	This study
c2x::MCP3	*mcp3* cytoplasmic domain sequence in pMAL c2x for MCP3 overexpression, *Amp^R*	This study
c2x::MCP4	*mcp4* cytoplasmic domain sequence in pMAL c2x for MCP4 overexpression, *Amp^R*	This study
c2x::MCP5	*mcp5* cytoplasmic domain sequence in pMAL c2x for MCP5 overexpression, *Amp^R*	This study
pQE30::CheX	*cheX* orf in pQE30 for CheX overexpression, *Amp^R*	Lab collection (222)
pQE30::CheY3	*cheY3* orf in pQE30 for CheY3 overexpression, *Amp^R*	Lab collection (208)
Teasy::*cheD*-RT	*cheD*-RT in pGEM-T Easy for qRT-PCR, *Amp^R*	This study
Teasy::*enolase*-RT	*enolase*-RT in pGEM-T Easy for qRT-PCR, *Amp^R*	Lab collection

**Kan^R*, kanamycin resistance; *Gent^R*, gentamicin resistance; *Amp^R*, ampicillin resistance

previously (143, 172). Briefly, the *cheD* gene (locus number *bb0606*) and flanking DNA was first amplified by PCR from the chromosomal DNA of *B. burgdorferi* strain B31-A3 using primers CheD-KO-F (GGAATCAGGCTTAAATCTTG) and CheD-KO-R (AAGCATGGAAAGTTGAAACC). The PCR product was cloned into plasmid pGEM-T Easy (Promega Inc.). The *cheD* gene was inactivated using a kanamycin resistance cassette (P_{flgB}-*aph1*) (224), which was inserted at the *Hin*dIII sites located within *cheD*. Competent B31-A3 cells were electroporated with *cheD*-P_{flgB}-*aph1* DNA that was linearized by *Not*I restriction digestion to remove the ampicillin restriction marker of the vector, preventing it from being introduced into *B. burgdorferi* (143, 172). The transformants were selected with kanamycin, and the kanamycin-resistant transformants were confirmed by PCR to have the P_{flgB}-*aph1* integrated within the *cheD* (143, 172, 182). Confirmation of the *cheD* gene inactivation was achieved by the lack of *cheD* transcripts in the *cheD* mutant cells (Δ*cheD*) by quantitative reverse transcriptase-PCR (qRT-PCR; see below).

The *cheD* mutant was complemented *in cis* by genomic integration using pXLF14301 suicide vector (183, 230, 231). To complement the mutant, the *cheD* gene and its native promoter (P_{cheD}) DNA sequences were PCR amplified from genomic DNA of *B. burgdorferi* strain B31-A3 using primers CheDcom.-F (AATTAAAATGATTTAACATATTTCCCAATAACATAGATAC) and CheDcom.-R (GCGGCCGCTTAAAAAACCTTTGTTCC), and P_{cheD}-F (ACTAGTATTGGCCATATCCCCATTAAGGC) and P_{cheD}-R (GTATCTATGTTATTGGGAAATATGTTAAATCATTTTAATT), respectively. The amplified DNA fragments were ligated by overlapping PCR, yielding P_{cheD}-*cheD* DNA

fragment, and then cloned into plasmid pGEM-T Easy (Promega Inc.). Finally, P_{cheD}-*cheD* was excised from the pGEM-T Easy using *Spe*I and *Not*I restriction digestions and then cloned into pXLF14301, yielding plasmid pXLFCheD. The plasmid was then electroporated into the Δ*cheD* mutant cells followed by selection with gentamicin and kanamycin. The resistant clones were analyzed by PCR for integration of P_{cheD}-*cheD* within the intergenic region of *bb0445* and *bb0446*. Restoration of *cheD* expression in the complemented *cheD* (*cheD*^{com}) clones was also verified by qRT-PCR (see below). Retention of *B. burgdorferi* endogenous plasmids in wild-type, mutant, and the complemented strains was verified by PCR as described previously (143, 182, 183, 225).

Reverse transcription-polymerase chain reaction (RT-PCR). Exponentially growing *B. burgdorferi* wild-type cells (2 x 10^7 cells/ml) were treated with RNAprotect™ followed by total RNA isolation using the RNeasy mini kit (Qiagen Inc.). Contaminating DNA in the RNA samples was removed by RNase-free Turbo® DNase I (Ambion Inc.) digestion for 3 hr. at 37°C followed by RNeasy mini purification. For RT-PCR, cDNA was prepared from 1 µg RNA using the AffinityScript QPCR cDNA synthesis kit (Agilent Technologies Inc.) according to the manufacturer's protocol. The iCycler detection system (Bio-Rad Inc.) was used to measure *cheD* transcript levels according to the manufacturer's instructions. *B. burgdorferi* enolase was used as a reference gene (171, 181-183). The gene specific primers (5'-3') were RT-enolase-F (TGGAGCGTACAAAGCCAACATT); RT-enolase-R (TGAAAAACCTCTGCTGCCATTC); CheD-qRT-F (CCTGGTGAAGCTTTTGTTTC); and

CheD-qRT-R (TTGATCAGGAGATATGTCAAGATC). The relative level of expression was calculated using the $2^{-\Delta\Delta CT}$ method (181-183, 232, 233).

Recombinant protein expression in *E. coli*. In order to express *B. burgdorferi cheD* in *E. coli*, a DNA fragment harboring the entire *cheD* open reading frame was amplified from chromosomal DNA of B31-A3 using primers R.CheD-F (TTAAATCATTTTAATTTTAA) and R. CheD-R (TTAAAAAACCTTTGTTCCGT), and cloned into the pASK-IBA7$^+$ expression vector (IBA Inc.) to generate the Strep-Tactin tagged CheD (Strep-CheD). *E. coli* BL21 (DE3) harboring the pASK-IBA7$^+$::*cheD* was induced with 200 ng/ml of anhydrotetracycline. Expression and purification of *E. coli* CheA, *B. burgdorferi* His-CheY3 and His-CheX proteins were described elsewhere (208, 222, 234). *B. burgdorferi mcp3*, *mcp4*, and *mcp5* open reading frames were cloned separately in the expression vector pMAL c2x (NEB Inc.) to generate MBP-MCP3, MBP-MCP4, and MBP-MCP5 recombinant proteins, respectively. *E. coli* codon-plus cells harboring pMAL c2x::*mcp3*, *mcp4* or *mcp5* was expressed and purified according to the manufacturer's protocol (NEB Inc.).The purity of the recombinant proteins were verified by Sodium dodecyl sulfate-polyacrylamide gel electrophoresis (SDS-PAGE) and quantified by comparison with standard bovine serum albumin (BSA).

SDS-PAGE and immunoblot analyses. SDS-PAGE and immunoblotting with an enhanced chemiluminescent detection method (GE Health Inc.) were carried out as reported previously (143, 172). The concentration of protein in cell lysates was determined by a Bio-Rad protein assay kit using BSA as a standard. Unless otherwise noted, 5 µg of lysate protein was subjected to SDS-PAGE and immunoblotting using *B. burgdorferi* specific antibodies.

Affinity blotting. Protein-protein interactions were determined using affinity blotting (235). Briefly, 2 µg of purified recombinant Strep-CheD protein was subjected to SDS-PAGE, and transferred to polyvinylidene difluoride (PDVF) membrane. The membranes were blocked overnight with shaking at 4°C in blocking solution (5% skim milk, 0.9% NaCl, 10 mM Tris, pH 7.4). After the incubation, 10 µg of purified His-CheX, His-CheY3, MBP-MCP3, MBP-MCP4, or MBP-MCP5 was added to the blocking solution for 3 hr. (235). The membranes were washed 4 times with immunoblotting wash buffer and then probed with proper antibodies. Detection was performed with the ECL immunoblotting detection kit (GE Healthcare Inc.).

Phosphorylation assays. Phosphorylation of CheA, phosphotransfer from CheA-P to CheY3, and dephosphorylation of CheY3-P by CheX phosphatase have been described (208, 221, 222). *B. burgdorferi* has two CheA proteins, CheA1 and CheA2, and both are capable of autophosphorylation by ATP (208). However, the expression level of *B. burgdorferi* CheA1 or CheA2 in *E. coli* is poor and they are also difficult to purify in native conditions (221). Alternatively, we performed the autophosphorylation assays using *E. coli* CheA. Purified *E. coli* CheA was kindly provided by Dr. Ruth Silversmith (University of North Carolina, Chapel Hill, NC) (236). To generate radio-labeled phosphorylated CheA (CheA-^{32}P), 20 pmole of purified CheA was incubated with 10 µCi of [γ-^{32}P]ATP and 30 mM of non-radio-labeled ATP for 30 minutes at room temperature. Autophosphorylated CheA was applied to Bio-Spin6 columns according to the manufacturer's instructions to remove unincorporated [γ-^{32}P]ATP (208, 222). CheA-^{32}P was then incubated with 160 pmole of purified CheY3 for 5 minutes, as described (208, 221). The CheA and CheY3 reaction mixture was then

incubated with 0.15 pmole of CheX or 0.15 pmole of CheX plus 15 pmole of CheD for various length of time. *In vitro* phosphorylation reactions were conducted in the TKM buffer (50 mM Tris-HCl, 50 mM KCl, 5 mM $MgCl_2$, pH 8.5), and reactions were stopped using the stop buffer (50 mM Tris-HCl, 100 mM dithiothreitol, 2% (w/v) SDS, 0.1% (w/v) bromophenol blue, 10% (v/v) glycerol, 5% (v/v) 2-mercaptoethanol, pH 6.8). Reactions were subjected to SDS-PAGE. The gels were dried, and the CheY3-^{32}P dephosphorylation levels were analyzed by phosphorimage analysis using Typhoon 9410 Phosphor Imager/Fluorescence Imager (GE Healthcare Inc.) (208, 221). The intensity of phosphorylated proteins was calculated using Quantity One 1-D Analysis Software ver. 4.6.9 (Bio-Rad Inc.) and is expressed as relative “volume”.

Dark-field microscopy, swarm plate chemotaxis assays, and colony swarm plate assays. Growing *B. burgdorferi* cells were imaged using a Zeiss Imager M1 dark-field microscope connected to a digital camera to determine morphology and motility. Swarm plate assays were performed to determine the spirochete’s chemotactic ability as described previously (222, 227). Briefly, approximately 1 x 10^6 cells in a 5 µl volume were spotted into 0.35% agarose plates containing BSK medium diluted in 1:10 in Dulbecco’s phosphate-buffered saline. Since *B. burgdorferi* is a slow-growing organism with a 5 to 12 h generation time (142), swarm plates were incubated for 5 days. Swarming images were documented using a digital camera (143, 165, 181, 182). To determine an individual colony’s swarm ability, *B. burgdorferi* clones were plated on separate semi-solid BSK plates (20-50 colonies per plate). Approximately a month after the inoculation, swarming diameter of each individual colony was measured. Each isolate was assayed in at least two independent experiments.

Mouse infection studies. Six to seven weeks old *Mus musculus* C3H/HeN mice were used for infection studies, as described (143, 181, 183, 225, 237). For infection via needle, 5 x 10^2 to 5 x 10^6 *in vitro*-grown spirochetes were injected intraperitoneally (143, 225, 238). The number of spirochetes was determined using a Petroff-Hausser chamber and each clone was verified for their retention of endogenous plasmids before the injection. Mice were bled 2 weeks post inoculation for immunoblot analysis with mouse sera against *B. burgdorferi* antigens to determine infectivity, as described (182, 183, 238, 239). Reisolation of *B. burgdorferi* from mouse skin, bladder and joint tissues was performed 3 weeks post injection to assess the ability of spirochetes to infect mice (182, 183, 225, 237, 240). Euthanized mouse tissues were placed in BSK-II growth medium and incubated for up to 35 days; the presence of spirochetes was determined by dark-field microscopy. The ID_{50} was calculated as described below.

Determination of Infectious dose 50 (ID_{50}) and statistical analysis. The dose required to infect 50% of the mice was experimentally determined for wild-type, Δ*cheD* mutant and the *cheD*^{com} strains, as described (181, 183). The data from the ID_{50} infection experiment and the single dose infection experiment for each strain were combined for the estimations of the 50% infectious dose. Comparison between strain ID_{50} values was made using a generalized linear model with a probit link function and the log of Dose. This method is also known as probit regression and in it we assume identical slopes in the response/log-dose relationship but different intercepts for each strain. Graphically those assumptions manifest themselves as dose response curves with lateral shifts corresponding to the changes in intercept. Additionally, an overdispersion parameter was fit in order to accommodate greater homogeneity in

infection rates that would otherwise be permitted by the model. All calculations were carried out using JMP V12 Software (SAS Institute Inc, Cary, NC). A $p \leq 0.05$ between samples was considered significant.

Assessment of spirochete acquisition and transmissions using mouse-tick-mouse infection assays. To assess if naïve *Ixodes scapularis* ticks are able to acquire *B. burgdorferi* from infected C3H/HeN mice, survive in the ticks, and then transmit from the ticks to the naïve mice, we performed mouse-tick-mouse cycle experiments (181-183). Briefly, naïve mice were injected with *in vitro*-grown spirochetes to infect 100% mice (100 x ID_{50}). Before performing any infection studies, spirochetes were verified by PCR to ensure that each clone retained all endogenous plasmids required for persistence infection in mouse and tick hosts (143, 159, 182, 183, 225). To verify the infection status, mice were bled 2 weeks post-inoculation and sera were tested using *B. burgdorferi* cell lysates by immunoblotting. Three weeks post-injection, naïve larval ticks were fed to repletion on separate spirochete infected mice (3 mice per bacterial strain; ~200 larvae/mouse) for 5 to 7 days and collected once they dropped off the mice to determine acquisition of spirochetes from mice to ticks. To determine percentage of spirochete-positive ticks for each *B. burgdorferi* clone, fed ticks were squashed individually to isolate genomic DNA followed by *B. burgdorferi flaB*-gene specific PCR, as described (181, 183, 230, 241). Seven days after drop-off, fed larvae was surface sterilized using 3% H_2O_2 followed by 70% ethanol, crushed individually in BSK-II medium, and plated in semi-solid BSK to determine viable spirochetes per tick (i.e., acquisition of spirochetes from infected mice to larval ticks) (143, 181, 225, 237, 240). In determining the total number of spirochetes per fed tick, 10 ticks were analyzed for each

strain and the results are expressed as a scatter plot with the mean. Statistical analysis was performed as described below. A second subset of fed larvae was allowed to molt. Two to three weeks after the molt, nymphal ticks were allowed to feed on naïve mice to determine transmission of spirochetes from infected nymphs to mice (143, 190). Naïve C3H/HeN mice were anesthetized and groups of nymphs were confined to capsules affixed to the shaved backs of the mice (3 mice per strain; 15 nymphs/mouse) (143, 242, 243). The ticks were allowed to feed until repletion (3 to 5 days) and then collected from the capsules. At 7 days post-repletion, ticks were squashed individually, and spirochete burdens were determined as described above. Statistical analysis was performed as described below. Mice were euthanized 3 weeks post-repletion, and the transmission of the spirochetes was evaluated by reisolation.

Statistical analysis. The significance of the difference between the mean values of the groups was analyzed as follows. Unless otherwise stated, for all data, normality was checked using Shapiro-Wilk normality test. If the data passed normality, a multiple-comparison analysis was performed by using a one-way analysis of variance (ANOVA) followed by a Tukey's post hoc test. If the data did not pass normality, a multiple-comparison analysis was performed by using a Kruskal-Wallis test, followed by Dunn test. A P-value of ≤0.05 between samples was considered significant.

RESULTS

Phosphatase activity of CheX is enhanced by CheD

Amino acid sequence analysis of *B. burgdorferi* CheD indicates that it shares approximately 30% identity with *B. subtilis* and *T. maritima* CheD. Most importantly, the essential residues of *B. subtilis* and *T. maritima* CheD are also conserved in *B. burgdorferi* (not shown; see (206)). In *B. subtilis*, CheD plays an important role in chemotaxis by modification of MCPs by deamidation of glutamine to glutamate residues or by enhancing chemotaxis CheC phosphatase activity to efficiently dephosphorylate the response regulator CheY, thereby regulating the levels of CheY-P (204-207). Because of the possession of the conserved residues, we predicted that *B. burgdorferi* CheD may exhibit similar functions as seen in other bacteria (204, 206, 220). *B. burgdorferi* genome lacks a homolog of CheC but possesses a functional phosphatase, CheX that efficiently dephosphorylate CheY3-P (222, 223). In order to test if *B. burgdorferi* CheD is able to stimulate the phosphatase activity, we first performed protein-protein interaction assays using affinity blotting as we supposed that CheD should bind to CheX in order to enhance the phosphatase activity. The affinity blotting data indicate that CheD interacts with CheX but not the chemotaxis response regulator CheY3 (Fig. 2.1). These observations suggest that CheD may be able to stimulate the phosphatase activity.

To determine if CheD is able to enhance phosphatase activity, we performed phosphorylation-dephosphorylation assays using recombinant purified CheA, CheY3, and CheX. When CheY3 was incubated with CheA-^{32}P for 5 minutes, CheY3 was

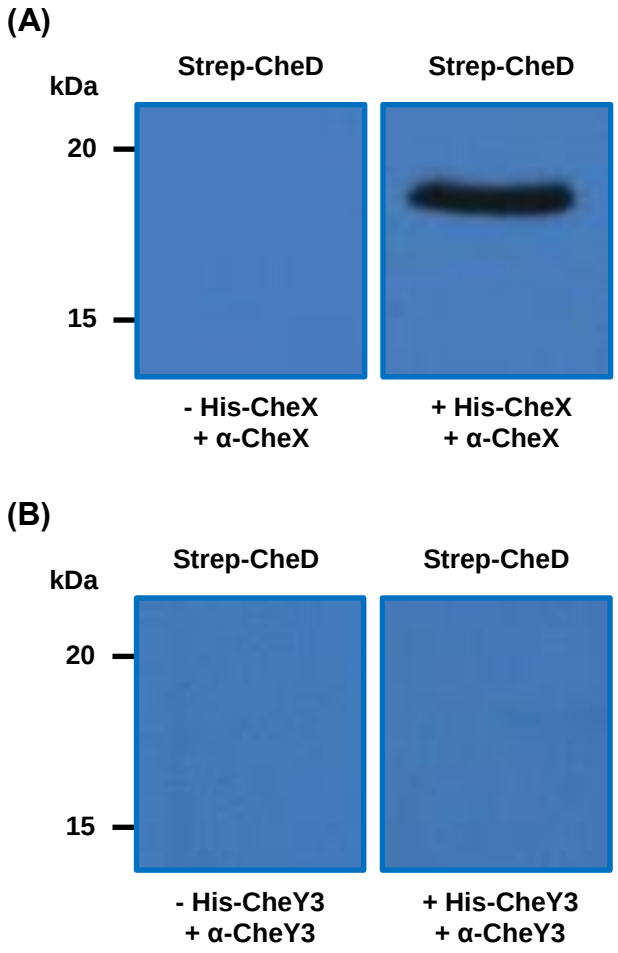

Figure 2.1. Affinity blot analysis indicate that CheD specifically interacts with CheX. (A) Purified Strep-CheD was incubated with (right) or without (left) His-CheX followed by immunoblotting with polyclonal anti-CheX. The band at an apparent molecular mass of 19 kDa (Strep-CheD) was observed in blots probed with His-CheX. **(B)** Purified Strep-CheD was probed with (right) or without (left) His-CheY3 followed by western blotting with polyclonal anti-CheY3. The bands at an apparent molecular mass of 19 kDa (Strep-CheD) were not detected with the His-CheY3 probe.

phosphorylated, as we have reported previously (Fig. 2.2.A, lane 2) (208, 221, 222). Moreover, incubation of CheY3-^{32}P with CheX for 2.5 minutes resulted in dephosphorylation of CheY3-^{32}P by CheX (Fig. 2.2.A, lane 3) (222). Importantly, when CheD was added in the CheA-CheY3-CheX reaction mixture for 2.5 minutes, the CheY3-^{32}P dephosphorylation was enhanced (Fig. 2.2.A, lane 4) and the level of CheY3-^{32}P was completely diminished within 5 minutes (Fig. 2.2.A, lane 8). CheD itself did not affect CheY3-^{32}P dephosphorylation (Fig. 2.2.A, lanes 5 and 9). Moreover, the enhancement of CheX phosphatase activity was dependent on the CheD concentration (Fig. 2.2.B, lanes 4 to 8), indicating that CheD efficiently enhances CheX phosphatase activity.

To determine if CheD is able to modify a *B. burgdorferi* chemoreceptor MCP protein, we performed deamidation assays using recombinant purified proteins, as described (206, 220). Even though we were able to detect deamidation with the positive control (*Bacillus subtilis* chemoreceptor) MCP-A, our multiple attempts with various assay conditions failed to deamidate any *B. burgdorferi* MCP. Since we were unable to detect deamidation of a MCP by CheD, we performed CheD-MCP protein-protein interaction assays alternatively, reasoning that CheD must first bind to a MCP in order to deamidate it. Using recombinant purified MCP and CheD proteins in an affinity blotting, we were able to determine CheD-MCP interactions. Specifically, we found that CheD interacts with MCP3 and MCP4, but not MCP5 (Fig. 2.3).

Construction of *cheD* mutant and complemented strains

In order to determine the role of CheD in motility, chemotaxis, or the infectious

Figure 2.2. CheD enhances phosphatase activity of CheX. Phosphorylation-dephosphorylation assays using purified recombinant CheA (A), CheY3 (Y), CheX (X), and CheD (D) proteins. **(A)** Twenty picomoles of CheA was autophosphorylated using 10 μCi of [γ-^{32}P]ATP (lane 1). CheA-^{32}P was then incubated separately with 160 pmol of CheY3 for 5 min (lanes 2 and 6). Radio-labeled CheY3-^{32}P was incubated with 0.15 pmol of CheX for 2.5 min or 5 min (lane 3 or 7, respectively). CheY3-^{32}P and CheX reaction mixture was incubated with (lanes 4 land 8) or without 15 pmol of CheD (lanes 5 and 9). Arrows indicate the positions of CheA-^{32}P and CheY3-^{32}P. **(B)** CheX phosphatase activity was efficiently enhanced by CheD. CheA was autophosphorylated as described above (lane 1). CheA-^{32}P was then incubated with 160 pmol of CheY3 for 10 min (lane 2). Radio-labeled CheY3-^{32}P was mixed with 0.15 pmol of CheX for 5 min without CheD (lane 3) or with 0.2 pmol (lane 4), 2 pmol (lane 5), 5 pmol (lane 6), 10 pmol (lane 7), or 20 pmol of CheD (lane 8). CheY3-^{32}P was also incubated with 20 pmol of CheD to confirm that CheD did not interfere with CheY3-P dephosphorylation (lane 9). An arrow indicates the position of CheA-^{32}P, CheY3-^{32}P or CheD. Lane numbers were shown at the bottom of each gel images. Relative intensities (PI “volumes”) of CheY3-^{32}P are shown in the right panels, and corresponding phosphor image lane numbers are shown at the top of the figures.

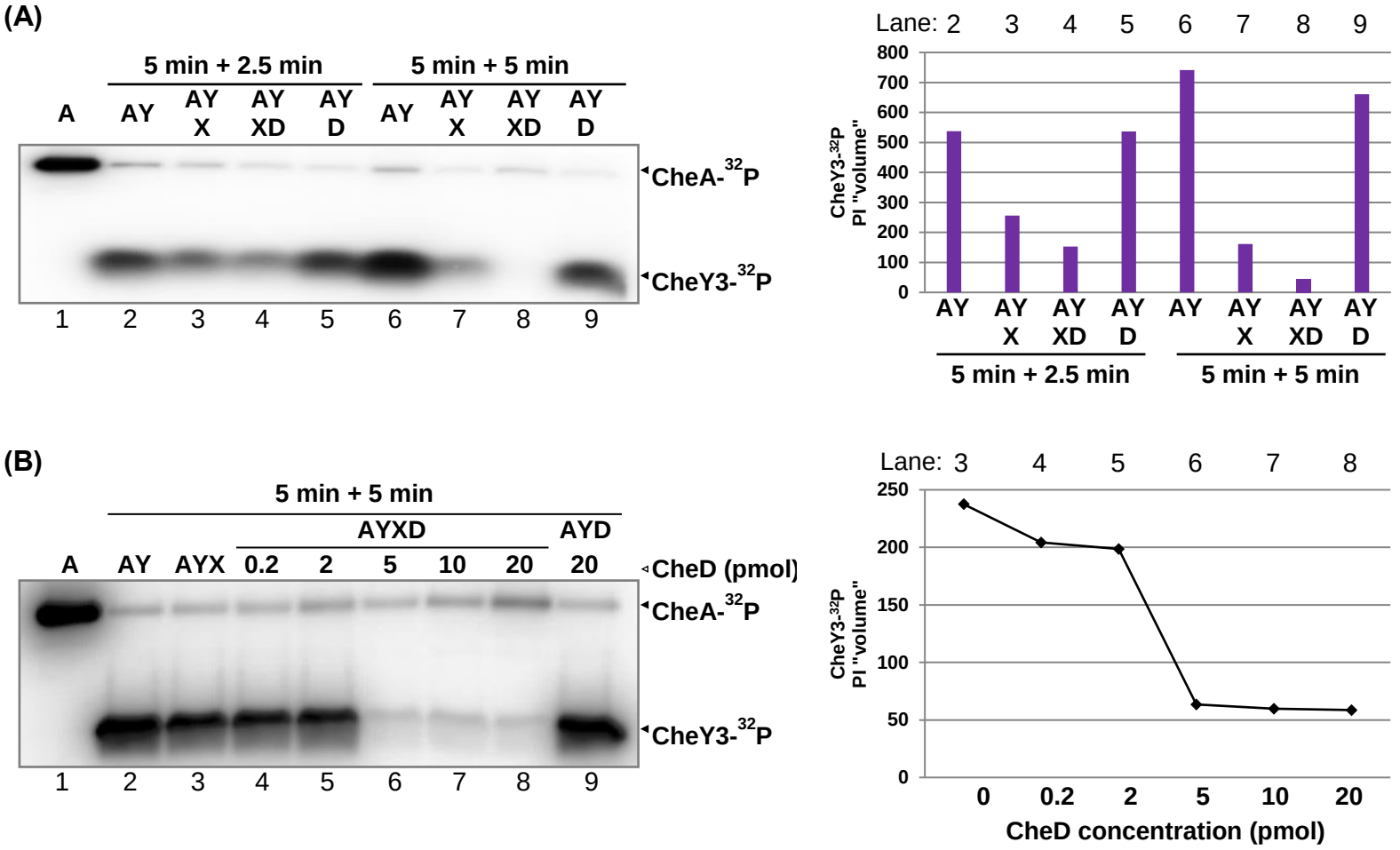
(A)
5 min + 2.5 min
5 min + 5 min
A
AY
AY X
AY XD
AY D
AY
AY X
AY XD
AY D
CheA-32P
CheY3-32P
1 2 3 4 5 6 7 8 9
Lane: 2 3 4 5 6 7 8 9
CheY3-32P PI "volume"
800
700
600
500
400
300
200
100
0
AY AY X AY XD AY D AY AY X AY XD AY D
5 min + 2.5 min
5 min + 5 min
(B)
5 min + 5 min
AYXD
AYD
A
AY
AYX
0.2
2
5
10
20
20
CheD (pmol)
CheA-32P
CheY3-32P
1 2 3 4 5 6 7 8 9
Lane: 3 4 5 6 7 8
CheY3-32P PI "volume"
250
200
150
100
50
0
0 0.2 2 5 10 20
CheD concentration (pmol)

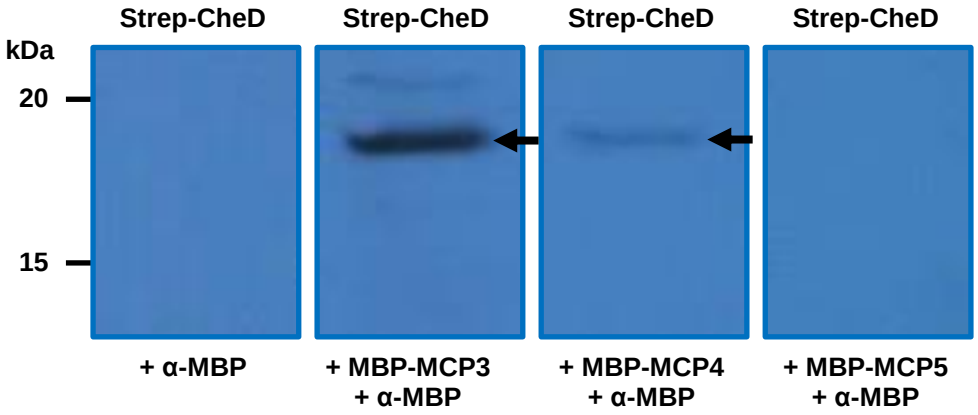

Figure 2.3. CheD specifically interacts with MCP3 and MCP4. Affinity blotting was performed as described above. Purified Strep-CheD was probed with MBP-MCP3, MBP-MCP4, or MBP-MCP5 followed by immunoblotting with monoclonal MBP antibodies (Thermo Scientific). The bands at an apparent molecular mass of 19 kDa (Strep-CheD; arrows) were always observed in blots probed with MCP3 and MCP4, but not MCP5.

cycle of *B. burgdorferi*, we inactivated the gene using a kanamycin resistance cassette (P_{flgB}-*aph1*) in the low-passage virulent wild-type clone B31-A3 (Fig. 2.4) (165, 181-183). PCR analysis of the kanamycin-resistant clones indicating that the P_{flgB}-*aph1* cassette was inserted in the *cheD* gene (not shown), resulting in successful construction of the mutant. Furthermore, we confirmed by PCR that the *cheD* mutant retained all linear and circular endogenous plasmids seen in the parental wild-type cells (data not shown).

The *cheD* mutant (Δ*cheD*) was complemented *in cis* by genomic integration to ensure that the phenotype of the mutant was solely attributed to the mutation and not due to a secondary mutation elsewhere in the genome (Fig. 2.4) (165, 183). Accordingly, the *cheD* gene and its native promoter (P_{cheD}) was fused together and inserted within *bb0445* and *bb0446* in the suicide vector pXLFCheD (230, 231). The insertion of P_{cheD}-*cheD* was downstream of both the *bb0445* and *bb0446*, and less likely to affect their expression, as reported previously (183, 230, 231). To detect the expression of *cheD* in the wild-type, Δ*cheD* mutant, and complemented *cheD* (*cheD*^{com}) cells, we performed qRT-PCR using gene-specific primers. Real-time PCR detected the *cheD* transcripts in wild-type and *cheD*^{com} cells, but not in the *cheD* mutant cells (Fig. 2.5). Moreover, the level of *cheD* transcripts synthesized in the *cheD*^{com} cells was approximately 84% of wild-type cells, indicating the restoration of *cheD* synthesis in the *cheD*^{com} cells (Fig. 2.5).

In vitro motility and chemotaxis phenotype of the Δ*cheD* mutant cells

We analyzed the Δ*cheD* mutant to determine any alteration of motility or

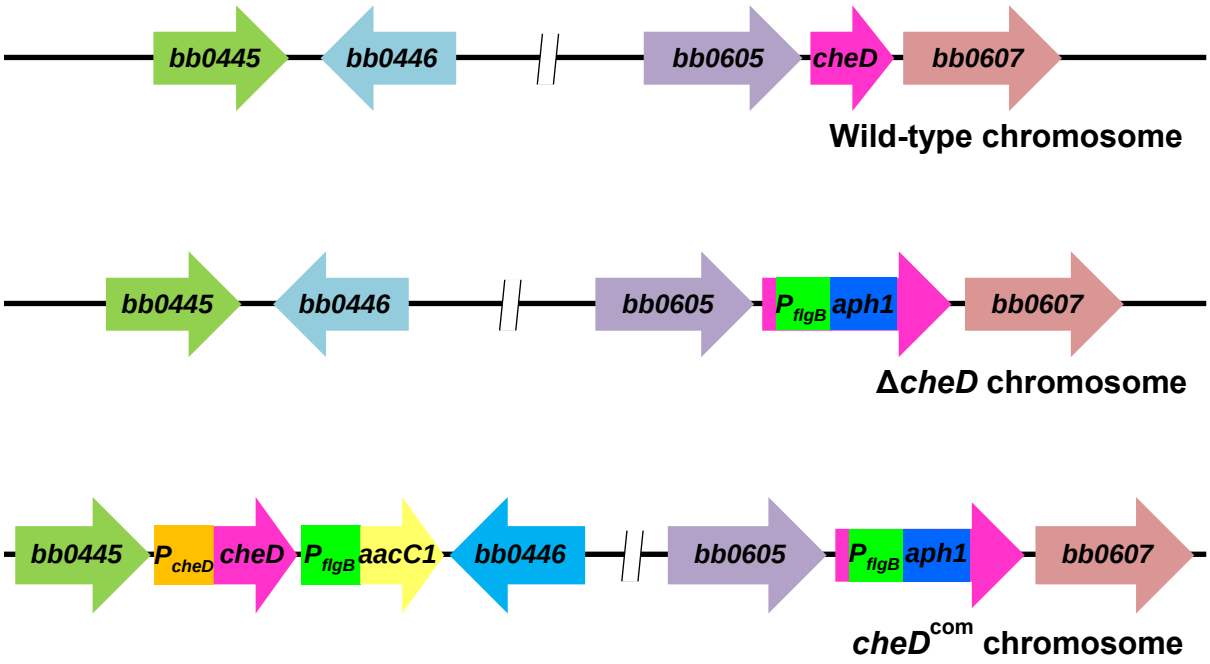

Figure 2.4. Schematic diagrams showing the construction of Δ*cheD* mutant and complemented strains. Inactivation of *cheD* using the P_{flgB}-*aph1* cassette. Wild-type *B. burgdorferi* with *cheD* polycistronic operon consisting of *bb0605-bb0606/cheD-bb0607* genes. The P_{flgB}-*aph1* cassette was inserted within the *cheD* gene using *Hin*dIII restriction digestion. The P_{cheD}-*cheD* DNA was inserted between genes *bb0445* and *bb0446* to complement the mutant *in cis* $cheD^{com}$ chromosome.

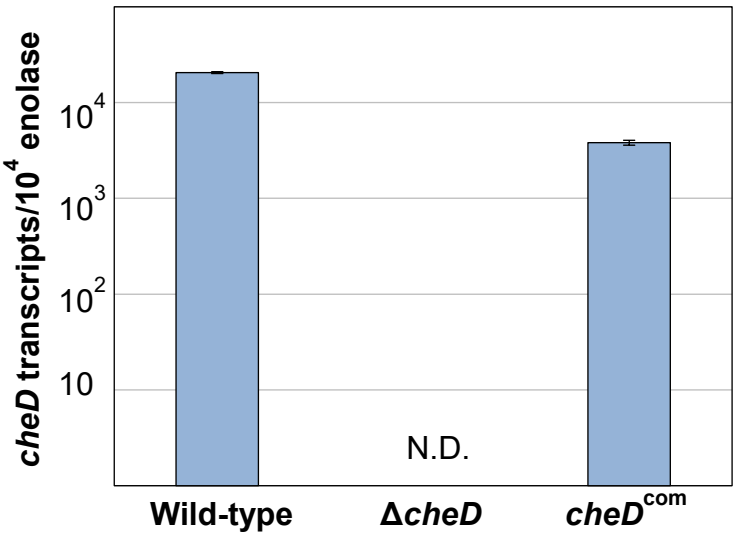

Figure 2.5. Expression of *cheD* was abolished in the mutant but was restored in the *cheD*^{com} cells as determined by qRT-PCR. The relative transcript levels of *cheD* was determined in the wild-type, Δ*cheD* and *cheD*^{com} cells which were then compared with the expression of *B. burgdorferi* enolase gene. The bars represent the mean ± standard deviation of the mean from three samples. A representative result from two independent studies is shown here. N.D., not detected.

chemotaxis behavior and compared those results with the wild-type or *cheD*^{com} cells. The *cheX* mutant was reported to exhibit a constant flexing swimming pattern whereas the wild-type cells run, flex/stop, and then reverse or change their swimming direction (222). Since we showed that CheD enhanced the phosphatase activity of CheX, we postulated that the *cheD* mutant cells might display an altered motility or chemotaxis phenotype. Dark-field microscopic analysis indicated that the motility patterns of the *cheD* mutant (run-flex/pause-reversal) and its flexing frequency during swimming were not noticeably different from the wild-type cells (9-12 flexes per minute; data not shown). However, the chemotaxis was found to be significantly reduced when compared to the wild-type (p=0.002) or the complemented *cheD*^{com} cells (p=0.007) (Fig. 2.6.A). In swarm plate assays, the average swarm diameters of the Δ*cheD* mutant were approximately 18% smaller than those of the wild-type or *cheD*^{com} cells (Fig. 2.6.A). Swarm plate assay is a group event where millions of bacteria attempt to migrate out from the initial site of inoculation (in a semi-solid plate) as they chemotax and metabolize neighboring nutrients resulting in a swarm ring. However, results obtained from such an assay may not accurately determine the chemotactic ability of an individual spirochete. Accordingly, we plated 20-50 *B. burgdorferi* cells in a semi-solid plate (same plates used for the swarm plate assay) to determine the chemotactic ability of individual cells by measuring their colony (swarm) size. Prolonged incubation of those plates produced colony sizes that were significantly smaller than the wild-type (p=0.0001) or *cheD*^{com} cells (p=0.014). On average, the colony size of Δ*cheD* mutants was approximately 13% smaller than wild-type or *cheD*^{com} cells (Fig. 2.6.B). Together, our results indicate that *cheD* plays an important role in *B. burgdorferi* chemotaxis.

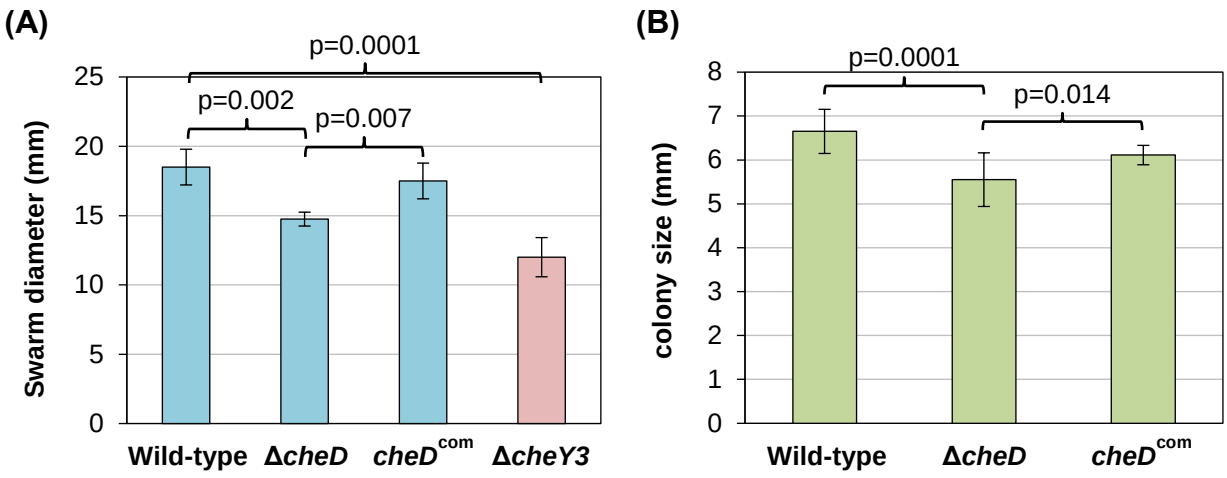

Figure 2.6. Δ*cheD* mutant cells are deficient in chemotaxis. (A) Swarm plate assays indicate a defect in chemotaxis exhibited by the Δ*cheD* cells. Approximately $1x10^6$ *B. burgdorferi* cells from the indicated strains were spotted into 0.35% soft agarose plates which were then incubated for 5 days. The swarm diameter of each clone was measured in millimeters. A non-chemotactic *cheY3* mutant was used as a control (208). Bars represent the mean ± standard deviation of the mean from each clone (data from at least 3 plates per clone). Statistical analysis was performed by using ANOVA, as described in the Materials & Methods. P-values between samples are shown at the top. **(B)** Δ*cheD* mutants display reduced colony size compared to the wild-type or complemented strains. *B. burgdorferi* cells from the indicated strains were plated on 0.4% soft agarose plates. Individual colony's swarm ability was determined four weeks after inoculation. The colony size of each clone was measured in millimeters. P-values were determined using ANOVA. Values are indicative of the mean ± standard deviation of the averages from at least 3 plates (20 individual colonies) per strain. P-values between samples are shown at the top where p≤0.05 was considered as significant.

***B. burgdorferi* Δ*cheD* mutant cells can establish infection in C3H/HeN mice by needle inoculation but display reduced infectivity.**

While the role of CheD in motility and chemotaxis has been demonstrated in other bacteria, its role in pathogenesis has not been determined in any bacterium. In order to evaluate the infection potential of the mutant, groups of C3H/HeN mice were challenged with 10-fold increasing doses of wild-type, Δ*cheD* or the complemented *cheD*^{com} cells to determine the 50% infectious dose (ID_{50}). Immediately before the injections, we confirmed by PCR that these strains retained their endogenous plasmids (data not shown) (143, 182, 183, 225). Two weeks post inoculation, the mice were bled and their sera were assessed for reactivity with *B. burgdorferi* antigen membrane protein A, also known as P39 (238, 239). Furthermore, to confirm the serology results, mice were euthanized three weeks post-inoculation and spirochetes were reisolated from ear, bladder and joint tissues. Serology results indicated that *cheD* mutant cells were attenuated in establishing an infection in mice (not shown) and correlated well with reisolation of spirochetes from tissues examined (Table 2.2). Whereas the *cheD*^{com} cells did not show a significant increase in the ID_{50} compared to the parental wild-type cells ($p=0.3$), the ID_{50} for the *cheD* mutant was approximately one logarithm higher than that of wild-type or *cheD*^{com}, indicating a significant attenuation in virulence ($p=0.012$ or $p=0.0005$, respectively) (Table 2.2).

***Ixodes scapularis* ticks are able to acquire and transmit mutant *B. burgdorferi*.**

Because infection of and survival within the mammalian host represents only one aspect of the *B. burgdorferi* enzootic life cycle, a more comprehensive evaluation of the

Table 2.2. Δ*cheD* mutant cells are able to establish infection in C3H/HeN mice but the infectivity is considerably reduced*

Strain	Dose (CFU)	No. of mice infected / No. tested	ID_{50}
WT	$7.5x10^2$	0/7	$1.8080x10^4$
	$7.5x10^3$	1/7	
	$7.5x10^4$	5/7	
	$9.3x10^5$	7/7	
Δ*cheD*	$6.2x10^2$	0/7	$1.5694x10^5$
	$6.2x10^3$	1/7	
	$6.2x10^4$	1/7	
	$1.00x10^6$	6/7	
	$1.00x10^7$	7/7	
***cheD*^{com}**	$5.6x10^2$	0/7	$1.9483x10^4$
	$5.6x10^3$	2/7	
	$5.6x10^4$	5/7	
	$8.2x10^5$	7/7	

*Mice were injected with the indicated *B. burgdorferi* clones and doses. Infectivity was determined by reisolation of *B. burgdorferi* from euthanized mouse tissues (ear skin, ankle joint, and urinary bladder). ID_{50} and statistical analyses were performed using Probit regression, as described in the Materials and Methods. The Δ*cheD* mutant spirochetes are significantly attenuated when compared to the ID_{50} of wild-type ($p=0.0125$) or the complemented *B. burgdorferi* ($p=0.0005$) where significance was defined as $p \leq 0.05$.

activities of these mutants in the tick vector was justified. Naïve *I. scapularis* larvae were allowed to feed on infected mice in order to determine acquisition as well as viability of *B. burgdorferi* in larval ticks. Seven days after feeding on infected mice, a subset of larvae were squashed individually and purified genomic DNA in order to determine spirochete-positive ticks by PCR using *B. burgdorferi flaB*-gene specific primers. Another set of fed larvae were squashed individually for plating in semi-solid medium in order to determine viable spirochetes per tick. PCR data shown in Figure 2.7.A indicate that 100% of larvae that fed on wild-type, Δ*cheD* or *cheD*^{com}-infected mice were able to acquire the spirochetes (i.e., spirochete-positive). The burden of the mutant spirochetes per tick was not significantly lower than that of the wild-type (p=0.129) (Fig. 2.7.B). However, the burden of mutant *B. burgdorferi* was statistically less than the burden seen in larval ticks infected with the complemented *cheD*^{com} (p=0.007).

In order to determine if the infected ticks are able to survive the molting and be able to transmit the mutant *B. burgdorferi* in naïve mice, a subset of fed larvae were allowed to molt. Two to three weeks after molting, infected nymphs were allowed to feed on naïve C3H/HeN mice (3 mice per strain, 15 nymphs per mouse). Seven days post-repletion, nymphs were analyzed individually by plating on semi-solid plates, as above. Plating results indicate that the mutant spirochete's burden in fed nymphs was considerably reduced compared to that of wild-type (p=0.013), however, the Δ*cheD* mutant's load was not statistically different from the *cheD*^{com} infected nymphs (p=0.452) (Fig. 2.7.C) despite the fact that 100% of the nymphs were spirochete-positive by all clones (not shown, see Fig. 2.7.A).

To determine the transmission of *B. burgdorferi* from infected nymphs to mice,

Figure 2.7. Naïve ticks are able to acquire and transmit Δ*cheD* mutant spirochetes during mouse-tick-mouse infection studies. (A) Naïve ticks were allowed to feed on infected mice to determine acquisition of spirochetes. Ten larvae fed upon the wild-type, Δ*cheD*, or the complemented spirochete-infected mice were squashed individually to isolate DNA. Those DNA samples were then used to detect *B. burgdorferi flaB* by PCR. PCR data indicate that 100% of larval ticks were able to acquire the spirochetes from *B. burgdorferi*-infected mice (all groups). A tick's DNA that we previously confirmed to be spirochete-positive was used as a positive control (+) and ddH_2O was used as a negative control (-). **(B)** Δ*cheD* mutant spirochetes are able to survive in fed larvae. Viable Δ*cheD* spirochetes in fed larvae are reduced compared to the wild-type or complemented cells. P-values shown at the top were determined by using ANOVA, as described in the Materials & Methods. A $p \leq 0.05$ between samples was considered significant. **(C)** Mutant spirochetes are able to survive in fed nymphs, but the number of viable Δ*cheD* cells in fed nymphs are considerably less than the wild-type ($p=0.013$) but not statistically different from the complemented $cheD^{com}$ cells ($p=0.452$). P-values were determined as described above where significance was defined as $p \leq 0.05$. A representative result from two independent studies with different batches of ticks is shown here. Bars represent the mean viable spirochetes per tick ± SEM.

(A)

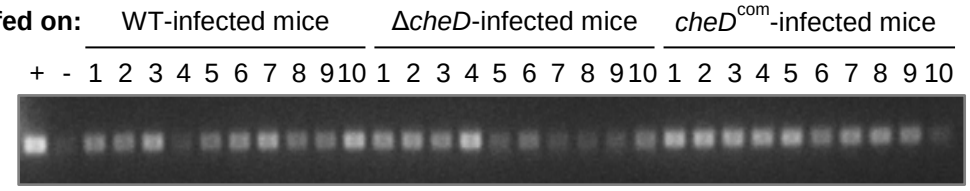
Larvae fed on:
WT-infected mice
ΔcheD-infected mice
cheD com -infected mice
+ - 1 2 3 4 5 6 7 8 9 10 1 2 3 4 5 6 7 8 9 10 1 2 3 4 5 6 7 8 9 10

(B)

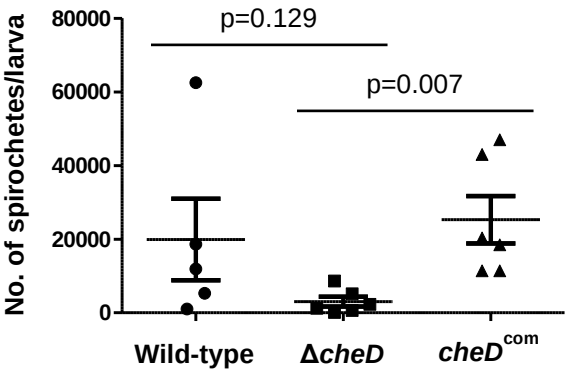
No. of spirochetes/larva
80000
60000
40000
20000
0
p=0.129
p=0.007
Wild-type
ΔcheD
cheD com

(C)

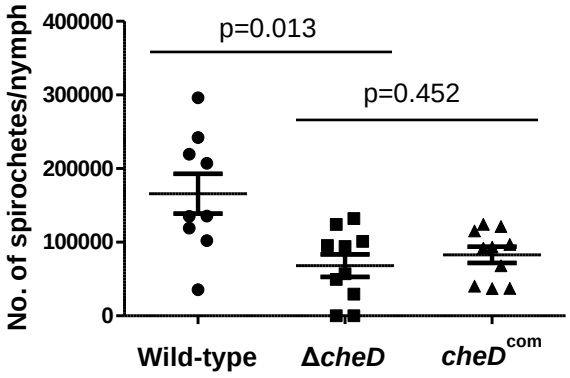
No. of spirochetes/nymph
400000
300000
200000
100000
0
p=0.013
p=0.452
Wild-type
ΔcheD
cheD com

the tick-fed animals were bled at two weeks post-feeding to perform serology followed by euthanization of mice to reisolate *B. burgdorferi* from ear, ankle joint, and urinary bladder tissues at 3 weeks post-repletion. Serology as well as bacterial outgrowth analyses indicate that the Δ*cheD* mutants are able to transmit and establish infection in all mice with no detectable deficiency (Fig. 2.8 and Table 2.3) even though we performed these *in vivo* studies twice using separate batches of ticks and mice.

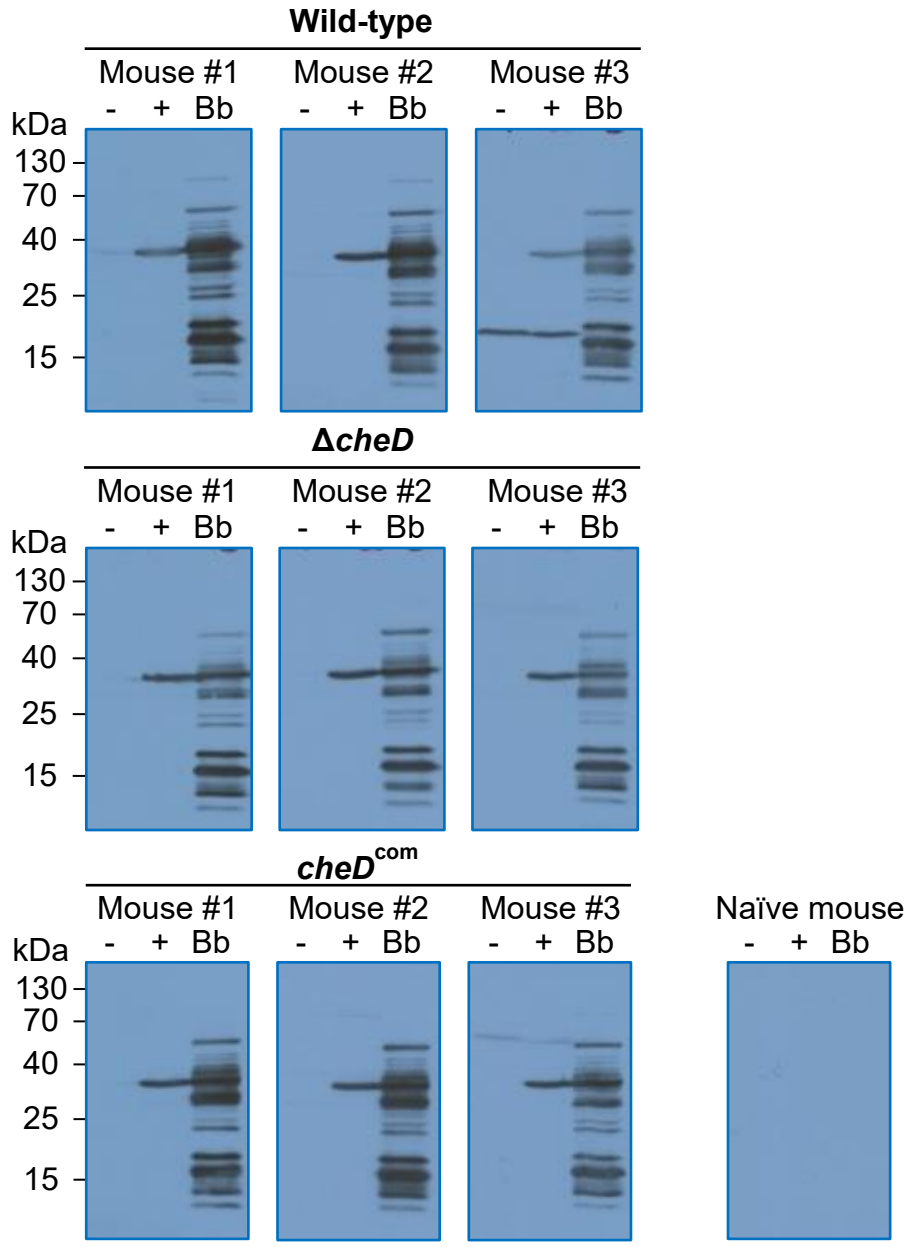

Figure 2.8. Serology results of mice fed by the infected nymphs. Sera were collected from tick-bitten mice three weeks post-feeding, and immune responses were detected by Western blot. -, *E. coli* XL1 (negative control); +, *E. coli* expressing *B. burgdorferi* antigen P39; Bb, *B. burgdorferi* wild-type cell lysate.

Table 2.3. Δ*cheD* spirochete-infected nymphal ticks are able to transmit the organisms into naïve C3H/HeN mice*

Strain	No. of tissues positive / No. examined	No. of mice infected / No. tested
Wild-type	8/9	3/3
Δ*cheD*	9/9	3/3
cheD^{com}	8/9	3/3

*Fifteen infected nymphs that are molted from larvae (from acquisition assay) were allowed to feed on one C3H/HeN mouse. Mice were euthanized 3 weeks post-repletion. Infectivity was determined by reisolation of *B. burgdorferi* from euthanized mouse tissues. A representative data from two independent studies is shown here.

DISCUSSION

In this study, we systematically demonstrated that CheD specifically interacts with CheX and enhances phosphatase activity (Fig. 2.1 and 2.2). It is notable that CheC-type of phosphatases are monomers that possess two CheY-P dephosphorylation sites whereas the CheX-type of phosphatases are dimers containing only one dephosphorylation site (206, 222, 223, 244). Considering this distinction, this is the first report demonstrating the stimulation of CheX-type of phosphatases by CheD. CheD was reported to possess various functions in *B. subtilis* (204, 220, 245). While we were able to determine CheD-CheX relationship, our multiple attempts to deamidate *B. burgdorferi* MCPs by CheD were unsuccessful despite the fact that our positive control *B. subtilis* MCP deamidation was successful (204, 206), and we performed those assays using various conditions (data not shown). We, however, were able to show that CheD specifically interacts with MCP3 and MCP4, but not MCP5 (Fig. 2.3). It is possible that CheD binds to other MCPs, however, we chose to use these three MCPs because MCP3 and MCP5 are homologs of the major chemoreceptors Tar and Tsp of *E. coli*, respectively, and MCP4 possesses three CheD binding sites (Table 2.4). CheD binding to MCP3 and MCP4 suggest that either our deamidation assay conditions were not optimized or the CheD/MCP proteins purified from *E. coli* cells were non-functional/inactive.

Because we found that CheD enhances CheX phosphatase activity and the *cheX* mutant constantly flexes (222), we supposed that the *cheD* mutant would also exhibit a motility phenotype. However, we failed to detect any noticeable difference in motility behavior exhibited by the Δ*cheD* cells. Even though the motility phenotype of the *cheD*

Table 2.4. Potential CheD modification substrate sites detected in *B. burgdorferi* chemoreceptors*

Chemoreceptor	Conserved sequence motif A/S X X **Q**/E **Q**/E X X A/S
B. subtilis MCP-A	A T V **Q** **Q** L S A
	G E L **Q** N M S A
B. subtilis MCP-C	A I S **Q** E S A A
B. burgdorferi MCP1	S R S **Q** E E F S
B. burgdorferi MCP2	S L L E **Q** N A S
	A S V E **Q** S S S
B. burgdorferi MCP3	S S L **Q** E Y S S
B. burgdorferi MCP4	S A L **Q** **Q** A S A
	A N V E **Q** I A S
	S S S E **Q** L S S
B. burgdorferi MCP5	S T L E **Q** M T A

B. burgdorferi* MCP chemoreceptor protein sequences were aligned with *B. subtilis* MCPs (George DG *Molecular Microbiology* 86(3):743-756 (2012)). Only the CheD modification amino acid residues from each MCP is shown here. Typically, CheD deamidates glutamine (Q**) to glutamate (E) residue.

mutant was indistinguishable from the wild-type cells, we demonstrated that CheD is important for chemotaxis (Fig. 2.6). The chemotaxis effect is unrelated to the mutant's growth rate *in vitro* since those cells grow normally in the BSK-II growth medium (not shown). Based on these findings, we propose that the enhancer function associated with the CheD is not likely to have a noticeable effect on CheX function in motility *in vitro*.

Our mouse infection studies demonstrated that the mutant cells are able to establish infection in C3H/HeN mice, however, the mutant was significantly attenuated (Table 2.2). These results were not completely surprising given the fact that the non-chemotactic *cheX* mutant cells are non-infectious in mice (M. A. Motaleb, unpublished data). In Δ*cheD* mutant cells, CheX, the only phosphatase in *B. burgdorferi*, is intact. Deletion of CheD likely had a minor effect on CheX proteins ability to dephosphorylate the CheY-P. Thus, the attenuation in mice we observed with the *cheD* mutant spirochetes is reasonable as the mutant did exhibit reduced chemotaxis phenotype (Fig. 2.9). It is also plausible that the attenuation we found with the mutant spirochetes could be a result of the chemoreceptors not being modified/deamidated normally due to the deletion of *cheD*. Moreover, we found that CheD is dispensable for acquisition or transmission of *B. burgdorferi* (Table 2.3 and Fig. 2.8) despite the fact that the viability of mutant spirochetes was reduced in ticks (both larvae and nymphs) and this reduced burden was detected consistently even though the P-values of wild-type vs. Δ*cheD* or *cheD*^{com} vs. Δ*cheD* were not always statistically significant (Fig. 2.7).

Chemotaxis is found to be important for disease processes by many bacteria including the spirochetes (138, 184, 185, 187, 189, 246), however, our findings with the

Figure 2.9. Role of chemotaxis in *B. burgdorferi*. In *B. burgdorferi* chemotaxis system, a histidine kinase CheA transfer its phosphate group to a response regulator CheY in order to phosphorylate it. The CheY-P then binds to the flagellar switch proteins to alter motility. CheX, the only phosphatase in *B. burgdorferi*, is able to dephosphorylate CheY-P (222, 223). However, the phosphatase activity is enhanced by CheD, resulting in fine-tuning the CheY-P levels in bacteria. Moreover, it appears that CheD plays an essential role in modifying some of the chemoreceptors to adapt/adjust sensing the environmental signals. Based on our observations to-date, we propose that chemotaxis is essential for transmission of *B. burgdorferi* and infection of the mammalian host.

Wild-type model

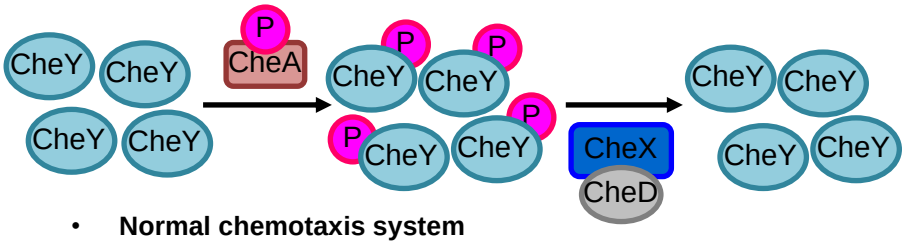

- **Normal chemotaxis system**
- **Full infectivity**

Δ*cheX* model

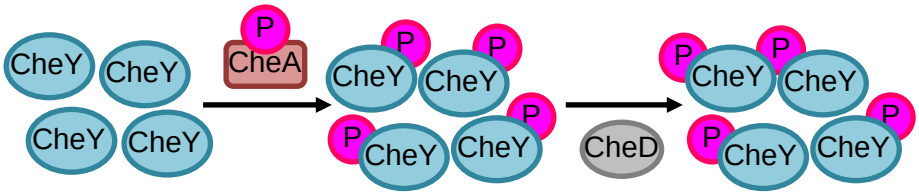

- **No dephosphorylation of CheY-P**
- **Non-chemotactic bacteria**
- **Non-infectious in mice**
- **No transmission by tick**
- **Viability is normal in ticks**

Δ*cheD* model

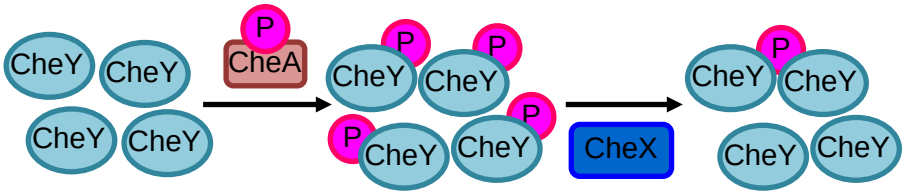

- **Delayed dephosphorylation of CheY-P**
- **Slightly reduced chemotaxis**
- **Reduced infectivity in mice**
- **Normal acquisition / transmission by tick**
- **Reduced survivability in ticks**

; Some of the *in vivo* function may be related to CheD's function in MCPs

Δ*cheD* mutant suggest that either the *in vitro* assay condition does not reflect the *in vivo* host conditions (*in vivo,* the *cheD* mutant may be normal with respect to its chemotactic ability) or the chemotaxis defect we observed with the Δ*cheD in vitro* was not reduced enough to affect acquisition or transmission of spirochetes. However, our coherent observation of marginal reduced burden of *cheD* mutant spirochetes in ticks could be related to its activity in CheX as the *cheX* mutant spirochetes burden in ticks are also marginally reduced when compared to the wild-type (M. A. Motaleb, unpublished data). Moreover, we postulate that this phenotype is linked to less mutant spirochetes were acquired by the ticks while feeding or the viability defect is connected to the receptor MCP modification function. Further evaluation of MCP proteins role in *B. burgdorferi* or how CheD affects the receptors and their subsequent effect on virulence needs to be demonstrated.

B. burgdorferi is a parasite that resides primarily in tick and rodents in the nature. Effective chemotaxis in these disparate habitats potentially explains the need for multiple chemotaxis systems in this organism. We propose that different adaptation systems (CheD or CheR1/CheR2-mediated) are likely employed to sense gradients of different scales and contours in these diverse environments. However, exactly how these chemotaxis systems contribute to the fitness of the Lyme disease spirochete is an open question.

CHAPTER THREE: SPIROCHETES FLAGELLAR COLLAR PROTEIN FLBB HAS ASTOUNDING EFFECTS IN ORIENTATION OF PERIPLASMIC FLAGELLA, BACTERIAL SHAPE, MOTILITY, AND ASSEMBLY OF MOTORS IN *BORRELIA BURGDORFERI*

ABSTRACT

Borrelia burgdorferi, the causative agent of Lyme disease, is a highly motile spirochete, and motility, which is provided by its periplasmic flagella, is critical for every part of the spirochete's enzootic life cycle. Unlike externally flagellated bacteria, spirochetes possess a unique periplasmic flagellar structure called the collar. This spirochete-specific novel component is linked to the flagellar basal body; however, nothing is known about the proteins encoding the collar or their function in any spirochete. To identify a collar protein and determine its function, we employed a comprehensive strategy that included genetic, biochemical, and microscopic analyses. We found that BB0286 (FlbB) is a novel flagellar motor protein, which is located around the flagellar basal body. Deletion of *bb0286* has a profound effect on collar formation, assembly of other flagellar structures, morphology, and motility of the spirochete. Orientation of the flagella toward the cell body is critical for determination of wild-type spirochete's wave-like morphology and motility. Here, we provide the first evidence that FlbB is a key determinant of normal orientation of the flagella and collar assembly.

INTRODUCTION

Lyme disease, which is caused by the spirochete, *Borrelia burgdorferi,* is the most prevalent vector-borne illness in the United States (1). In nature, survival of *B. burgdorferi* depends on migration by the bacteria to sites of colonization in *Ixodes* ticks and mammalian hosts (33, 34). The spirochete is a motile organism and motility is reported to be crucial for every part of the spirochete's pathogenic life cycle, e.g., viability of *B. burgdorferi* in ticks, transmission from ticks to mice, persistent infection and dissemination in the mammalian host (143, 188, 190).

The bacterial flagellar motor, such as those examined in *Escherichia coli,* is a highly efficient nano-machine, with a rotation frequency greater than 100 Hz, even though the diameter of the motor is only ca. 45 nm. The flagellum is a complex structure that is composed of three substructures whose assembly requires at least 25 different proteins. The basal body-motor portion of the flagellum is connected to the filament by the rod-hook assembly. When torque is generated by proton (or sodium in some organisms) flux, the flagellum stator rotates the filament propelling the organism to run or swim. The C-ring or switch complex, which is composed of FliG, FliM, and FliN proteins, is attached to the MS-ring basal body (FliF proteins) and stator (MotA-MotB). The C-ring determines whether a motor rotates clockwise (CW) or counter-clockwise (CCW) (247-250).

Spirochetes are a group of motile bacteria that are distinct from other externally flagellated bacteria such as those seen in *E. coli* in many different aspects (138, 162, 164). For example, *B. burgdorferi* is a long organism (10-20 µm) that possesses 7-11 flagella inserted at each pole of the cell (up to 22 flagella per cell). Unlike *E. coli*, *B.*

burgdorferi flagella are located between the outer membrane and peptidoglycan layer i.e., in the periplasmic space (138, 188, 198, 251, 252). *B. burgdorferi* motility and chemotaxis genes are controlled by housekeeping σ^{70} promoters. This results in the flagella of this spirochete being assembled in a sequential manner. Moreover, the flagellar motors of spirochetes, specifically those of *B. burgdorferi*, are much larger than *E. coli* motors (~80 vs. ~45 nm) and thus require more gene products for their assembly (138, 163, 173).

The periplasmic flagella originate near the cell poles and extend toward the other pole of the cell or toward the cell body. In motile cells, the periplasmic flagellar filaments form a ribbon-like structure that wraps around the cell body, resulting in a distinctive flat-wave morphology (188, 190, 198, 251). It has been proposed that the spirochete's flagella rotate asymmetrically during a "run" mode, i.e., flagella at one pole rotate CW whereas the flagella at the other end rotate CCW. When flagella at both poles rotate in the same direction, the spirochete flexes/tumbles (138, 210). While flagella in most other bacteria are involved in motility, periplasmic flagella in *B. burgdorferi* determine the cellular morphology as well as motility. For example, a mutant that lacks FlaB encoding the protein component of the periplasmic flagellar filaments produces a rod-shaped cell in addition to being non-motile (143, 172). Due to their involvement in cellular morphology and the fact that these flagella rotate within the periplasmic space, it is not surprising that spirochetes possess extra or unique flagellar structures that offer flexibility or rigidity that is required to rotate their flagella within the periplasmic space. Recently, cryo-electron tomography (cryo-ET) of spirochete flagellar motors revealed unique features that are absent from all other bacterial motors studied to-date. One of

these structures is called the “collar” (Fig. 3.1) (162, 164, 253-255). The collar appears to be located adjacent to FliL. FliL homologs are found in several species of bacteria and its function is distinct in those organisms (165, 256-261). In *B. burgdorferi*, we found that periplasmic flagellar filaments were partially and abnormally tilted toward the cell pole in the Δ*fliL* mutant (165).

Importantly, the collar is apparently integrated with the major components of the periplasmic flagella such as the MS-ring. Because of these connections and its central location in the motor, we hypothesize that the collar is critical for flagellar assembly as well as for providing proper rigidity or flexibility of flagella during rotation. However, nothing is known about the proteins encoding the unique collar structure or their function in any spirochete. In this communication, we show that mutations in *bb0286 (flbB*) has a profound effect on collar formation, flagellar orientation, morphology, motility, and the assembly of FliL as well as the stator. Moreover, using green fluorescent protein (GFP) we determined the location of FlbB in the collar. A mechanism underlying the orientation of the periplasmic flagella is also demonstrated.

Figure 3.1. Unique collar structures are conserved in all spirochetes. (A) External flagellar motor of *Escherichia coli*; **(B-D)** periplasmic flagellar motors of the spirochetes, *Leptospira interrogans*, *Treponema pallidum*, and *Borrelia burgdorferi*. The distinctive collar structure is indicated using an arrow. Because of the dynamic nature of the *E. coli* stator, it was not visualized by cryo-ET (A). **(E, F)** Schematic models of the external flagellar motor of *E. coli* (E) and the periplasmic flagellar motor of *B. burgdorferi* (F). Periplasmic flagella are distinct from the external flagella, as they are enclosed within the outer membrane and their flagellar motors are considerably larger and more complex. However, the core architecture of the two flagellar types is comparable. Shared structures include the export apparatus, stator, the MS-ring, the C-ring, the rod connecting the hook with the MS-ring, hook, and filament (not shown) (164). Unique collar structure in the periplasmic flagellar apparatus is shown using an orange color. IM, inner membrane; OM, outer membrane; PG, peptidoglycan layer.

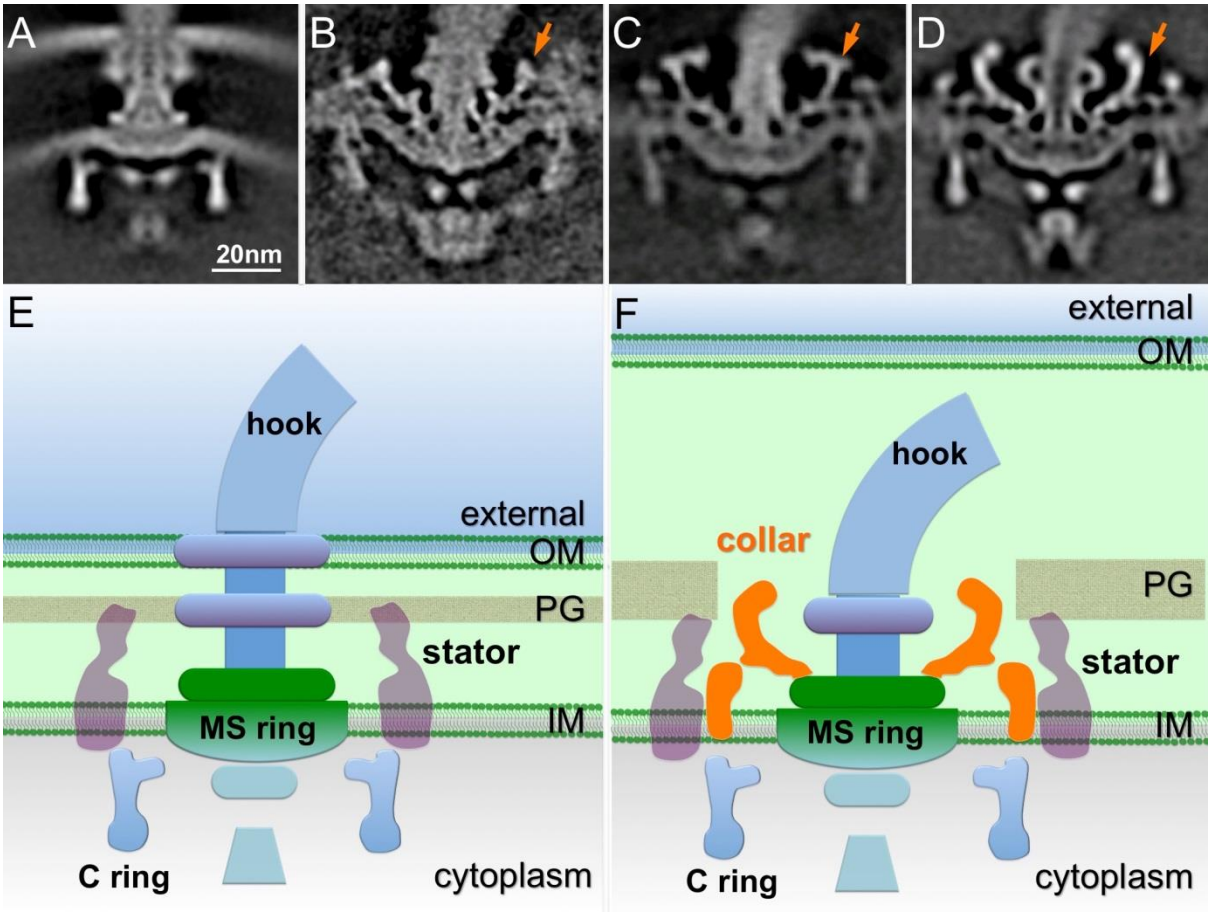
A
B
C
D
20nm
E
hook
external
OM
PG
stator
MS ring
IM
C ring
cytoplasm
F
external
OM
hook
collar
PG
stator
MS ring
IM
C ring
cytoplasm

MATERIALS AND METHODS

Bacterial strains, plasmids, and growth conditions. The bacterial strains and plasmids used in this study are listed in Table 3.1. High-passage, avirulent *B. burgdorferi* strain B31-A was used as a wild-type clone throughout the study (224, 225). Construction of a *flbB* (*bb0286*) deletion mutation was achieved as described below. *B. burgdorferi* cells were cultured in liquid Barbour-Stoenner-Kelly (BSK-II) medium, and plating BSK was prepared using 0.4% agarose (143, 227). Cells were grown at 35°C in a 2.5% CO_2 incubator as described previously (227). *E. coli* cells were grown at 30°C or 37°C in Luria-Bertani (LB) broth or LB agar (229). Antibiotics, indicators, and inducers, when required, were included in the bacterial culture medium with the following concentrations: 100 µg/ml ampicillin, 50 µg/ml kanamycin, 100 µg/ml streptomycin, 40 µg/ml gentamicin, 80 µg/ml 5-bromo-4-chloro-3-indolyl-β-D-galactopyranoside (X-gal), 0.5 mM isopropyl-β-D-thiogalactoside (IPTG).

Construction of the *flbB*-deletion mutant. Construction of the *flbB*-deletion plasmids, electroporation, and plating conditions were described previously (143, 182, 183, 227). Briefly, the 5'- (1198 bp), and 3'-flaking (432 bp) DNA of *flbB* gene were amplified by PCR from chromosomal DNA of *B. burgdorferi* strain B31-A using primers FlbB.KO.P1F (GACGATTAGAACCTACTTTCG) and FlbB.KO.P1R (TAAAATTGCTTTTAACTATTATTCACTTTCATTCC), and FlbB.KO.P2F (CGATGAGTTTTTCTAATCATTGGAGTAGTGTG) and FlbB.KO.P2R (TTGGTCCTTAGAGTCATCT), respectively. Promoter-less kanamycin resistance cassette [*Pl-kan*, 846 bp] was similarly PCR amplified from P_{flgB}-*aph1* using primers FlbB.KO.KanF (GGAATGAAAGTGAATAATAGTTAAAAGCAATTTTA) and

Table 3.1. Bacterial strains and plasmids used in this study

Strains or Plasmids	Relevant characteristics*	Reference or Source
Borrelia burgdorferi		
B. burgdorferi B31-A	B31 (ATCC 35210), the prototype strain of *B. burgdorferi* sensu stricto, originally isolated from a tick collected on Shelter Island, NY, A high passage, non-infectious clone	(224, 225)
B. burgdorferi B31-A Δ*flbB*	B31-A derived, Δ*flbB*, *Kan*^{R}	This study
B. burgdorferi B31-A GFP	B31-A derived, cp26-*P*$_{flgB}$-*gfp*, *Gent*^{R}	Lab collection
B. burgdorferi B31-A Δ*flbB*/*flbB-GFP*	B31-A Δ*flbB* derived, pBSV2G::*P*$_{flgB}$-*flbB-gfp*, *Kan*^{R} *Gent*^{R}	This study
B. burgdorferi B31-A Δ*flaB*	B31-A derived, Δ*flaB*, *Kan*^{R}	Lab collection (172)
B. burgdorferi B31-A Δ*fliL*	B31-A derived, Δ*fliL*, *Strp*^{R}	Lab collection (165)
Escherichia coli		
E. coli DH5α	Transformation host for cloning vector, F$^-$ *Φ*80d*lacZ*ΔM15, Δ(*lacZYA-argF*) U169 *recA*1 *endA*1 *hsdR*17(r_k^-,m_k^+) *phoA*, *supE*44 *thi*-1 *gyrA*96 *relA*1	Promega Inc.
E. coli BTH101	Host for BACTH system. F$^-$, *cya-99*, *araD139, galE15, galK16, rpsL1 (Strp*^{R}*)*, *hsdR2, mcrA1, mcrB1*	Euromedex Inc.
Plasmids		
pGEM-T Easy	Cloning vector for PCR product, ColE1 ori, *Amp*^{R}	Promega Inc.
pBSV2G	Shuttle vector, ColE1 ori, *Gent*^{R}	(264)
pMC2498	Suicide vector, *P*$_{flaB}$-*gfp*, *Amp*^{R}	(262, 263)

Table 3.1. Bacterial strains and plasmids used in this study (~continue)

Strains or Plasmids	Relevant characteristics*	Reference or Source
Plasmids		
pKT25	BACTH vector designated to express a given polypeptide fused in frame at its N-terminal end with T25 fragment (amino acids 1-224 of CyaA), p15A ori, *Kan*^{R}	Euromedex Inc.
pUT18C	BACTH vector designated to express a given polypeptide fused in frame at its N-terminal end with T18 fragment (amino acids 225-399 of CyaA), ColE1 ori, *Amp*^{R}	Euromedex Inc.
pKT25-zip	BACTH positive control vector, derivative of pKT25 in which the leucine zipper of GCN4 is genetically fused in frame to the T25 fragment	Euromedex Inc.
pUT18C-zip	BACTH positive control vector, derivative of pUT18C in which the leucine zipper of GCN4 is genetically fused in frame to the T18 fragment	Euromedex Inc.
Teasy::*flbB*_KO	*flbB-Pl-aph1* in pGEM-T Easy for *flbB* knockout, *Amp*^{R}	This study
pBSV2G::P_{flgB}-*flbB-gfp*	P_{flgB}-*flbB-gfp* in pBSV2G for expression of FlbB-GFP, *Amp*^{R}	This study
pKT25::*fliL*	*fliL* orf in pKT25, *Kan*^{R}	This study
pKT25::*flbB*	*flbB* orf in pKT25, *Kan*^{R}	This study
pKT25::*motA*	*motA* orf in pKT25, *Kan*^{R}	This study
pKT25::*motB*	*motB* orf in pKT25, *Kan*^{R}	This study
pUT18C::*fliL*	*fliL* orf in pUT18C, *Amp*^{R}	This study
pUT18C::*flbB*	*flbB* orf in pUT18C, *Amp*^{R}	This study
pUT18C::*motA*	*motA* orf in pUT18C, *Amp*^{R}	This study

Table 3.1. Bacterial strains and plasmids used in this study (~continue)

Strains or Plasmids	Relevant characteristics*	Reference or Source
Plasmids		
pUT18C::*motB*	*motB* orf in pUT18C, *Amp*^{R}	This study

**Kan*^{R}, kanamycin resistance; *Gent*^{R}, gentamicin resistance; *Strp*^{R}, streptomycin resistance; *Amp*^{R}, ampicillin resistance

FlbB.KO.KanR (CACACTACTCCAATGATTAGAAAAACTCATCG) (182). These three pieces of DNA fragments were linked by overlapping PCR, yielding *bb0285-Pl-kan-bb0287* (*flbB*_KO_*Pl-kan*), then cloned into the pGEM-T Easy (Promega Inc.), yielding plasmid Teasy::*flbB*_KO_*Pl-kan*. Competent B31-A cells were electroporated with *flbB*_KO_*Pl-kan* PCR amplified linear DNA. The transformants were selected with 200 µg/ml kanamycin. The kanamycin-resistant transformants were isolated and confirmed the replacement of *flbB* gene with the *Pl-kan* by PCR, and lack of FlbB protein expression was confirmed by immunoblotting as described below.

Construction of a plasmid expressing FlbB-GFP. To construct a *B. burgdorferi* strain that expresses GFP coupled with FlbB, the *flgB* promoter (P_{flgB}), and *flbB* gene were PCR amplified from chromosomal DNA of strain B31-A using primers P_{flgB}-*Bam*HI.F (GGATCCCGAGCTTCAAGGAAGATTTCC) and P_{flgB}-*flbB*.R (ATAAAAAATTATTCACATGGAAACCTCCCTCATTTAAAA), and P_{flgB}-*flbB*.F (TGAGGGAGGTTTCCATGTGAATAATTTTTTATCGTTC) and *flbB-gfp*.R (TCTTCTCCTTTACTCTCCAATGAACTAACAG), respectively (*Bam*HI restriction site is underlined). *gfp* was PCR amplified from pMC2498 plasmid using primers *flbB-gfp*.R (CTGTTAGTTCATTGGAGAGTAAAGGAGAAGA) and *gfp-Hin*dIII.R (AAGCTTCTATTTGTATAGTTCATCCATGCCATG) (*Hin*dIII restriction site is underlined) (262, 263). These three pieces of DNA fragments were linked by overlapping PCR and cloned into the pGEM-T Easy, yielding plasmid Teasy::P_{flgB}-*flbB-gfp*. This and the *B. burgdorferi* shuttle vector pBSV2G were digested with *Bam*HI and *Hin*dIII, and ligated to yield pBSV2G::P_{flgB}-*flbB-gfp* (264). Approximately 50 µg of pBSV2G::P_{flgB}-*flbB-gfp* plasmid DNA was electroporated into the Δ*flbB* mutant cells.

Transformants were selected with kanamycin and gentamicin. Resistant transformants were analyzed by PCR to confirm the presence of the pBSV2G::P_{flgB}-*flbB-gfp* plasmids in the transformants (Δ*flbB/flbB-GFP* cells). Furthermore, the expression of GFP and FlbB proteins in the Δ*flbB/flbB-GFP* cells were confirmed by immunoblotting with *B. burgdorferi* FlbB-specific polyclonal and Anti-GFP monoclonal (Roche Life Science) antibodies, respectively. Anti-FlbB was raised in rabbits which immunized with purified recombinant His_6-FlbB, as described (Alpha Diagnostic International) (165).

SDS-PAGE and immunoblot analyses. Sodium dodecyl sulfate-polyacrylamide gel electrophoresis (SDS-PAGE) and immunoblotting with an enhanced chemiluminescent detection method (GE Health Inc.) were carried out as reported previously (143, 172). The concentration of protein in cell lysates was determined by a Bio-Rad protein assay kit. Unless otherwise noted, 10 μg of lysate protein was subjected to SDS-PAGE and immunoblotting using proper antibodies.

Dark-field microscopy and measurement of colony size. Growing *B. burgdorferi* cells (2-4 $x10^7$ cells/ml) were imaged using a Zeiss Imager M1 dark-field microscope connected to a Zeiss AxioCam MRc digital camera to determine morphology. For measurement of *B. burgdorferi* colony swarm diameter, approximately 20 to 50 cells were plated on semi-solid BSK-II medium containing 0.4% agarose. Four weeks after inoculation, we measured the diameter of 20 representative colonies from each clone (265).

Confocal laser scanning microscopy. *B. burgdorferi* cells were examined with a confocal microscope (LSM 510; Carl Zeiss, Inc., Thornwood, NY, USA) using 488 nm Argon ion laser excitation and a 505-550 bandpass filter to collect GFP fluorescence

emission, with simultaneous collection of a transmitted light image using differential interference contrast (DIC) optics. Images were acquired and analyzed using Zen 2009 software (Zeiss Inc.).

Cryo-electron tomography (cryo-ET) and subtomogram averaging. Frozen-hydrated specimens were prepared as described previously (163, 190). Briefly, growing *B. burgdorferi* wild-type, Δ*flbB* mutant, and *flbB-GFP* cells were harvested at low 1,500xg speed, and suspended in 40 µl phosphate buffered saline (PBS, pH 7.4) at a final concentration of ~2 x 10^9 cells/ml. Resuspended cells were mixed with 10 nm gold clusters, then 5 µl was deposited onto freshly glow-discharged holey carbon grids for 1 min. Grids were blotted with filter paper to remove excess fluid, followed by rapid freezing in liquid ethane maintained at -180°C using a gravity-driven plunger apparatus (163, 266). The resulting frozen-hydrated specimens were imaged at -170°C using a Polara G2 electron microscope (FEI Company) equipped with a field emission gun and a K2 direct electron detector (Gatan). The microscope was operated at 300 kV with a magnification of x9,400, resulting in an effective pixel size of 4.6 Å. Using the FEI batch tomography program, low-dose single-axis tilt series were collected from each bacterium at a -6 µm defocus with a cumulative dose of ~60 $e^-/Å^2$ distributed over 60 images. Tilt angles were in the range of -60° and +60° with an angular increment of 2°. Tilt series were aligned and reconstructed using IMOD software and tomoauto (267, 268).

In total, 285 and 190 reconstructions were generated from Δ*flbB* mutant and *flbB-GFP* cells, respectively. A total of 1,742 motor sub-tomograms (256x256x256 voxels) were visually identified, then extracted from the reconstructions. The initial orientation of

each particle was estimated by the C-ring and the hook, thereby providing two of the three Euler angles. To accelerate image analysis, 4x4x4 binned sub-tomograms (64x64x64 voxels) were used for initial alignment. The original data was then used for the refinement and averaging as described previously (163, 266).

3D visualization. Reconstructions of *B. burgdorferi* cells were visualized and segmented manually using IMOD (267). UCSF Chimera, a visualization system for exploratory research and analysis, was utilized for 3-D surface rendering of sub-tomogram averages (269).

Co-immunoprecipitation (co-IP). FlbB and FliL protein-protein interactions were determined using a Dynabeads® Protein A Immunoprecipitation kit, according to the manufacture's protocol (Novex Inc.). Briefly, 36 µg of rabbit polyclonal FlbB antibodies were diluted in 600 µl of PBS with 0.01% Tween 20, and then coupled the antibody with 1.5 mg of Dynabeads. To prepare cell extracts, wild-type or Δ*flbB* mutant *B. burgdorferi* cells were harvested. Cell pellets were resuspended in PBS with 0.01% Tween 20 and then lysed by sonication. Sonicated cell extracts were centrifuged at 16,000 x g for 15 min at 4°C to remove bacterial debris. Approximately 750 µg cell extracts were incubated with FlbB antibody-conjugated Dynabeads with gentle shaking for 10 min at room temperature, and washed with 1 ml of washing buffer for four times. 50 µl of SDS loading dye was added directly to the FlbB antibody-conjugated Dynabeads after the washes, and then heated for 10 minutes in boiling water bath. The boiled samples were subjected to SDS-PAGE and immunoblotting using *B. burgdorferi* FliL-specific antibodies (165). FlbB-MotB and FliL-MotB co-IP assays were similarly performed using *B. burgdorferi* FlbB, FliL, or MotB-specific polyclonal antisera (190).

Bacterial two-hybrid system. Protein-protein interactions between FlbB and FliL were measured with the bacterial adenylate cyclase two hybrid system, according to the manufacture's protocol (BACTH; Euromedex Inc.). Briefly, *flbB* and *fliL* genes were amplified by PCR from chromosomal DNA of *B. burgdorferi* strain B31-A using primers FlbB.*Bam*HI.F (**GGATCC**CAATAATTTTTTATCG) and FlbB.*Kpn*I.R (**GGTACCCTC**CAATGAACTAAC), and FliL.*Bam*HI.F (**GGATCC**CCCTAATAAAGACG) and FliL.*Kpn*I.R (**GGTACC**CATATCAAAAATATCAATT), respectively (restriction enzyme sites are shown in bold). These DNA fragments were cloned into the pUT18C and pKT25. Both pUT18C::*flbB* (or *fliL*) and pKT25::*fliL* (or *flbB*) were co-transformed into the BTH101 *E. coli* host cell. Transformants were grown on LB plates containing X-gal, ampicillin, and kanamycin. Appearance of blue colored colonies in those plates is an indication of a positive protein-protein interaction. FliL-MotA, FliL-MotB, FlbB-MotA, and FlbB-MotB interactions were performed as described for FliL-FlbB.

Statistical analysis. A paired Student's *t*-test was used to determine statistical significance. A P-value of ≤0.05 between samples was considered significant.

RESULTS

Identification of a protein encoding the collar structure

Genomic analysis suggests that over 50 genes or 5–6% of the *B. burgdorferi* genome are potentially involved in motility and chemotaxis (138, 151). In order to identify proteins involved in the collar structure, we employed a strategy by subtracting common gene homologs that are present in other bacterial genomes especially those with externally flagellated bacteria whose motors have been determined by cryo-ET (162). To ensure that we did not overlook any gene that may share low homology but could encode a collar protein, we systematically mutated almost all genes annotated as "flagellar/motility-related" in the *B. burgdorferi* genome (138, 151) (our unpublished observation). Through these analyses, BB0286 (FlbB) was identified as a potential candidate for the collar structure. *flbB* is a spirochete-specific gene that is located within the flagellar *flgB* polycistronic operon, increasing the likelihood that this protein may encode for a flagellar gene (138, 270, 271). FlbB is a small protein (205 a.a.) that possess a transmembrane domain at its N-terminal end and shares no significant amino acid sequence identity with proteins from non-spirochetal bacteria (data not shown; see below).

Δ*flbB* mutant cells are rod-shaped and non-motile

We deleted the *flbB* gene by using a promoter-less kanamycin resistance cassette that results in nonpolar mutations (Fig. 3.2.A) (181-183). PCR analysis of the kanamycin-resistant *B. burgdorferi* clones confirmed the deletion of the *flbB* (data not shown). Immunoblotting with anti-FlbB antisera indicated that FlbB protein synthesis

Figure 3.2. Construction of Δ*flbB* mutant and determination of polar effect on downstream genes expression. (A) Schematic diagrams of wild-type and Δ*flbB* mutant genomes. *flaB* gene (*bb0147*) is separated from the targeted *flbB* gene (*bb0286*) by approximately 100 kb. Inactivation of *flbB* gene using the *pl-aph1* cassette is described elsewhere (182, 183). Wild-type *B. burgdorferi* with *flgB* polycistronic operon is shown (top). The *pl-aph1* cassette replaced with *flbB* gene by allelic exchange (bottom) (182). The model lists only a few of the 26 genes in the *flgB* operon, and other genes are indicated by the multiple arrowheads. **(B)** Confirmation of *flbB* gene inactivation and determination of polar effect by Western blotting. Wild-type and Δ*flbB* mutant cell lysates were subjected to SDS-PAGE (left) and transferred to a PVDF transfer membrane for immunoblot analysis (right). Immunoblots were performed with *B. burgdorferi* FlbB, FlgE, MotB, FliL, or FlaB-specific antibodies. DnaK was used as a loading control.

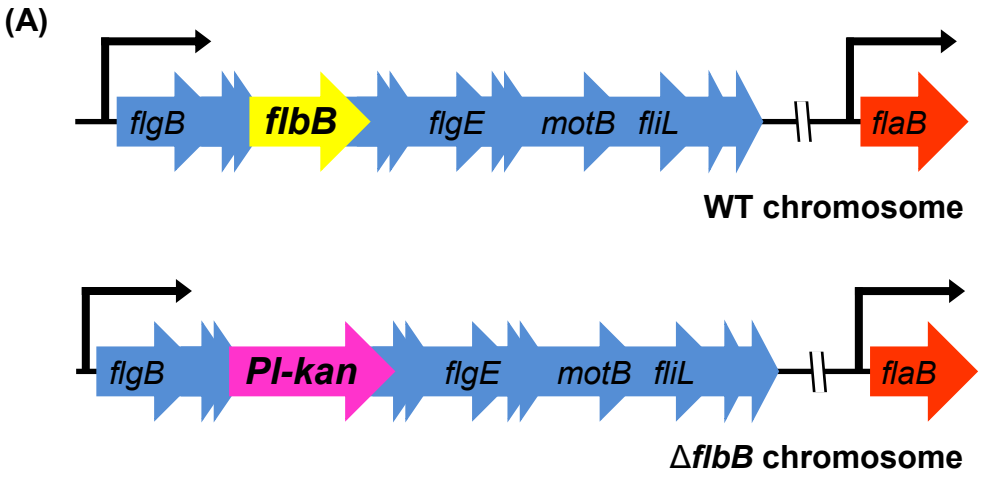
(A)
flgB
flbB
flgE
motB
fliL
flaB
WT chromosome
flgB
Pl-kan
flgE
motB
fliL
flaB
ΔflbB chromosome

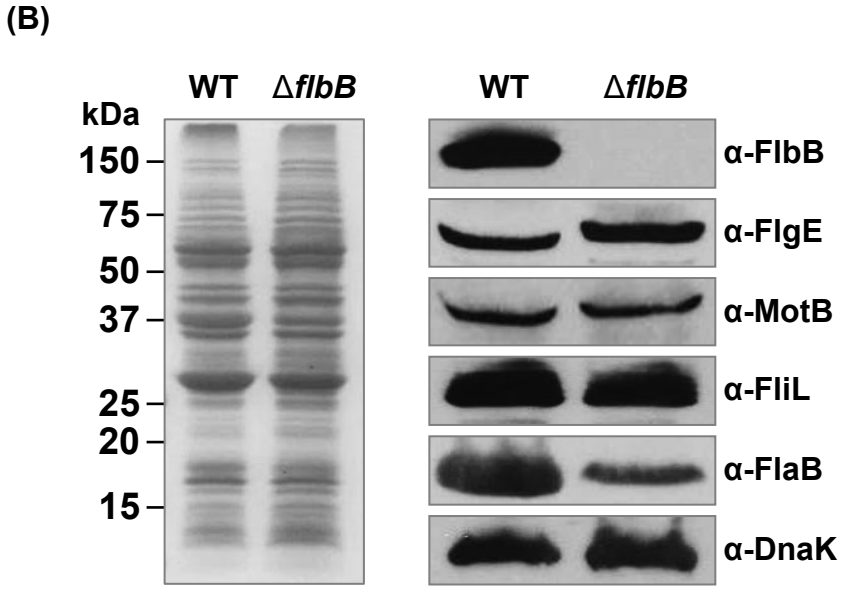
(B)
WT
ΔflbB
kDa
150
75
50
37
25
20
15
WT
ΔflbB
α-FlbB
α-FlgE
α-MotB
α-FliL
α-FlaB
α-DnaK

was inhibited in the Δ*flbB* mutant cells; yet, expression of proteins encoded by genes downstream of *flbB*, i.e., *flgE*, *motB*, and *fliL*, were not altered in the mutant cells compared to the wild-type *B. burgdorferi* (Fig. 3.2.B). This suggests that the mutant phenotype is due solely to loss of *flbB* function (see below). Although the mutant did not exhibit a polar effect on downstream genes expression, we attempted to complement the Δ*flbB* mutant both *in cis* (genetic recombination) and *in trans* (using a shuttle vector). While multiple attempts to genetically complement the Δ*flbB* mutant have failed, we report our findings with the mutant as others have done in the past (165, 237, 272-277).

Dark-field microscopy and swarm plate assays were used to assess cell morphology and motility of Δ*flbB* cells (227, 265). These measurements indicated that the mutant cells are non-motile and display a rod-shaped morphology (Fig. 3.3), despite the synthesis of periplasmic flagella, FlaB, albeit at a reduced level compared to the wild-type (Fig. 3.2.B). Furthermore, swarm plate motility assays indicate that the mutant cells produced colony diameters that are significantly smaller than the wild-type cells (~1 mm vs. ~6 mm swarm produced by the wild-type; Fig. 3.3.B). The morphology and motility phenotypes of the Δ*flbB* mutant cells are similar to the non-motile, rod-shaped Δ*flaB* mutants that lack flagellar filaments (143, 172). Taken together, our results indicate that FlbB is important for morphology and motility of *B. burgdorferi*.

Δ*flbB* mutant displays abnormal periplasmic flagellar orientation

Previous studies showed that periplasmic flagella are crucial not only for motility but also for the cellular flat-wave morphology of *B. burgdorferi* (143, 172). Because the

Figure 3.3. Morphology and motility phenotype of the Δ*flbB* mutant cells. (A) Dark-field microscopic images showing the distinct rod-shaped morphology of Δ*flbB* spirochetes (right) whereas the wild-type (WT) cells exhibit a flat-wave morphology (left). Growing *B. burgdorferi* cells were visualized using a dark-field microscope (40x) and images were captured using a digital camera. The mutant cells were also non-motile. **(B)** Swarm plate motility assays in 0.4% agarose. Δ*flbB* mutant cells display significantly reduced swarm diameter compared to wild-type cells. Individual colony's swarm ability was measured four weeks after inoculation. The colony size of each clone is measured in millimeters. Non-motile Δ*flaB* mutant was used as a control (172). Statistical analysis was performed by using Student's *t*-test. P-values between samples are shown at the top.

(A)

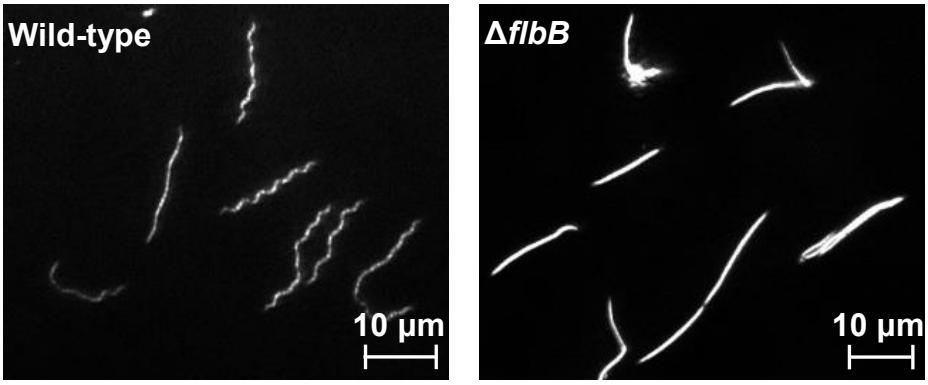
Wild-type
10 µm
ΔflbB
10 µm

(B)

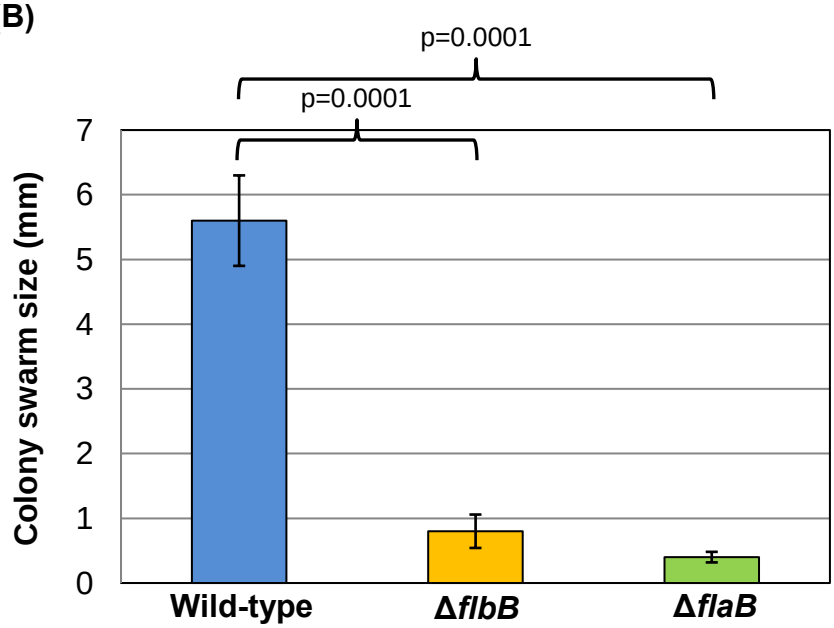
p=0.0001
p=0.0001
Colony swarm size (mm)
0
1
2
3
4
5
6
7
Wild-type
ΔflbB
ΔflaB

Δ*flbB* mutant cells synthesize periplasmic flagella but are rod-shaped, we investigated the basis of those defects using cryo-ET (Fig. 3.4). Our reconstructions of the native cellular structures shown in Figures 3.4.C and D indicate that the wild-type periplasmic flagella form ribbon-like structures that are oriented inwards toward the center of the cell. In contrast, the mutant's periplasmic flagella are short and the flagellar ribbon is distorted. Most striking and opposite to wild-type, Δ*flbB* flagella are oriented abnormally toward the cell pole (compare Figs. 3.4.A-B with 3.4.C-D). In fact, the majority of periplasmic flagella (82% vs. 1-2% in the wild-type) are found to be abnormally oriented toward the cell pole in the mutant cells (Table 3.2). These results indicate that FlbB is essential for normal orientation of periplasmic flagella (toward the cell body).

The collar structure is absent in the Δ*flbB* mutant cells

We compared the motor structures in wild-type and the Δ*flbB* mutant cells by cryo-ET and found that the collar structure is absent from the mutant's periplasmic flagella (Figs. 3.5.A, B). To reveal the motor structure in detail, we used subtomogram averaging to analyze approximately 1000 motor structures extracted from tomographic reconstructions. The averaged structure reveals major features of the flagellar motor, such as the export apparatus, the C-ring, the MS-ring, the rod, and the P-ring (Fig. 3.5.C). These major features of the wild-type motor are also detected in the Δ*flbB* motor (Fig. 3.5.D). However, a large portion of densities surrounding the central rod and the P-ring are absent in the Δ*flbB* motor (Fig. 3.5.D). Specifically, the Δ*flbB* motor lacks the collar structure detected in wild-type cells (compare Figs. 3.5.C, E with 3.5.D, F).

By comparing structures from a deletion mutation in *motB* (J. Liu and M. Motaleb-

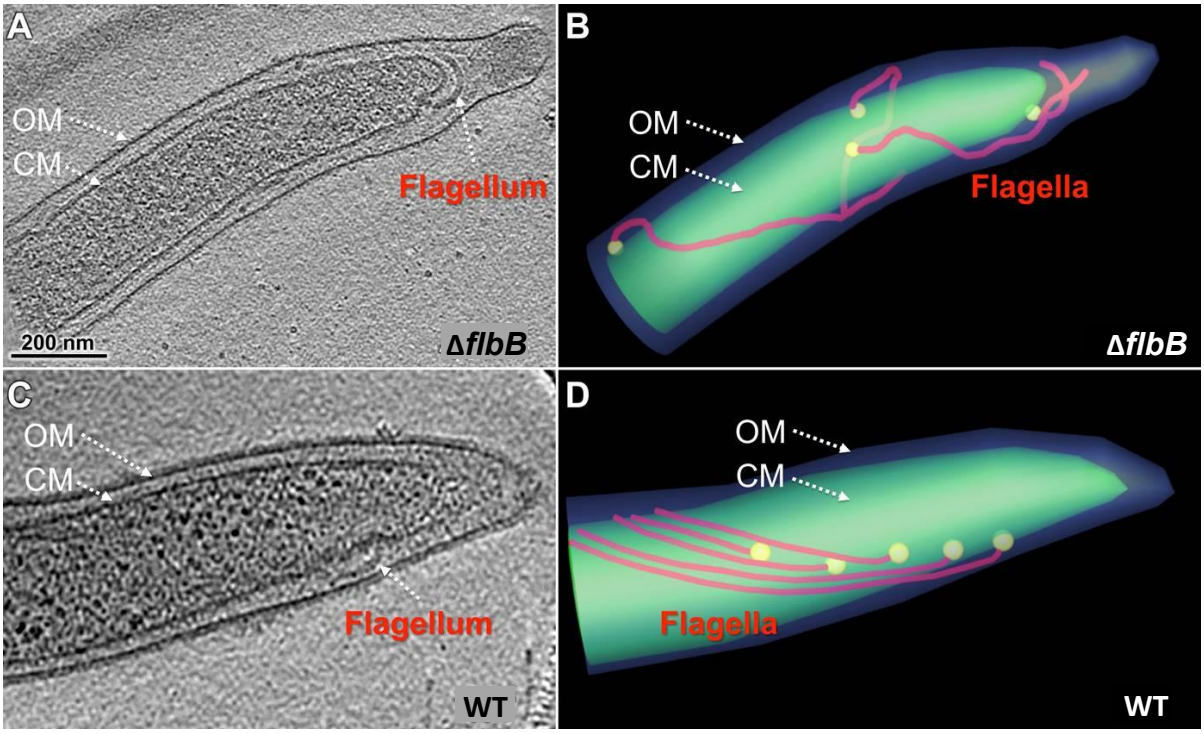

Figure 3.4. Periplasmic flagellar orientation in wild-type and Δ*flbB* mutant. (A) A representative tomographic slice of a Δ*flbB* cell showing that the periplasmic flagella are abnormally oriented toward the cell pole. **(B)** A cartoon model of the Δ*flbB* mutant shown in (A) clearly illustrated the abnormal tilting of the flagella. **(C)** A representative tomographic slice of a WT cell showing the periplasmic flagella that are extended toward the cell body but not the cell pole. **(D)** A cartoon model of the WT cell showing the normal orientation of the flagella toward the cell body.

Table 3.2. Δ*flbB* mutant cells periplasmic flagella are oriented abnormally toward the cell pole

Strain	No. of cells analyzed	No. of irregular periplasmic flagella*	No. of normal periplasmic flagella+	% irregular periplasmic flagella
Wild-type	43	5	288	1.7
Δ*fliL*	41	55	208	21
Δ*flbB*	44	144	32	82

*Irregular periplasmic flagella were tilted toward the cell pole.

+Normal periplasmic flagella were tilted toward the cell body. Δ*fliL* mutant was used as a reference strain (165).

Figure 3.5. Comparative analysis of *in situ* flagellar motors from wild-type and Δ*flbB* reveals the 3D collar structure for the first time. (A) A tomographic section from a WT cell shows the motors that are embedded in the cytoplasmic inner membrane (IM/CM). **(B)** A tomographic section from a Δ*flbB* cell shows a motor that is embedded in the cytoplasmic membrane. **(C)** The central section (left) and schematic diagram (right) of the WT flagellar motor. **(D)** The central section (left) and schematic diagram (right) of the Δ*flbB* flagellar motor. **(E)** The surface rendering of the 3D averaged WT and **(F)** Δ*flbB* motor structures are shown in side view. **(G)** The surface rendering of the 3D averaged WT motor structure is shown in tilted top view (90°). Compared to the motor structures from WT (C, E, G), the Δ*flbB* motor lacks the entire collar (blue), the stator (orange-red), and FliL (pink) structures. Noticeably, the collar is a large and complex structure comparing to FliL and the stator. OM, outer membrane; PG, peptidoglycan layer; P, P-ring; R, central rod; exp, export apparatus.

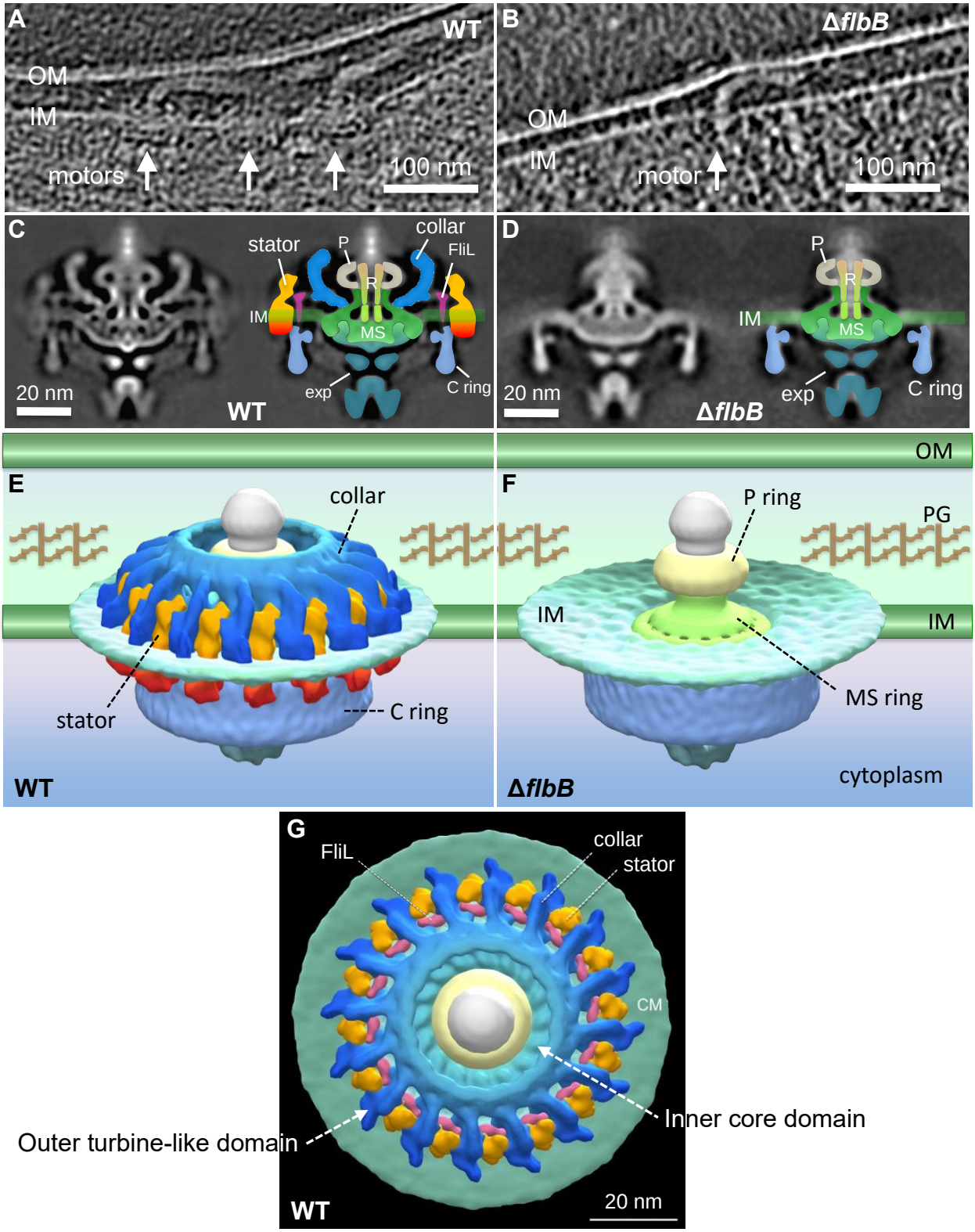
A
WT
OM
IM
motors
100 nm
B
ΔflbB
OM
IM
motor
100 nm
C
stator
P
collar
FliL
R
IM
MS
exp
C ring
20 nm
WT
D
P
R
IM
MS
exp
C ring
20 nm
ΔflbB
OM
E
collar
stator
C ring
WT
F
P ring
PG
IM
IM
MS ring
cytoplasm
ΔflbB
G
FliL
collar
stator
CM
Outer turbine-like domain
Inner core domain
WT
20 nm

unpublished), *fliL* (165), and the current Δ*flbB* strain, we were able to define the 3D structure of the collar and the stator (Figs. 3.5.E, G). The overall dimension of the collar is ~71 nm in diameter and ~24 nm in height. This unique structure consists of two major layers along the radial direction—for clarity, labeled here as the inner core domain and the outer turbine-like domain (Fig. 3.5.G). The inner domain of the intact collar appears to consist of 16 truss-like subassemblies joined together to form a chamber-like structure that surrounds the rod and the P-ring (Figs. 3.5.E, G). FliL is attached to each subassembly at the membrane region (Figs. 3.5.C, G). The outer domain—the sixteen extended "turbine blades"—is the most distinct feature appearing in the spirochetal flagellar motor. Sixteen stator units are inserted between two adjacent "turbine blades", forming a stator ring that packs around the C-ring in the cytoplasm (Figs. 3.5.E, G). Furthermore, the stator (MotA-MotB) and FliL structures are also disappeared in the mutant even though MotB and FliL proteins are stably expressed at wild-type levels, suggesting that FlbB/collar is important for the assembly of those flagellar structures (compare Figs. 3.5.C, E with 3.5.D, F). Together, our cryo-ET data indicate that FlbB is essential for the formation of the collar structure and the assembly or stability of FliL and the stator.

FlbB—FliL interactions

As shown above, majority of Δ*flbB* mutant's periplasmic flagella are abnormally tilted toward the cell pole. Interestingly, we observed a similar phenotype with our Δ*fliL* mutant cells (Table 3.2) (165). These results led us to predict that (a) FlbB and FliL proteins interact and direct the periplasmic flagella to orient toward the cell body but not the cell pole; (b) FlbB and FliL are located in close proximity to each other; and (c)

FlbB/collar is assembled before FliL and the stator because the FliL and stator structures are not assembled in the Δ*flbB*. To determine if FlbB interacts with FliL, we performed co-immunoprecipitation (co-IP) assays with wild-type and Δ*flbB* cell extracts. Our co-IP data indicate that FlbB specifically interacts with FliL (Fig. 3.6.A). The FlbB-FliL binding is verified further by using an alternative bacterial two-hybrid assay (BACTH). Our two-hybrid assays also confirmed that FlbB interacts with FliL (Fig. 3.6.B). These FliL-FlbB interaction results suggest that FlbB is located adjacent to the FliL, near the base of the collar structure (see below).

Our motor structures show that the periplasmic domain of the stator is adjacent to the collar and that the stator structure is missing in the Δ*flbB* (Fig. 3.5). To test if there is any interaction between the stator and FlbB, and this interaction is important for the assembly of the stator, we performed co-IP and BACTH assays, as described above. Using these assays, we failed to detect any FlbB-MotA or FlbB-MotB interaction (data not shown), indicating that FlbB is not directly interacting with the stator and supporting our proposal that FlbB is just a small part of the collar that is located at its base (below).

Localization of FlbB by GFP fusion

To determine the location of FlbB in the periplasmic flagella, the gene encoding GFP was fused at the 3'-end of *flbB* (*flbB-gfp*) and then ligated such that *flgB* promoter drives the expression of *flbB-gfp* (P_{flgB}-*flbB-gfp*) from the shuttle vector pBSV2G. The placement of *gfp* at the 3'-end of *flbB* is suitable for the expression of FlbB-GFP since the N-terminal region (7-29 amino acid residues) of FlbB is found to possess a transmembrane domain using TMHMM Server, ver. 2.0 (Fig. 3.7) (278, 279).

Figure 3.6. FlbB directly interact with FliL. (A) A co-IP assay showing the interaction between FlbB and FliL. FlbB-specific antibody conjugated with Dynabeads was incubated with wild-type or Δ*flbB* cell extracts. The proteins that were immunoprecipitated with the FlbB-antibody were separated using a gel, transferred to a PVDF-membrane, and subsequently, the membrane was blotted with anti-FliL (165). FliL proteins are co-precipitated with *B. burgdorferi* wild-type cell extracts (lane 1), but not with Δ*flbB* mutant extracts (lane 2). PBS buffer was used as a negative control (lane 3). To check for the non-specific protein binding on Dynabeads, we used empty Dynabeads (no Ab/antisera) in the co-IP with wild-type extracts (lane 4). Arrowheads indicate the positions of antibody heavy chain (~55 kDa), light chain (~25 kDa), or FliL (~20 kDa). Lane numbers are shown at the bottom of the figure. **(B)** BACTH assays showing the interaction between FlbB and FliL, and self-interactions of FlbB-FlbB or FliL-FliL. *E. coli* cells harboring *flbB* or *fliL* gene in the vector pUT18C or pKT25 was transformed on a plate containing X-gal. Appearance of blue colored colonies indicate a positive protein-protein interaction. (**-**), negative control; (+), positive control; 1, pUT18C::*flbB*—pKT25::*fliL* co-transformant; 2, pUT18C::*fliL*—pKT25::*flbB* co-transformant; 3, pUT18C::*fliL*—pKT25::*fliL* co-transformant; 4, pUT18C::*flbB*—pKT25::*flbB* co-transformant.

(A)

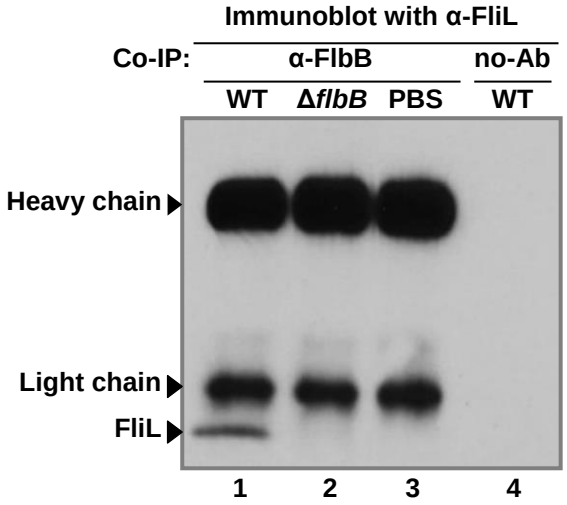

(B)

BACTH system showing FlbB-FliL interactions

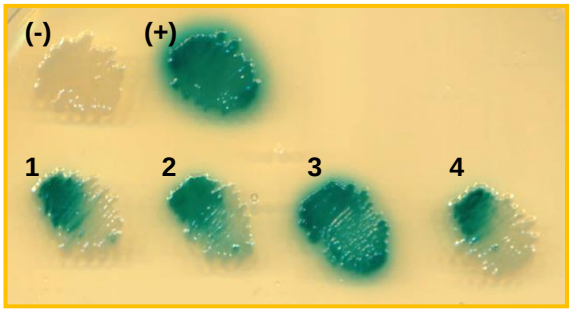

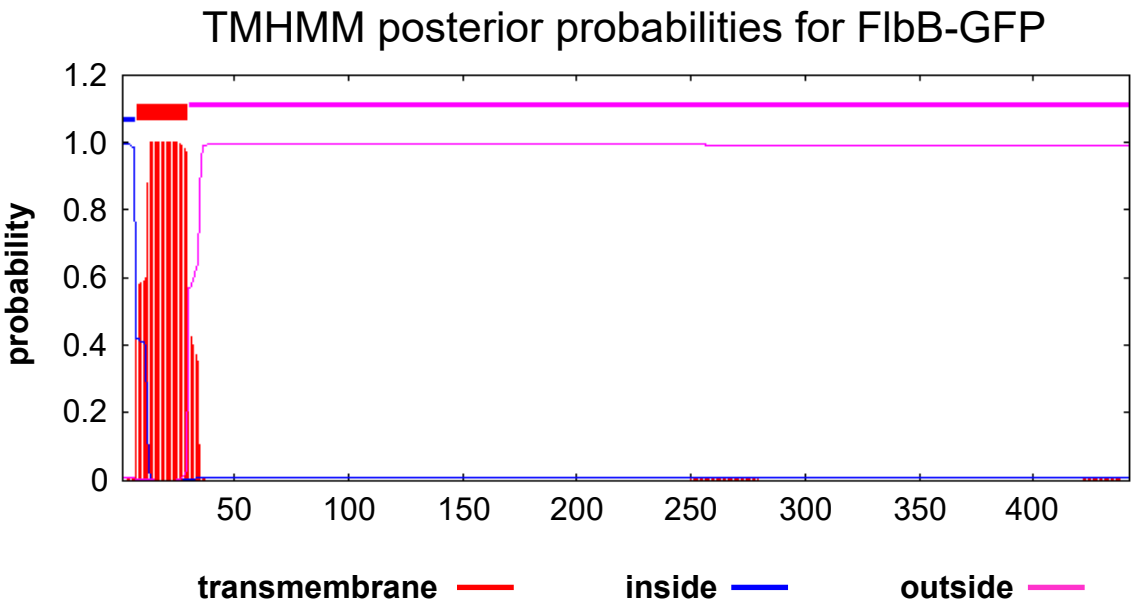

FlbB-GFP full-length: 442 a.a. (FlbB 1-205/GFP 206-442)
FlbB-GFP No. of predicted transmembrane (TM) helix: 1

FlbB-GFP TMHMM2.0 inside	1-6 a.a.
FlbB-GFP TMHMM2.0 TM helix	7-29 a.a.
FlbB-GFP TMHMM2.0 outside	30-442 a.a.

Figure 3.7. Transmembrane domain prediction of FlbB-GFP fusion protein.

FlbB possesses a transmembrane domain as predicted by TMHMM Server ver. 2.0 software with default options. Predicted transmembrane region is indicated by red box (7-29 amino acid residues). FlbB-GFP amino acid sequence was used for the prediction.

Subsequent introduction of pBSV2G::P_{flgB}-*flbB-gfp* into Δ*flbB* mutant cells resulted in expression of FlbB-GFP, as confirmed by immunoblotting using anti-GFP and anti-FlbB (not shown). Confocal microscopy shows the FlbB-GFP clusters at ~73% of the cell tips of the Δ*flbB*/pBSV2G::P_{flgB}-*flbB-gfp* cells where motors are typically located (Δ*flbB/flbB-GFP* cells; Fig. 3.8, middle). As expected, this pattern (FlbB-GFP clusters) was not observed in the wild-type cells expressing only GFP using pBSV2G::P_{flgB}-*gfp* plasmid (wild-type GFP; Fig. 3.8, left) or in the Δ*flbB* mutant negative control cells that does not express GFP (Fig. 3.8, right).

To conclusively determine FlbB location, cryo-ET and subtomogram averaging were utilized to visualize the motor structure of the Δ*flbB/flbB-GFP* cells. Compared to the cellular density of Δ*flbB* motor, the Δ*flbB/flbB-GFP* motor shows extra densities near the basal body MS-ring structure as shown in Figure 3.9, suggesting the location of FlbB-GFP. Together, these data imply that FlbB proteins are located at the base of the collar and they are anchored to the cytoplasmic membrane to form the base for the assembly of the collar complex.

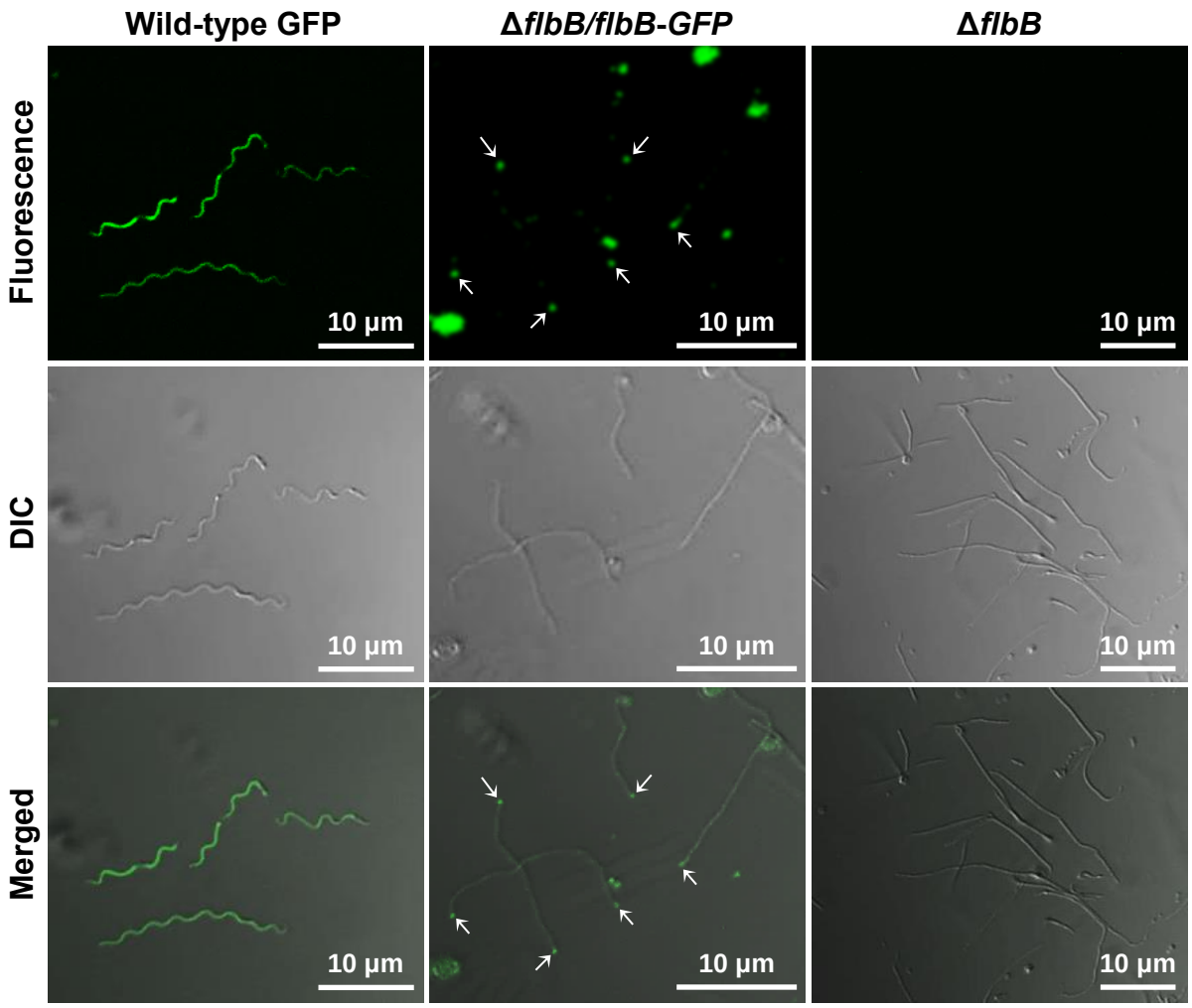

Figure 3.8. Expression and location of FlbB-GFP in *B. burgdorferi*. Confocal microscopy showing the fluorescence (top), *differential interference contrast* (DIC; middle), and merged (bottom) micrographs of the wild-type GFP, Δ*flbB*/*flbB-GFP*, and Δ*flbB* cells at 64x. The white arrows indicate the location of FlbB-GFP in the Δ*flbB*/*flbB-GFP* cell tips (FlbB-GFP clusters were detected in approximately 73% cells tips). Even distribution of the GFP signal was observed throughout the wild-type GFP cells, as expected.

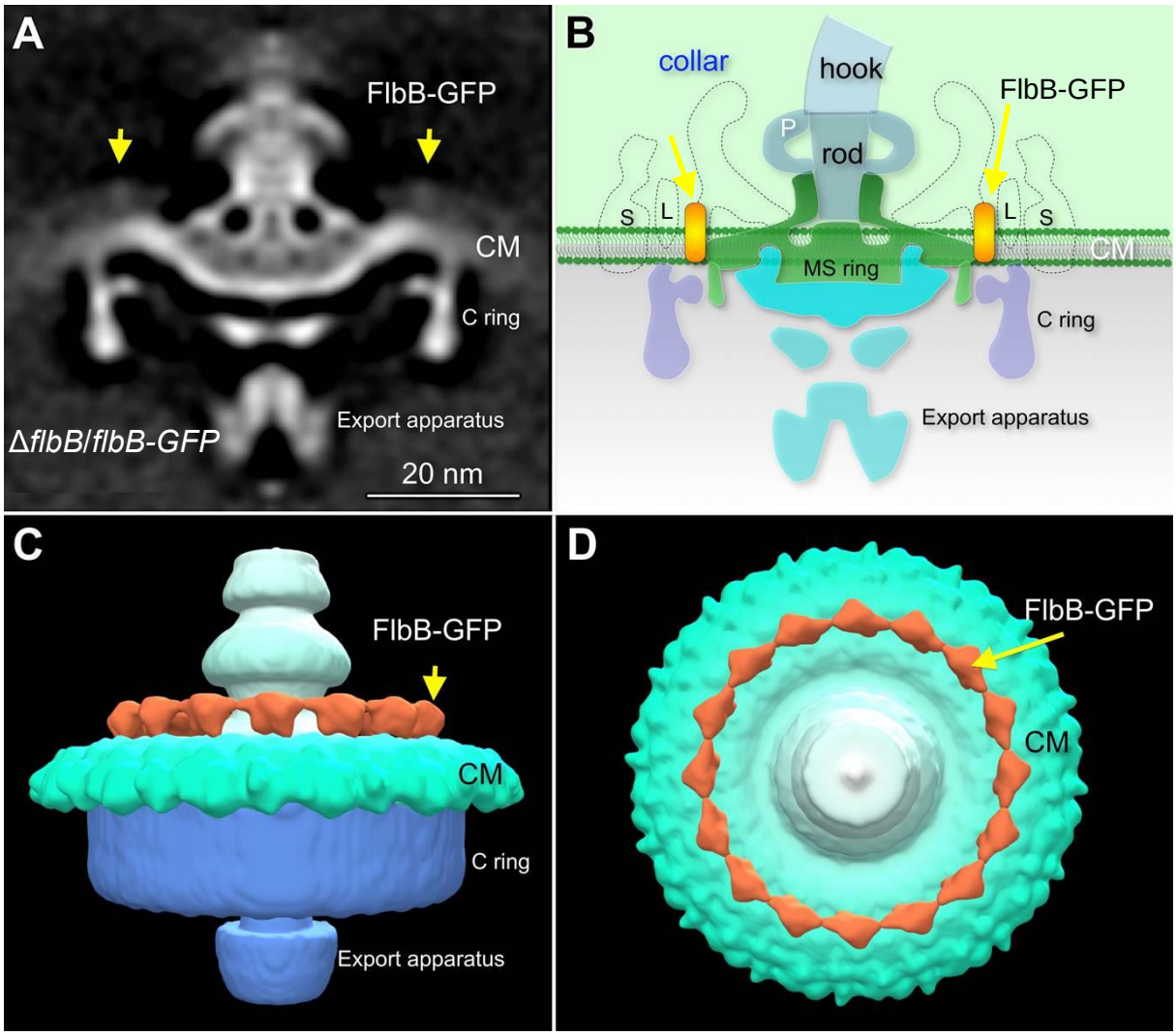

Figure 3.9. Location of FlbB-GFP as determined by cryo-ET. (A) The averaged 3D motor structures of the Δ*flbB*/*flbB-GFP* cells, and **(B)** schematic diagram of the Δ*flbB*/*flbB-GFP* flagellar motor illustrating the location of FlbB at the base of the collar. **(C)** Three dimensional isosurface rendering of the Δ*flbB*/*flbB-GFP* flagellar motor is shown in side view. **(D)** Three dimensional isosurface rendering of the Δ*flbB*/*flbB-GFP* flagellar motor is shown in tilted (top) view. The yellow arrows indicate the location of FlbB-GFP. S, stator; L, FliL; P, P-ring; CM, cytoplasmic membrane.

DISCUSSION

Despite the fact that periplasmic flagellar motility is crucial for host colonization or disease production by the spirochetes including *B. burgdorferi*, there is still very limited knowledge about what genes encode for the spirochete-specific flagellar components. FlbB identified as a collar protein in this communication has profound effects in motility, morphology, orientation of periplasmic flagella, and assembly of motor proteins. The Δ*flbB* mutant cells are rod-shaped and non-motile despite the possession of periplasmic flagella (Figs. 3.2, 3.3, and 3.4), however, those flagella are inactive due to their missing stators (Figs. 3.5.D, F). Stator proteins use proton flux to produce torque in order for the flagella to rotate, which in turn enables the organism to translocate. Because the periplasmic flagella are oriented abnormally and their stators are missing, it was obvious that those *B. burgdorferi* mutant cells exhibited rod-shaped and non-motile phenotypes. However, the number of periplasmic flagella or level of flagellar filament FlaB protein is reduced in the mutant compared to the wild-type cells (Fig. 3.1.B). The *flaB* gene is not genetically linked with the targeted *flbB* or other genes in the *flgB* operon. However, we observed this reduced FlaB protein synthesis or fewer flagellar filaments not only in Δ*flbB* but also in other non-motile mutants such as Δ*motB* (190). These observations suggest that the stator or collar-stator is important for the wild-type level of periplasmic flagellar filament synthesis in *B. burgdorferi*.

One of the most remarkable findings here is the abnormal orientation of flagella in the Δ*flbB* mutant (Fig. 3.4 and Table 3.2). Normal orientation of the flagella toward the cell body and not the cell pole is critical in producing the wild-type spirochete's wave-like morphology and smooth swimming (Figs. 3.3 and 3.4) (165). We have

previously reported that FliL is partially responsible for determination of flagellar orientation (165). As shown in Figure 3.4 and Table 3.2, 82% of the flagella in the Δ*flbB* are abnormally oriented. Thus, based on Δ*flbB* and Δ*fliL* flagellar orientation phenotypes as well as protein-protein interaction data shown in Figure 3.6, we propose that FlbB/collar—FliL structures enforce the periplasmic flagella to orient toward the cell body—an observation that has never been demonstrated in any spirochete. We, however, postulate that this irregular periplasmic flagellar phenotype associated with the mutant is a combined effect of collar-stator-FliL rather than just the FlbB/collar since the stator and FliL structures were diminished along with the collar (in the Δ*flbB* mutant). Moreover, it is important to note that the Δ*flbB* mutant was not complemented. Thus, the phenotypes observed with the mutant could be due to a secondary mutation elsewhere in the genome rather than just because of the deletion of *flbB* even though the mutant is non-polar (Fig. 3.2.B).

The stator and FliL structures were not present in the mutants despite the synthesis of MotB and FliL proteins at the wild-type levels (Figs. 3.2 and 3.5.D, F), indicating that those structures were not assembled due to the lack of the collar structure. It is noteworthy to mention that the collar structure is intact in our Δ*motB* (J. Liu and M. Motaleb-unpublished) or Δ*fliL* mutants (165). Furthermore, the stator is intact in the Δ*fliL* mutant—a very good indication that FliL and stator structures were diminished not because of a secondary alteration or polar effect (165). These results also suggest that the collar is assembled before FliL or the stator. Moreover, FliL and stator structures were not assembled in the Δ*flbB* likely because the collar provides the stability/foundation for those two motor structures similar to what was observed with the

flagellar filament proteins, FlaA and FlaB. FlaA and FlaB proteins interact and we found that unless the filament FlaB is synthesized and assembled, FlaA protein is not assembled in the Δ*flaB* (143, 172).

In *E. coli* or *Salmonella typhimurium*, FliL was reported to interact with the stator (280). However, we could not detect any interactions between FliL-MotA, FliL-MotB, FlbB-MotA, or FlbB-MotB. These results suggest that FliL or FlbB may not interact with the stator directly. Alternatively, our BACTH vectors (pKT25 and pUT18C) could not express MotA or MotB properly or our co-IP reaction conditions were not optimized. However, in *Rhodobacter sphaeroides*, FliL is able to interact with itself but not with the MotB leading to the proposal that FliL may participate in coupling with the flagellar stator in an indirect manner (256). Moreover, in *Vibrio alginolyticus,* FliL was suggested to interact with the stator directly or indirectly (261). Subsequently, we propose that *B. burgdorferi* FliL (or FlbB/collar) interacts with the stator indirectly using a yet to be identified protein(s) which is important for the assembly of the stator.

It is noteworthy that the full collar structure was not assembled in the Δ*flbB* cells expressing FlbB-GFP (Fig. 3.9), and morphology and motility phenotype were also not restored in those cells (not shown). This result is not surprising because in order for the collar structure or function to be restored in the Δ*flbB*, the FlbB-GFP protein's stoichiometry should be the same as that of other collar proteins since most motor complexes maintain a ratio (such as the FliG:FliM:FliN protein copies in a switch complex are 34:34:100, and MotA:MotB ratio is 4:2 in a stator complex) (281-283). When GFP or mCherry was fused with flagellar motor MotA or MotB or their homologs, assembly and/or function was reported to be abolished in other bacteria (284, 285).

The collar is a colossal structural component of the periplasmic flagella. It is noticeably larger than the C-ring or stator (Fig. 3.5). Considering that the C-ring is composed of three proteins (FliG, FliM, and FliN), the collar is likely comprised of multiple proteins. FlbB is a small protein (205 amino acids) that is comparable to its binding partner FliL (178 amino acids) or MotB (260 amino acids). FliL appears to form a small and elongated structure right next to the edge of the collar (Figs. 3.5.C, G) (165). Therefore, we propose that FlbB is arranged in a small structure at the base of the collar by embedding in the cytoplasmic membrane using its transmembrane domain (Figs. 3.7 and 3.9). Other (unidentified) collar proteins are expected to assemble onto the FlbB base. As such, deletion of *flbB* had a dramatic effect on the entire collar, and thus, its associated structures are not assembled in the Δ*flbB*.

Altogether, our data demonstrate that the collar is a highly complex structure that has profound impacts in *B. burgdorferi*. Importantly, we show for the first time that FlbB assembles around the flagellar basal body and plays critical roles in collar formation. Furthermore, we provided the first 3D structure of the collar and revealed its unprecedented complexity. Moreover, we show that FlbB and FliL are crucial for normal orientation of periplasmic flagella.

CHAPTER FOUR: SUMMARY AND FUTURE DIRECTIONS

Borrelia burgdorferi is the causative agent of Lyme disease, which is the most prevalent vector-borne illness in the United States and Europe (1, 31). The disease is caused by at least three genospecies of bacteria in humans; *B. afzelii*, *B. garinii*, and *B. burgdorferi* sensu stricto (7). Among these, only *B. burgdorfei* sensu stricto causes Lyme disease in North America (1). This organism is an obligate parasite, and cycles between the *Ixodes* ticks and mammalian hosts in the nature. It is transmitted to mammalian hosts through the bite of a spirochete-infected tick (2, 3, 286). Completion of the enzootic cycle requires that *B. burgdorferi* not only traverse through dense and complex tissues within the tick to migrate from the midgut to the salivary glands, where they are transmitted to the next host during tick feeding (2, 143, 287), but also that *B. burgdorferi*, after being deposited into the dermis of a mammalian host, navigate the intracellular matrix, to the circulatory system of the host, and disseminate to distant organs, such as tibiotarsal joints, bladder, heart, and the nervous system, to produce various clinical manifestations (2, 143, 287, 288). The spirochete must complete these tasks all by simultaneously detecting what environment it is in, where it needs to go, and evading the immune systems of both hosts. Indeed, motility is shown to be absolutely required for migration of *B. burgdorferi* from skin to the distant tissues, for persistent infection in mice, transmission from the tick vector to the murine host, and optimal survival in the ticks (143, 190, 289). In addition, chemotaxis activities are important for successful completion of the enzootic life cycle of Lyme disease in order to allow the spirochetes to navigate from the mouse into the larval tick, during dissemination as well as from the nymphal tick into the mouse during transmission (189, 209).

Chapter 2 of this dissertation describes: 1) the biochemical roles of CheD in *B. burgdorferi*; 2) the role of *cheD* in *B. burgdorferi* motility and chemotaxis; and 3) defines the functions of *cheD* in the infectious life cycle of *B. burgdorferi*.

Specifically, we have shown that CheD directly interacts with two of the five chemoreceptors, MCP3 and MCP4. However, CheD failed to deamidate those two chemoreceptors under various conditions tested. Since CheD is able to interact with those MCPs, we assume it can also deamidates MCP3-4 if the reaction conditions are optimized. Although not tested, we postulate that CheD is able to interact and deamidate the other MCPs (MCP1-2) since these two MCPs also possess the CheD substrate sites. These assays can further our understanding of the complex chemotaxis signalling pathways in *B. burgdorferi*. Most interestingly, ligands for these receptor MCPs have not yet been identified. It is tempting to speculate that some of the receptors initiate chemotaxis signalling by engaging tick-specific ligands whereas others are activated by the mammalian host-specific nutrients. In support of this proposition, we found that Mother Nature has offered the spirochete two distinct chemotaxis signalling pathways (CheA1-CheY2 and CheA2-CheY3). It will be interesting to see if these predictions turn out to be true.

We have shown experimental evidence that CheD enhances the CheX-type phosphatase. In other bacteria, such as *B. subtilis*, CheD enhances CheC phosphatase, and these CheC-type of phosphatases are monomers that possess two CheY-P dephosphorylation sites (205, 206), whereas CheX is a dimer containing only one dephosphorylation site (206, 222, 223, 244). To better understand how CheD stimulates CheX activity, X-ray co-crystal of CheD-CheX can be obtained to demonstrate the

differences between CheD-CheC and CheD-CheX interactions. This CheD-CheX structural analysis may provide some idea as to how CheD enhances CheX-type of phosphatases.

Additionally and most importantly, we show for the first time that the *cheD* mutant displayed significantly attenuated infectivity in mice, and reduced viability in ticks. We also show the CheD does not play an important role in the acquisition and transmission of *B. burgdorferi* during the enzootic cycle; however, it is important to the survivability of *B. burgdorferi* within mammalian and tick hosts (Fig. 4.1). This *in vivo* phenotype is consistent with our hypothetical model (Fig. 2.9). We propose that in the *cheD* mutant, CheX is still intact but is less active due to the deletion of the enhancer CheD. Consequently, dephosphorylation of CheY-P by CheX still occurs but is delayed. This reduced infectivity of the *cheD* mutant makes sense in relation to the *cheX* mutant, which is deficient in chemotaxis and is unable to establish an infection in mice.

Interestingly, the *cheX* mutant can survive normally in ticks (unpublished data) whereas the *cheD* mutant shows reduced viability. This reduced viability of the *cheD* mutant in tick host is still unclear. We postulate that this phenotype is likely linked to the MCP deamidation by CheD. This MCP modification by the CheD may involve in the *B. burgodorferi* survivability in tick hosts.

It is noteworthy that the *cheD* mutant cells are able to establish an infection through transmission by ticks without any defect. However, the *in vitro* cultured *cheD* mutant displayed reduced virulence via needle inoculation. The reason for this discrepancy is that the host-adapted spirochetes display a hyper-virulent phenotype

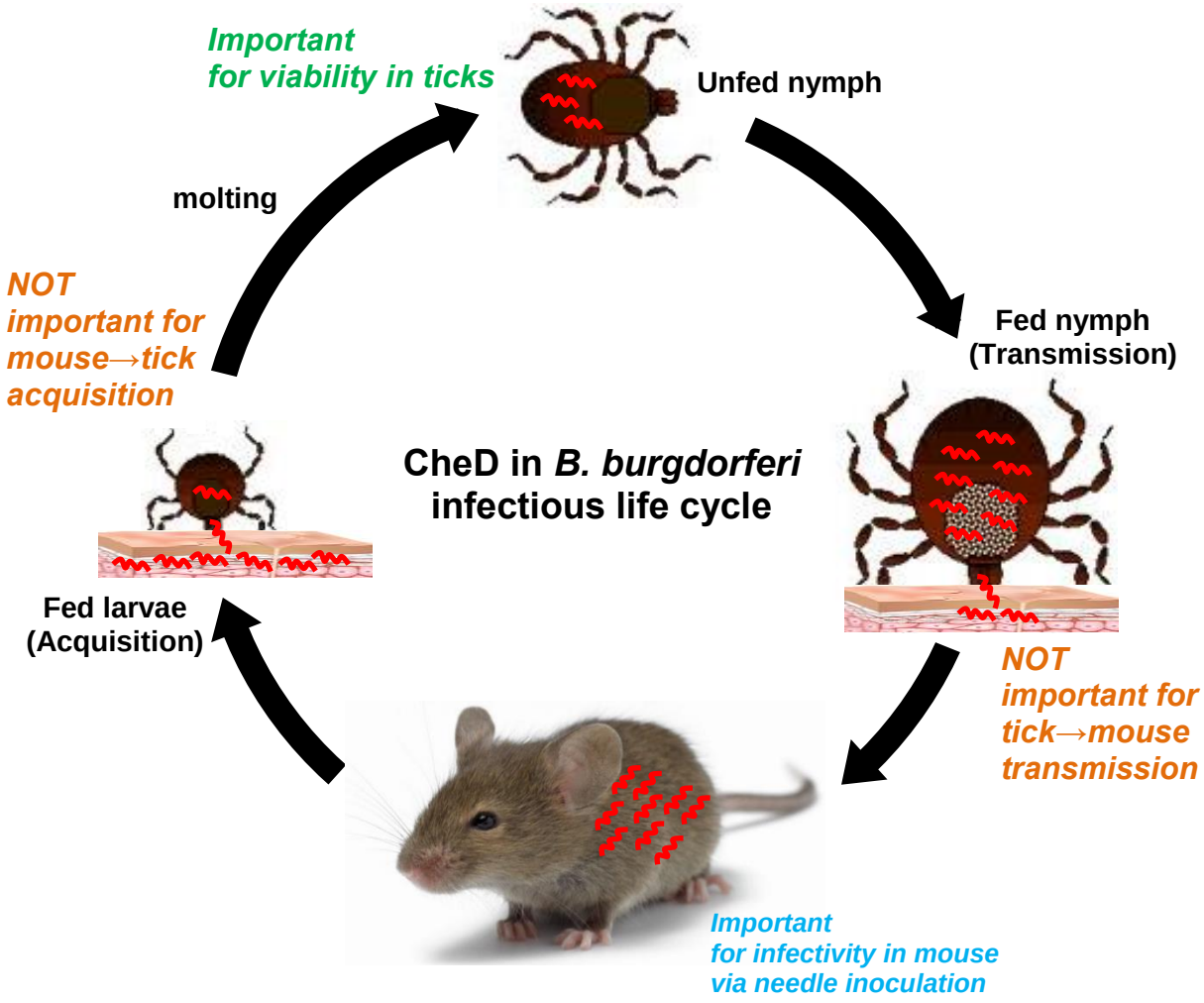

Figure 4.1. A model of CheD in the enzootic cycle of *B. burgdorferi*. In the enzootic cycle of *B. burgdorferi*, CheD is functional in the mammalian and tick hosts and important for infectivity in mouse and viability in ticks. However, it does not play an important role during aquisition from infected mouse to naïve larvae, nor during transmission from infected fed nymphs to mammals.

compared to the *in vitro* cultured spirochetes (290).

Motility and chemotaxis work hand-in-hand as motility is governed by the chemotaxis system (138, 196, 200, 201, 203, 217). The Lyme disease spirochete is a motile organism, and motility, provided by its periplasmic flagella, is critical for every stage of the infectious life cycle of *B. burgdorferi* (143, 172, 188, 190). The periplasmic flagellar motors contain a novel structural component called the collar. Chapter 3 of this research project demonstrated 1) the identification of a collar protein; 2) determines the role of collar protein in motility, flagellar assembly, and periplasmic flagellar orientation; 3) and identified additional collar proteins.

Chapter 3 demonstrated the identification of a gene *flbB* that we found to be important for collar assembly for the first time. We have shown its role in motility, morphology, periplasmic flagellar orientation, and stability of other flagellar motors. In addition, we verified the location of FlbB in the flagellar motor. To ensure that FlbB is a spirochete-specific protein that is essential for the collar assembly, we will attempt to determine the role of FlbB in other representative spirochetes such as *Treponema denticola* or *Leptospira biflexa* as FlbB shares significant amino acid sequence identity in these other spirochetes [*T. denticola* FlbB (E-value 5e-20, 30% identity) and *L. biflexa* FlbB (2e-09, 25% identity)]. While not genetically tractable, we will attempt to complement a *B. burgdorferi* or *T. denticola* or *L. biflexa flbB* mutant with an intact wild-type *Treponema pallidum flbB* gene. If we are able to complement a Δ*flbB*, it will show that the function of FlbB is also conserved in other spirochetes.

As shown in chapter 3, the collar is a large structural complex and we, therefore,

proposed that the collar is comprised of multiple proteins. FlbB is a small protein (205 amino acids) and using GFP, we have shown that it forms only a small structure at the base of the collar structure where FlbB is likely to be embedded in the membrane using its membrane-binding domain. Additional (unidentified) collar proteins are expected to assemble onto the base FlbB. Since we have inactivated all proteins annonated as flagellar/motility-related in the *B. burgdorferi* genome and found only FlbB to be involved in collar structure, we took advantage of a protein-protein interaction (PPI) map developed in another spirochete—*T. pallidum*—the causative agent of syphilis to identify additional proteins involved in collar assembly.

Accordingly, we performed bioinformatics using the PPI map (291), and found several proteins including BB0236. BB0236 is shown to interact directly with the FlbB homolog in that map (Fig. 4.2). This BB0236 is annotated as a hypothetical protein and is away from any known motility/flagellar-related operons in *B. burgdorferi*. BB0236 encodes a tetratricopeptide repeat (TPR) domain protein, which serves as a chaperone that helps stabilize multiprotein complexes in other bacteria (292, 293). Our preliminary data indicate that BB0236 interacts with FlbB in a co-immunoprecipitation assay. Moreover, mutant analyses indicate that BB0236 is crucial for motility, morphology, and the stability of other flagellar structures. Most importantly, our preliminary data indicate that BB0236 is a collar protein because the collar structure is absent in the *bb0236* mutant but is restored in the *bb0236* complemented cells as determined by cryo-ET. Identification of BB0236 strongly suggests that the collar is a multiprotein complex because TPR proteins are shown to be involved in various multiprotein complexes in other bacteria. In the future, we will attempt to identify the remaining collar proteins by

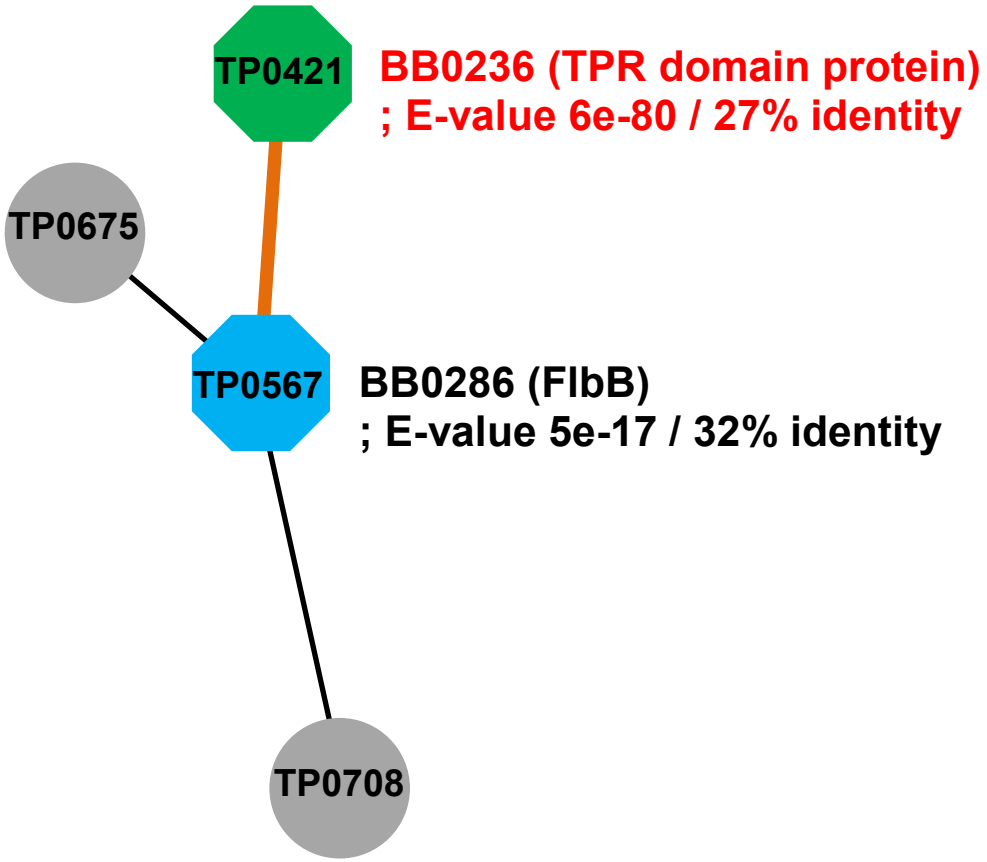

Figure 4.2. Protein interaction network of *Treponema pallidum*. The protein-protein interaction (PPI) map was produced between known motility proteins and proteins of unknown function by the yeast two-hybrid system (291). *T. pallidum* protein TP0567 shows 32% amino acid sequence identity with *B. burgdorferi* BB0286 (FlbB) and TP0567 is shown to interact with TP0421, TP0675, and TP0708. Only TP0421 shares considerable sequence homology with *B. burgdorferi* BB0236 (27% identity).

analyzing the potential candidates identified using the PPI map and determine their roles in motility and flagellar assembly.

The long-term goal of this research project is to understand the mechanism of the spirochete's distinctive motility and assembly of periplasmic flagella in *B. burgdorferi*, which can serve as a model to study the large macromolecular complexes in medically significant yet uncultivable spirochetal pathogens, such as *T. pallidum,* as well as many other significant spirochetes. Identification of virulence-associated flagellar structural proteins can lead to the development of a pharmacological agent to treat or prevent not only Lyme disease, but also other spirochete-borne diseases, such as syphilis and leptospirosis.

REFERENCES

1. **Mead, P. S.** 2015. Epidemiology of Lyme Disease. Infect Dis Clin North Am. **29:**187-210.

2. **Radolf, J. D., M. J. Caimano, B. Stevenson, and L. T. Hu.** 2012. Of ticks, mice and men: understanding the dual-host lifestyle of Lyme disease spirochaetes. Nature Reviews Microbiology. **10:**87-99.

3. **Murray, T. S., and E. D. Shapiro.** 2010. Lyme disease. Clin Lab Med. **30:**311-328.

4. **Steere, A., S. Malawista, D. Snydman, R. Shope, W. Andiman, M. Ross, and F. Steele.** 1977. Lyme arthritis: an epidemic of oligoarticular arthritis in children and adults in three Connecticut communities. Arthritis Rheum. **20:** 7-17.

5. **Burgdorfer, W., A. G. Barbour, S. F. Hayes, J. L. Benach, E. Grunwaldt, and J. P. Davis.** 1982. Lyme disease-a tick-borne spirochetosis? Science. **216:**1317-1319.

6. **Burgdorfer, W.** 1984. Discovery of the Lyme disease spirochete and its relation to tick vectors. Yale J Biol Med. **57:**515-520.

7. **Johnson, R. C., G. P. Schmid, F. W. Hyde, A. Steigerwalt, and D. J. Brenner.** 1984. *Borrelia burgdorferi* sp. nov.: etiologic agent of Lyme disease. Int J Syst Bacteriol. **34:**496-497.

8. **Keller, A., A. Graefen, M. Ball, M. Matzas, V. Boisguerin, F. Maixner, P. Leidinger, C. Backes, R. Khairat, and M. Forster.** 2012. New insights into the Tyrolean Iceman's origin and phenotype as inferred by whole-genome sequencing. Nature Communications. **3:**698.

9. **Poinar Jr, G.** 2014. Spirochete-like cells in a Dominican amber *Ambylomma* tick (Arachnida: Ixodidae). Hist Biol. **27:**565-570.

10. **Steere, A. C., N. H. Bartenhagen, J. E. Craft, G. J. Hutchinson, J. H. Newman, D. W. Rahn, L. H. Sigal, P. N. Spieler, K. S. Stenn, and S. E. Malawista.** 1983. The early clinical manifestations of Lyme disease. Ann Intern Med. **99:**76-82.

11. **Åsbrink, E., and A. Hovmark.** 1988. Early and Late Cutaneous Manifestations in *Ixodes*-borne Borreliosis (Erythema Migrans Borreliosis, Lyme Borreliosis). Ann N. Y. Acad Sci. **539:**4-15.

12. **Nadelman, R. B., and G. P. Wormser.** 1998. Lyme borreliosis. The Lancet. **352:**557-565.

13. **Pachner, A. R., P. Duray, and A. C. Steere.** 1989. Central nervous system manifestations of Lyme disease. Arch Neurol. **46:**790-795.

14. **Sanchez, J. L.** 2015. Clinical Manifestations and Treatment of Lyme Disease. Clin Lab Med. **35:**765-778.

15. **Samuels, D. S.** 2010. *Borrelia*: molecular biology, host interaction and pathogenesis. Horizon Scientific Press.

16. **Tibbles, C. D., and J. A. Edlow.** 2007. Does this patient have erythema migrans? Jama. **297:**2617-2627.

17. **Steere, A. C., and V. K. Sikand.** 2003. The presenting manifestations of Lyme disease and the outcomes of treatment. N Engl J Med. **348:**2472-2474.

18. **Nadelman, R. B., J. Nowakowski, G. Forseter, N. S. Goldberg, S. Bittker, D. Cooper, M. Aguero-Rosenfeld, and G. P. Wormser.** 1996. The clinical spectrum of early Lyme borreliosis in patients with culture-confirmed erythema migrans. Am J Med. **100:**502-508.

19. **Smith, R. P., R. T. Schoen, D. W. Rahn, V. K. Sikand, J. Nowakowski, D. L. Parenti, M. S. Holman, D. H. Persing, and A. C. Steere.** 2002. Clinical characteristics and treatment outcome of early Lyme disease in patients with microbiologically confirmed erythema migrans. Ann Intern Med. **136:**421-428.

20. **Stanek, G., G. P. Wormser, J. Gray, and F. Strle.** 2012. Lyme borreliosis. The Lancet. **379:**461-473.

21. **Wormser, G. P., R. J. Dattwyler, E. D. Shapiro, J. J. Halperin, A. C. Steere, M. S. Klempner, P. J. Krause, J. S. Bakken, F. Strle, G. Stanek, L. Bockenstedt, D. Fish, J. S. Dumler, and R. B. Nadelman.** 2006. The clinical assessment, treatment, and prevention of Lyme disease, human granulocytic anaplasmosis, and babesiosis: clinical practice guidelines by the Infectious Diseases Society of America. Clin Infect Dis. **43:**1089-1134.

22. **Wormser, G. P., D. McKenna, J. Carlin, R. B. Nadelman, L. F. Cavaliere, D. Holmgren, D. W. Byrne, and J. Nowakowski.** 2005. Brief communication: hematogenous dissemination in early Lyme disease. Ann Intern Med. **142:**751-755.

23. **Arvikar, S. L., and A. C. Steere.** 2015. Diagnosis and Treatment of Lyme Arthritis. Infect Dis Clin North Am. **29:**269-280.

24. **Feder Jr, H. M., B. J. Johnson, S. O'Connell, E. D. Shapiro, A. C. Steere, and G. P. Wormser.** 2007. A critical appraisal of “chronic Lyme disease”. N Engl J Med. **357:**1422-1430.

25. **Carlson, D., J. Hernandez, B. J. Bloom, J. Coburn, J. M. Aversa, and A. C. Steere.** 1999. Lack of *Borrelia burgdorferi* DNA in synovial samples from patients with antibiotic treatment–resistant Lyme arthritis. Arthritis Rheum. **42:**2705-2709.

26. **Bacon, R. M., K. J. Kugeler, and P. S. Mead.** 2008. Surveillance for Lyme disease--United States, 1992-2006. Department of Health & Human Services, Centers for Disease Control and Prevention. MMWR Surveill Summ. **57:**1-9.

27. **Forrester, J. D., J. Meiman, J. Mullins, R. Nelson, S. Ertel, M. Cartter, C. M. Brown, V. Lijewski, E. Schiffman, and D. Neitzel.** 2014. Notes from the field: update on lyme carditis, groups at high risk, and frequency of associated sudden cardiac death—United States. MMWR Morb Mortal Wkly Rep. **63:**982-983.

28. **Balmelli, T., and J. Piffaretti.** 1995. Association between different clinical manifestations of Lyme disease and different species of *Borrelia burgdorferi* sensu lato. Res Microbiol. **146:**329-340.

29. **van Dam, A. P., H. Kuiper, K. Vos, A. Widjojokusumo, B. M. de Jongh, L. Spanjaard, A. C. Ramselaar, M. D. Kramer, and J. Dankert.** 1993. Different genospecies of *Borrelia burgdorferi* are associated with distinct clinical manifestations of Lyme borreliosis. Clin Infect Dis. **17:**708-717.

30. **Busch, U., C. Hizo-Teufel, R. Böhmer, V. Fingerle, D. RöbZler, B. Wilske, and V. Preac-Mursic.** 1996. *Borrelia burgdorferi* sensu lato strains isolated from cutaneous Lyme borreliosis biopsies differentiated by pulsed-field gel electrophoresis. Scand J Infect Dis. **28:**583-589.

31. **Centers for Disease Control and Prevention (CDC).** 2012. Summary of notifiable diseases--United States, 2010. MMWR Morb Mortal Wkly Rep. **59:**1-111.

32. **Maes, E., P. Lecomte, and N. Ray.** 1998. A cost-of-illness study of Lyme disease in the United States. Clin Ther. **20:**993-1008.

33. **Zhang, X., M. I. Meltzer, C. A. Pena, A. B. Hopkins, L. Wroth, and A. D. Fix.** 2006. Economic impact of Lyme disease. Emerg Infect Dis. **12:**653-660.

34. **Kuehn, B. M.** 2013. CDC estimates 300,000 US cases of Lyme disease annually. Jama. **310:**1110.

35. **Centers for Disease Control and Prevention.** 2015. Notice to Readers: Final 2014 Reports of Nationally Notifiable Infectious Diseases. MMWR Morb Mortal Wkly Rep. **64:**1019-1033.

36. **Marcus, L. C., A. C. Steere, P. H. Duray, A. E. Anderson, and E. B. Mahoney.** 1985. Fatal pancarditis in a patient with coexistent Lyme disease and babesiosis: demonstration of spirochetes in the myocardium. Ann Intern Med. **103:**374-376.

37. **Kirsch, M., F. L. Ruben, A. C. Steere, P. H. Duray, C. W. Norden, and A. Winkelstein.** 1988. Fatal adult respiratory distress syndrome in a patient with Lyme disease. Jama. **259:**2737-2739.

38. **Waniek, C., I. Prohovnik, A. A. Kaufman, and A. J. Dwork.** 1995. Rapidly progressive frontal-type dementia associated with Lyme disease. J Neuropsychiatry Clin Neurosci. **7:**345-347.

39. **Tavora, F., A. Burke, L. Li, T. J. Franks, and R. Virmani.** 2008. Postmortem confirmation of Lyme carditis with polymerase chain reaction. Cardiovascular Pathology. **17:**103-107.

40. **Cary, N. R., B. Fox, D. J. Wright, S. J. Cutler, L. M. Shapiro, and A. A. Grace.** 1990. Fatal Lyme carditis and endodermal heterotopia of the atrioventricular node. Postgrad Med J. **66:**134-136.

41. **Reimers, C., J. De Koning, U. Neubert, V. Preac-Mursic, J. Koster, W. Müller-Felber, D. Pongratz, and P. Duray.** 1993. *Borrelia burgdorferi* myositis: report of eight patients. J Neurol. **240:**278-283.

42. **Deresinski, S.** 2014. Sudden unexpected cardiac death from Lyme disease. J Infect Dis. **33:**37-39.

43. **Kugeler, K. J., K. S. Griffith, L. H. Gould, K. Kochanek, M. J. Delorey, B. J. Biggerstaff, and P. S. Mead.** 2011. A review of death certificates listing Lyme disease as a cause of death in the United States. Clin Infect Dis. **52:**364-367.

44. **Centers for Disease Control and Prevention (CDC).** 2013. Three sudden cardiac deaths associated with Lyme carditis - United States, November 2012-July 2013. MMWR Morb Mortal Wkly Rep. **62:**993-996.

45. **Centers for Disease Control and Prevention (CDC).** 2016. Lyme Disease-Division of Vector-borne Infectious Diseases. doi: In: http://www.cdc.gov/ncidod/dvbid/lyme/index.htm.

46. **DePietropaolo, D. L., J. H. Powers, J. M. Gill, and A. J. Foy.** 2006. Diagnosis of Lyme disease. Del Med. J. **78:**11-18.

47. **Wright, W. F., D. J. Riedel, R. Talwani, and B. L. Gilliam.** 2012. Diagnosis and management of Lyme disease. Am Fam Physician. **85:**1086.

48. **Shapiro, E. D.** 2014. Clinical practice. Lyme disease. N Engl J Med. **370:**1724-1731.

49. **Wormser, G. P., E. Masters, J. Nowakowski, D. McKenna, D. Holmgren, K. Ma, L. Ihde, L. F. Cavaliere, and R. B. Nadelman.** 2005. Prospective clinical evaluation of patients from Missouri and New York with erythema migrans-like skin lesions. Clin Infect Dis. **41:**958-965.

50. **Centers for Disease Control and Prevention (CDC).** 1995. Recommendations for test performance and interpretation from the Second National Conference on Serologic Diagnosis of Lyme Disease. MMWR Morb Mortal Wkly Rep. **44:**590-591.

51. **Schriefer, M. E.** 2015. Lyme disease diagnosis: serology. Clin Lab Med. **35:**797-814.

52. **Dressler, F., J. A. Whalen, B. N. Reinhardt, and A. C. Steere.** 1993. Western blotting in the serodiagnosis of Lyme disease. J Infect Dis. **167:**392-400.

53. **Engstrom, S. M., E. Shoop, and R. C. Johnson.** 1995. Immunoblot interpretation criteria for serodiagnosis of early Lyme disease. J Clin Microbiol. **33:**419-427.

54. **Bockenstedt, L. K., and G. P. Wormser.** 2014. Review: unraveling Lyme disease. Arthritis Rheum. **66:**2313-2323.

55. **Dumler, J. S.** 2001. Molecular diagnosis of Lyme disease: review and meta-analysis. Molecular Diagnosis. **6:**1-11.

56. **Babady, N. E., L. M. Sloan, E. A. Vetter, R. Patel, and M. J. Binnicker.** 2008. Percent positive rate of Lyme real-time polymerase chain reaction in blood, cerebrospinal fluid, synovial fluid, and tissue. Diagn Microbiol Infect Dis. **62:**464-466.

57. **Bratton, R. L., J. W. Whiteside, M. J. Hovan, R. L. Engle, and F. D. Edwards.** 2008. Diagnosis and treatment of Lyme disease. Mayo Clinic Proceedings. **83:**566-571.

58. **Klempner, M. S., C. H. Schmid, L. Hu, A. C. Steere, G. Johnson, B. McCloud, R. Noring, and A. Weinstein.** 2001. Intralaboratory reliability of serologic and urine testing for Lyme disease. Am J Med. **110:**217-219.

59. **Steere, A. C., P. H. Duray, and E. C. Butcher.** 1988. Spirochetal antigens and lymphoid cell surface markers in Lyme synovitis. Arthritis Rheum. **31:**487-495.

60. **Guerau-de-Arellano, M., and B. T. Huber.** 2002. Development of autoimmunity in Lyme arthritis. Curr Opin Rheumatol. **14:**388-393.

61. **Steere, A. C., D. Gross, A. L. Meyer, and B. T. Huber.** 2001. Autoimmune mechanisms in antibiotic treatment-resistant Lyme arthritis. J Autoimmun. **16:**263-268.

62. **Steere, A., and L. Baxter-Lowe.** 1998. Association of chronic, treatment-resistant Lyme arthritis with rheumatoid arthritis (RA) alleles., p. S81-S81. *In* Anonymous ARTHRITIS AND RHEUMATISM. LIPPINCOTT WILLIAMS & WILKINS 227 EAST WASHINGTON SQ, PHILADELPHIA, PA 19106 USA.

63. **Steere, A. C., W. Klitz, E. E. Drouin, B. A. Falk, W. W. Kwok, G. T. Nepom, and L. A. Baxter-Lowe.** 2006. Antibiotic-refractory Lyme arthritis is associated with HLA-DR molecules that bind a *Borrelia burgdorferi* peptide. J Exp Med. **203:**961-971.

64. **Winchester, R., E. Dwyer, and S. Rose.** 1992. The genetic basis of rheumatoid arthritis. The shared epitope hypothesis. Rheum Dis Clin North Am. **18:**761-783.

65. **Grygorczuk, S., J. Zajkowska, M. Kondrusik, A. Moniuszko, S. Pancewicz, and W. Pawlak-Zalewska.** 2008. Failures of antibiotic treatment in Lyme arthritis. Przegl Epidemiol. **62:**581-588.

66. **Jones, K. L., G. A. McHugh, L. J. Glickstein, and A. C. Steere.** 2009. Analysis of *Borrelia burgdorferi* genotypes in patients with Lyme arthritis: High frequency of ribosomal RNA intergenic spacer type 1 strains in antibiotic-refractory arthritis. Arthritis Rheum. **60:**2174-2182.

67. **Feng, J., T. Wang, W. Shi, S. Zhang, D. Sullivan, P. G. Auwaerter, and Y. Zhang.** 2014. Identification of novel activity against *Borrelia burgdorferi* persisters using an FDA approved drug library. Emerging Microbes & Infections. **3:**e49.

68. **Jones, K. E., N. G. Patel, M. A. Levy, A. Storeygard, D. Balk, J. L. Gittleman, and P. Daszak.** 2008. Global trends in emerging infectious diseases. Nature. **451:**990-993.

69. **Terekhova, D., M. L. Sartakova, G. P. Wormser, I. Schwartz, and F. C. Cabello.** 2002. Erythromycin resistance in *Borrelia burgdorferi*. Antimicrob Agents Chemother. **46:**3637-3640.

70. **Samuels, D. S., R. T. Marconi, W. M. Huang, and C. F. Garon.** 1994. *gyrB* mutations in coumermycin A1-resistant *Borrelia burgdorferi*. J Bacteriol. **176:**3072-3075.

71. **Shadick, N. A., M. H. Liang, C. B. Phillips, K. Fossel, and K. M. Kuntz.** 2001. The cost-effectiveness of vaccination against Lyme disease. Arch Intern Med. **161:**554-561.

72. **Meltzer, M. I., D. T. Dennis, and K. A. Orloski.** 1999. The cost effectiveness of vaccinating against Lyme disease. Emerg Infect Dis. **5:**321-328.

73. **Embers, M. E., and S. Narasimhan.** 2013. Vaccination against Lyme disease: past, present, and future. Front Cell Infect Microbiol. **3:**6.

74. **Steere, A. C., V. K. Sikand, F. Meurice, D. L. Parenti, E. Fikrig, R. T. Schoen, J. Nowakowski, C. H. Schmid, S. Laukamp, and C. Buscarino.** 1998. Vaccination against Lyme disease with recombinant *Borrelia burgdorferi* outer-surface lipoprotein A with adjuvant. N Engl J Med. **339:**209-215.

75. **Sigal, L. H., J. M. Zahradnik, P. Lavin, S. J. Patella, G. Bryant, R. Haselby, E. Hilton, M. Kunkel, D. Adler-Klein, and T. Doherty.** 1998. A vaccine consisting of recombinant *Borrelia burgdorferi* outer-surface protein A to prevent Lyme disease. N Engl J Med. **339:**216-222.

76. **Poland, G. A., and R. M. Jacobson.** 2001. The prevention of Lyme disease with vaccine. Vaccine. **19:**2303-2308.

77. **Poland, G. A.** 2001. Prevention of Lyme disease: a review of the evidence, p. 713-724. *In* Anonymous Mayo Clinic Proceedings. Elsevier.

78. **Poland, G. A.** 2011. Vaccines against Lyme disease: What happened and what lessons can we learn? Clin Infect Dis. **52 Suppl 3:**s253-8.

79. **Kalish, R. A., J. M. Leong, and A. C. Steere.** 1993. Association of treatment-resistant chronic Lyme arthritis with HLA-DR4 and antibody reactivity to OspA and OspB of *Borrelia burgdorferi*. Infect Immun. **61:**2774-2779.

80. **Pal, U., X. Li, T. Wang, R. R. Montgomery, N. Ramamoorthi, F. Bao, X. Yang, M. Pypaert, D. Pradhan, and F. S. Kantor.** 2004. TROSPA, an *Ixodes scapularis* receptor for *Borrelia burgdorferi*. Cell. **119:**457-468.

81. **de Silva, A. M., S. R. Telford 3rd, L. R. Brunet, S. W. Barthold, and E. Fikrig.** 1996. *Borrelia burgdorferi* OspA is an arthropod-specific transmission-blocking Lyme disease vaccine. J Exp Med. **183:**271-275.

82. **Ohnishi, J., J. Piesman, and A. M. de Silva.** 2001. Antigenic and genetic heterogeneity of *Borrelia burgdorferi* populations transmitted by ticks. Proc Natl Acad Sci U. S. A. **98:**670-675.

83. **Schwan, T. G., and J. Piesman.** 2000. Temporal changes in outer surface proteins A and C of the lyme disease-associated spirochete, *Borrelia burgdorferi*, during the chain of infection in ticks and mice. J Clin Microbiol. **38:**382-388.

84. **Bockenstedt, L. K., E. Hodzic, S. Feng, K. W. Bourrel, A. de Silva, R. R. Montgomery, E. Fikrig, J. D. Radolf, and S. W. Barthold.** 1997. *Borrelia burgdorferi* strain-specific Osp C-mediated immunity in mice. Infect Immun. **65:**4661-4667.

85. **Gilmore, R. D.,Jr, K. J. Kappel, M. C. Dolan, T. R. Burkot, and B. J. Johnson.** 1996. Outer surface protein C (OspC), but not P39, is a protective immunogen against a tick-transmitted *Borrelia burgdorferi* challenge: evidence for a conformational protective epitope in OspC. Infect Immun. **64:**2234-2239.

86. **Seinost, G., D. E. Dykhuizen, R. J. Dattwyler, W. T. Golde, J. J. Dunn, I. N. Wang, G. P. Wormser, M. E. Schriefer, and B. J. Luft.** 1999. Four clones of *Borrelia*

burgdorferi sensu stricto cause invasive infection in humans. Infect Immun. **67:**3518-3524.

87. **Wang, I. N., D. E. Dykhuizen, W. Qiu, J. J. Dunn, E. M. Bosler, and B. J. Luft.** 1999. Genetic diversity of *ospC* in a local population of *Borrelia burgdorferi* sensu stricto. Genetics. **151:**15-30.

88. **Earnhart, C. G., and R. T. Marconi.** 2007. OspC phylogenetic analyses support the feasibility of a broadly protective polyvalent chimeric Lyme disease vaccine. Clin Vaccine Immunol. **14:**628-634.

89. **Earnhart, C. G., and R. T. Marconi.** 2007. An octavalent Lyme disease vaccine induces antibodies that recognize all incorporated OspC type-specific sequences. Human Vaccines. **3:**281-289.

90. **Earnhart, C. G., E. L. Buckles, and R. T. Marconi.** 2007. Development of an OspC-based tetravalent, recombinant, chimeric vaccinogen that elicits bactericidal antibody against diverse Lyme disease spirochete strains. Vaccine. **25:**466-480.

91. **Scheiblhofer, S., R. Weiss, H. Dürnberger, S. Mostböck, M. Breitenbach, I. Livey, and J. Thalhamer.** 2003. A DNA vaccine encoding the outer surface protein C from *Borrelia burgdorferi* is able to induce protective immune responses. Microb Infect. **5:**939-946.

92. **Adams, D. A., R. A. Jajosky, U. Ajani, J. Kriseman, P. Sharp, D. H. Onwen, A. W. Schley, W. J. Anderson, A. Grigoryan, A. E. Aranas, M. S. Wodajo, J. P. Abellera, and Centers for Disease Control and Prevention (CDC).** 2014. Summary of notifiable diseases--United States, 2012. MMWR Morb Mortal Wkly Rep. **61:**1-121.

93. **Centers for Disease Control and Prevention.** 2014. Notice to readers: final 2013 reports of nationally notifiable infectious diseases. MMWR Morb Mortal Wkly Rep. **63:**702.

94. **Adams, D., K. Fullerton, R. Jajosky, P. Sharp, D. Onweh, A. Schley, W. Anderson, A. Faulkner, and K. Kugeler.** 2015. Summary of Notifiable Infectious Diseases and Conditions - United States, 2013. MMWR Morb Mortal Wkly Rep. **62:**1-122.

95. **Mather, T. N., M. L. Wilson, S. I. Moore, J. M. Ribeiro, and A. Spielman.** 1989. Comparing the relative potential of rodents as reservoirs of the Lyme disease spirochete (*Borrelia burgdorferi*). Am J Epidemiol. **130:**143-150.

96. **Genchi, C.** 1992. Arthropoda as zoonoses and their implications. Vet Parasitol. **44:**21-33.

97. **Lane, R., J. Mun, L. Eisen, and R. Eisen.** 2006. Refractoriness of the western fence lizard (*Sceloporus occidentalis*) to the Lyme disease group spirochete *Borrelia bissettii*. J Parasitol. **92:**691-696.

98. **Kuo, M. M., R. S. Lane, and P. C. Giclas.** 2000. A comparative study of mammalian and reptilian alternative pathway of complement-mediated killing of the Lyme disease spirochete (*Borrelia burgdorferi*). J Parasitol. **86:**1223-1228.

99. **Giery, S. T., and R. S. Ostfeld.** 2007. The role of lizards in the ecology of Lyme disease in two endemic zones of the northeastern United States. J Parasitol. **93:**511-517.

100. **Salkeld, D. J., and R. S. Lane.** 2010. Community ecology and disease risk: lizards, squirrels, and the Lyme disease spirochete in California, USA. Ecology. **91:**293-298.

101. **Swei, A., R. S. Ostfeld, R. S. Lane, and C. J. Briggs.** 2011. Impact of the experimental removal of lizards on Lyme disease risk. Proc Biol Sci. **278:**2970-2978.

102. **Liveris, D., G. Wang, G. Girao, D. W. Byrne, J. Nowakowski, D. McKenna, R. Nadelman, G. P. Wormser, and I. Schwartz.** 2002. Quantitative detection of *Borrelia burgdorferi* in 2-millimeter skin samples of erythema migrans lesions: correlation of results with clinical and laboratory findings. J Clin Microbiol. **40:**1249-1253.

103. **Lane, R., J. Piesman, and W. Burgdorfer.** 1991. Lyme borreliosis: relation of its causative agent to its vectors and hosts in North America and Europe. Annu Rev Entomol. **36:**587-609.

104. **Piesman, J., J. G. Donahue, T. N. Mather, and A. Spielman.** 1986. Transovarially acquired Lyme disease spirochetes (*Borrelia burgdorferi*) in field-collected larval *Ixodes dammini* (Acari: Ixodidae). J Med Entomol. **23:**219.

105. **Rollend, L., D. Fish, and J. E. Childs.** 2013. Transovarial transmission of *Borrelia* spirochetes by *Ixodes scapularis*: a summary of the literature and recent observations. Ticks and Tick-Borne Diseases. **4:**46-51.

106. **Schulze, T. L., G. S. Bowen, M. F. Lakat, W. E. Parkin, and J. K. Shisler.** 1985. The role of adult *Ixodes dammini* (Acari: Ixodidae) in the transmission of Lyme disease in New Jersey, USA. J Med Entomol. **22:**88-93.

107. **Richter, D., A. Debski, Z. Hubalek, and F. Matuschka.** 2012. Absence of Lyme disease spirochetes in larval *Ixodes ricinus* ticks. Vector-Borne and Zoonotic Diseases. **12:**21-27.

108. **Burgess, E. C., T. E. Amundson, J. P. Davis, R. A. Kaslow, and R. Edelman.** 1986. Experimental inoculation of *Peromyscus* spp. with *Borrelia burgdorferi*: evidence of contact transmission. Am J Trop Med Hyg. **35:**355-359.

109. **Wright, S. D., and S. W. Nielsen.** 1990. Experimental infection of the white-footed mouse with *Borrelia burgdorferi*. Am J Vet Res. **51:**1980-1987.

110. **Altaie, S., S. Mookherjee, E. Assian, F. Al-Taie, S. Nakeeb, S. Siddiqui, and L. Duffy.** 1996. Transmission of *Borrelia burgdorferi* from experimentally infected mating pairs to offspring in a murine model. FDA Science Forum. 1-17.

111. **Gustafson, J. M.** 1993. The in utero and seminal transmission of *Borrelia burgdorferi* in Canidae. University of Wisconsin--Madison.

112. **Bach, G.** 2001. Recovery of Lyme spirochetes by PCR in semen samples of previously diagnosed Lyme disease patients. 14th International Scientific Conference on Lyme Disease.

113. **Harvey, W., and P. Salvato.** 2003. 'Lyme disease': ancient engine of an unrecognized borreliosis pandemic? Med Hypotheses. **60:**742-759.

114. **Stricker, R., D. Moore, and E. Winger.** 2004. Clinical and immunologic evidence for transmission of Lyme disease through intimate human contact: 412. J Invest Med. **52:**S151.

115. **Middelveen, M. J., J. Burke, E. Sapi, C. Bandoski, K. R. Filush, Y. Wang, A. Franco, A. Timmaraju, H. A. Schlinger, and P. J. Mayne.** 2015. Culture and identification of *Borrelia* spirochetes in human vaginal and seminal secretions. F1000Research. **3:**309.

116. **Stricker, R. B., and M. J. Middelveen.** 2015. Sexual transmission of Lyme disease: challenging the tickborne disease paradigm. Expert Review of Anti-Infective Therapy. **13:**1303-1306.

117. **Gerber, M. A., E. D. Shapiro, P. J. Krause, R. G. Cable, S. J. Badon, and R. W. Ryan.** 1994. The risk of acquiring Lyme disease or babesiosis from a blood transfusion. J Infect Dis. **170:**231-234.

118. **Ginzburg, Y., D. Kessler, S. Kang, B. Shaz, and G. P. Wormser.** 2013. Why has *Borrelia burgdorferi* not been transmitted by blood transfusion? Transfusion. **53:**2822-2826.

119. **Thorp, A. M., and L. Tonnetti.** 2015. Distribution and survival of *Borrelia miyamotoi* in human blood components. Transfusion. **56:**705-711.

120. **Gabitzsch, E. S., J. Piesman, M. C. Dolan, C. M. Sykes, and N. S. Zeidner.** 2006. Transfer of *Borrelia burgdorferi* ss infection via blood transfusion in a murine model. J Parasitol. **92:**869-870.

121. **Paster, B., E. Stackebrandt, R. Hespell, C. Hahn, and C. Woese.** 1984. The phylogeny of the spirochetes. Syst Appl Microbiol. **5:**337-351.

122. **Paster, B. J., and F. E. Dewhirst.** 2000. Phylogenetic foundation of spirochetes. J Mol Microbiol Biotechnol. **2:**341-344.

123. **Hengge, U. R., A. Tannapfel, S. K. Tyring, R. Erbel, G. Arendt, and T. Ruzicka.** 2003. Lyme borreliosis. The Lancet Infectious Diseases. **3:**489-500.

124. **Baranton, G., D. Postic, I. Saint Girons, P. Boerlin, J. Piffaretti, M. Assous, and P. A. Grimont.** 1992. Delineation of *Borrelia burgdorferi* sensu stricto, *Borrelia garinii* sp. nov., and group VS461 associated with Lyme borreliosis. Int J Syst Evol Microbiol. **42:**378-383.

125. **Canica, M. M., F. Nato, L. d. Merle, J. C. Mazie, G. Baranton, and D. Postic.** 1993. Monoclonal antibodies for identification of *Borrelia afzelii* sp. nov. associated with late cutaneous manifestations of Lyme borreliosis. Scand J Infect Dis. **25:**441-448.

126. **Kawabata, H., T. Masuzawa, and Y. Yanagihara.** 1993. Genomic analysis of *Borrelia japonica* sp. nov. isolated from Ixodes ovatus in Japan. Microbiol Immunol. **37:**843-848.

127. **Wang, G., A. P. Van Dam, A. Le Fleche, D. Postic, O. Peter, G. Baranton, R. De Boer, L. Spanjaard, and J. Dankert.** 1997. Genetic and phenotypic analysis of *Borrelia valaisiana* sp. nov.(*Borrelia* genomic groups VS116 and M19). Int J Syst Evol Microbiol. **47:**926-932.

128. **Le Fleche, A., D. Postic, K. Girardet, O. Peter, and G. Baranton.** 1997. Characterization of *Borrelia lusitaniae* sp. nov. by 16S ribosomal DNA sequence analysis. Int J Syst Evol Microbiol. **47:**921-925.

129. **Marconi, R. T., D. Liveris, and I. Schwartz.** 1995. Identification of novel insertion elements, restriction fragment length polymorphism patterns, and discontinuous 23S rRNA in Lyme disease spirochetes: phylogenetic analyses of rRNA genes and their intergenic spacers in *Borrelia japonica* sp. nov. and genomic group 21038 (*Borrelia andersonii* sp. nov.) isolates. J Clin Microbiol. **33:**2427-2434.

130. **Fukunaga, M., A. Hamase, K. Okada, and M. Nakao.** 1996. *Borrelia tanukii* sp. nov. and *Borrelia turdae* sp. nov. found from ixodid ticks in Japan: rapid species identification by 16S rRNA gene-targeted PCR analysis. Microbiol Immunol. **40:**877-881.

131. **Elferink, O.** 1997. Validation of the Publication of New Names and New Combinations Previously Effectively Published Outside the IJSB. Int J Syst Bacteriol. **47:**1274.

132. **Postic, D., M. V. Assous, P. A. Grimont, and G. Baranton.** 1994. Diversity of *Borrelia burgdorferi* Sensu Lato Evidenced by Restriction Fragment Length Polymorphism of *rrf* (5S)-*rrl* (23S) Intergenic Spacer Amplicons. Int J Syst Evol Microbiol. **44:**743-752.

133. **Postic, D., N. M. Ras, R. S. Lane, M. Hendson, and G. Baranton.** 1998. Expanded diversity among Californian borrelia isolates and description of *Borrelia bissettii* sp. nov. (formerly *Borrelia* group DN127). J Clin Microbiol. **36:**3497-3504.

134. **Barbour, A. G., and S. F. Hayes.** 1986. Biology of *Borrelia* species. Microbiol Rev. **50:**381-400.

135. **Holt, S. C.** 1978. Anatomy and chemistry of spirochetes. Microbiol Rev. **42:**114-160.

136. **Johnson, R. C.** 1977. The spirochetes. Annu Rev Microbiol. **31:**89-106.

137. **Goldstein, S. F., K. F. Buttle, and N. W. Charon.** 1996. Structural analysis of the Leptospiraceae and *Borrelia burgdorferi* by high-voltage electron microscopy. J Bacteriol. **178:**6539-6545.

138. **Charon, N. W., A. Cockburn, C. Li, J. Liu, K. A. Miller, M. R. Miller, M. A. Motaleb, and C. W. Wolgemuth.** 2012. The unique paradigm of spirochete motility and chemotaxis. Annu Rev Microbiol. **66:**349-370.

139. **Polovinchik, Y.** 2000. Study of BSK II and BSK H Media for Culturing Lyme Disease Spirochetes. Science [Internet]. Available from: Nature.Berkeley.Edu/Classes/es196/Projects/2000final/Polovinchik.Pdf.

140. **Kelly, R.** 1971. Cultivation of *Borrelia hermsi*. Science. **173:**443-444.

141. **Barbour, A. G.** 1984. Isolation and cultivation of Lyme disease spirochetes. Yale J Biol Med. **57:**521-525.

142. **Rosa, P. A., K. Tilly, and P. E. Stewart.** 2005. The burgeoning molecular genetics of the Lyme disease spirochaete. Nature Reviews Microbiology. **3:**129-143.

143. **Sultan, S. Z., A. Manne, P. E. Stewart, A. Bestor, P. A. Rosa, N. W. Charon, and M. A. Motaleb.** 2013. Motility is crucial for the infectious life cycle of *Borrelia burgdorferi*. Infect Immun. **81:**2012-2021.

144. **Chandler, M., R. Bird, and L. Caro.** 1975. The replication time of the *Escherichia coli* K12 chromosome as a function of cell doubling time. J Mol Biol. **94:**127-132.

145. **Belisle, J. T., M. E. Brandt, J. D. Radolf, and M. V. Norgard.** 1994. Fatty acids of *Treponema pallidum* and *Borrelia burgdorferi* lipoproteins. J Bacteriol. **176:**2151-2157.

146. **Takayama, K., R. J. Rothenberg, and A. G. Barbour.** 1987. Absence of lipopolysaccharide in the Lyme disease spirochete, *Borrelia burgdorferi*. Infect Immun. **55:**2311-2313.

147. **Bergström, S., V. Bundoc, and A. Barbour.** 1989. Molecular analysis of linear plasmid-encoded major surface proteins, OspA and OspB, of the Lyme disease spirochaete *Borrelia burgdorferi*. Mol Microbiol. **3:**479-486.

148. **Brandt, M. E., B. S. Riley, J. D. Radolf, and M. V. Norgard.** 1990. Immunogenic integral membrane proteins of *Borrelia burgdorferi* are lipoproteins. Infect Immun. **58:**983-991.

149. **Eiffert, H., H. Lotter, K. Jarecki-Khan, and R. Thomssen.** 1991. Identification of an immunoreactive non-proteinaleous component in *Borrelia burgdorferi*. Med Microbiol Immunol. **180:**229-237.

150. **Radolf, J. D., K. W. Bourell, D. R. Akins, J. S. Brusca, and M. V. Norgard.** 1994. Analysis of *Borrelia burgdorferi* membrane architecture by freeze-fracture electron microscopy. J Bacteriol. **176:**21-31.

151. **Fraser, C. M., S. Casjens, W. M. Huang, G. G. Sutton, R. Clayton, R. Lathigra, O. White, K. A. Ketchum, R. Dodson, and E. K. Hickey.** 1997. Genomic sequence of a Lyme disease spirochaete, *Borrelia burgdorferi*. Nature. **390:**580-586.

152. **Casjens, S., N. Palmer, R. Van Vugt, W. Mun Huang, B. Stevenson, P. Rosa, R. Lathigra, G. Sutton, J. Peterson, and R. J. Dodson.** 2000. A bacterial genome in flux: the twelve linear and nine circular extrachromosomal DNAs in an infectious isolate of the Lyme disease spirochete *Borrelia burgdorferi*. Mol Microbiol. **35:**490-516.

153. **Barbour, A. G., and C. F. Garon.** 1987. Linear plasmids of the bacterium *Borrelia burgdorferi* have covalently closed ends. Science. **237:**409-411.

154. **Barbour, A. G.** 1988. Plasmid analysis of *Borrelia burgdorferi*, the Lyme disease agent. J Clin Microbiol. **26:**475-478.

155. **Casjens, S., R. van Vugt, K. Tilly, P. A. Rosa, and B. Stevenson.** 1997. Homology throughout the multiple 32-kilobase circular plasmids present in Lyme disease spirochetes. J Bacteriol. **179:**217-227.

156. **Hinnebusch, J., and A. G. Barbour.** 1992. Linear- and circular-plasmid copy numbers in *Borrelia burgdorferi*. J Bacteriol. **174:**5251-5257.

157. **Norris, S. J., J. K. Howell, S. A. Garza, M. S. Ferdows, and A. G. Barbour.** 1995. High- and low-infectivity phenotypes of clonal populations of *in vitro*-cultured *Borrelia burgdorferi*. Infect Immun. **63:**2206-2212.

158. **Zhang, J., J. M. Hardham, A. G. Barbour, and S. J. Norris.** 1997. Antigenic variation in Lyme disease borreliae by promiscuous recombination of VMP-like sequence cassettes. Cell. **89:**275-285.

159. **Purser, J. E., and S. J. Norris.** 2000. Correlation between plasmid content and infectivity in *Borrelia burgdorferi*. Proc Natl Acad Sci U. S. A. **97:**13865-13870.

160. **Casjens, S.** 2000. *Borrelia* genomes in the year 2000. J Mol Microbiol Biotechnol. **2:**401-410.

161. **Limberger, R. J.** 2004. The periplasmic flagellum of spirochetes. J Mol Microbiol Biotechnol. **7:**30-40.

162. **Chen, S., M. Beeby, G. E. Murphy, J. R. Leadbetter, D. R. Hendrixson, A. Briegel, Z. Li, J. Shi, E. I. Tocheva, and A. Müller.** 2011. Structural diversity of bacterial flagellar motors. Embo J. **30:**2972-2981.

163. **Zhao, X., K. Zhang, T. Boquoi, B. Hu, M. A. Motaleb, K. A. Miller, M. E. James, N. W. Charon, M. D. Manson, S. J. Norris, C. Li, and J. Liu.** 2013. Cryoelectron tomography reveals the sequential assembly of bacterial flagella in *Borrelia burgdorferi*. Proc Natl Acad Sci U. S. A. **110:**14390-14395.

164. **Zhao, X., S. J. Norris, and J. Liu.** 2014. Molecular architecture of the bacterial flagellar motor in cells. Biochemistry. **53:**4323-4333.

165. **Motaleb, M. A., J. E. Pitzer, S. Z. Sultan, and J. Liu.** 2011. A novel gene inactivation system reveals altered periplasmic flagellar orientation in a *Borrelia burgdorferi fliL* mutant. J Bacteriol. **193:**3324-3331.

166. **Sal, M. S., C. Li, M. A. Motalab, S. Shibata, S. Aizawa, and N. W. Charon.** 2008. *Borrelia burgdorferi* uniquely regulates its motility genes and has an intricate flagellar hook-basal body structure. J Bacteriol. **190:**1912-1921.

167. **Samatey, F. A., H. Matsunami, K. Imada, S. Nagashima, T. R. Shaikh, D. R. Thomas, J. Z. Chen, D. J. DeRosier, A. Kitao, and K. Namba.** 2004. Structure of the bacterial flagellar hook and implication for the molecular universal joint mechanism. Nature. **431:**1062-1068.

168. **Miller, K. A., M. A. Motaleb, J. Liu, B. Hu, M. J. Caimano, M. R. Miller, and N. W. Charon.** 2014. Initial characterization of the FlgE hook high molecular weight complex of *Borrelia burgdorferi*. PLoS One. **9:**e98338.

169. **Charon, N. W., and S. F. Goldstein.** 2002. Genetics of motility and chemotaxis of a fascinating group of bacteria: the spirochetes. Annu Rev Genet. **36:**47-73.

170. **Ge, Y., and N. W. Charon.** 1997. An unexpected *flaA* homolog is present and expressed in *Borrelia burgdorferi*. J Bacteriol. **179:**552-556.

171. **Motaleb, M. A., M. S. Sal, and N. W. Charon.** 2004. The decrease in FlaA observed in a *flaB* mutant of *Borrelia burgdorferi* occurs posttranscriptionally. J Bacteriol. **186:**3703-3711.

172. **Motaleb, M. A., L. Corum, J. L. Bono, A. F. Elias, P. Rosa, D. S. Samuels, and N. W. Charon.** 2000. *Borrelia burgdorferi* periplasmic flagella have both skeletal and motility functions. Proc Natl Acad Sci U. S. A. **97:**10899-10904.

173. **Chevance, F. F., and K. T. Hughes.** 2008. Coordinating assembly of a bacterial macromolecular machine. Nature Reviews Microbiology. **6:**455-465.

174. **Sze, C. W., D. R. Morado, J. Liu, N. W. Charon, H. Xu, and C. Li.** 2011. Carbon storage regulator A ($CsrA_{Bb}$) is a repressor of *Borrelia burgdorferi* flagellin protein FlaB. Mol Microbiol. **82:**851-864.

175. **Smith, A. H., J. S. Blevins, G. N. Bachlani, X. F. Yang, and M. V. Norgard.** 2007. Evidence that RpoS (sigmaS) in *Borrelia burgdorferi* is controlled directly by RpoN (sigma54/sigmaN). J Bacteriol. **189:**2139-2144.

176. **Xu, H., M. J. Caimano, T. Lin, M. He, J. D. Radolf, S. J. Norris, F. Gheradini, A. J. Wolfe, and X. F. Yang.** 2010. Role of acetyl-phosphate in activation of the Rrp2-RpoN-RpoS pathway in *Borrelia burgdorferi*. PLoS Pathog. **6:**e1001104.

177. **Ouyang, Z., J. S. Blevins, and M. V. Norgard.** 2008. Transcriptional interplay among the regulators Rrp2, RpoN and RpoS in *Borrelia burgdorferi*. Microbiology. **154:**2641-2658.

178. **Caimano, M. J., R. Iyer, C. H. Eggers, C. Gonzalez, E. A. Morton, M. A. Gilbert, I. Schwartz, and J. D. Radolf.** 2007. Analysis of the RpoS regulon in *Borrelia burgdorferi* in response to mammalian host signals provides insight into RpoS function during the enzootic cycle. Mol Microbiol. **65:**1193-1217.

179. **Fisher, M. A., D. Grimm, A. K. Henion, A. F. Elias, P. E. Stewart, P. A. Rosa, and F. C. Gherardini.** 2005. *Borrelia burgdorferi* sigma54 is required for mammalian infection and vector transmission but not for tick colonization. Proc Natl Acad Sci U. S. A. **102:**5162-5167.

180. **Kostick, J. L., L. T. Szkotnicki, E. A. Rogers, P. Bocci, N. Raffaelli, and R. T. Marconi.** 2011. The diguanylate cyclase, Rrp1, regulates critical steps in the enzootic cycle of the Lyme disease spirochetes. Mol Microbiol. **81:**219-231.

181. **Sultan, S. Z., J. E. Pitzer, T. Boquoi, G. Hobbs, M. R. Miller, and M. A. Motaleb.** 2011. Analysis of the HD-GYP domain cyclic dimeric GMP phosphodiesterase reveals a role in motility and the enzootic life cycle of *Borrelia burgdorferi*. Infect Immun. **79:**3273-3283.

182. **Sultan, S. Z., J. E. Pitzer, M. R. Miller, and M. A. Motaleb.** 2010. Analysis of a *Borrelia burgdorferi* phosphodiesterase demonstrates a role for cyclic-di-guanosine monophosphate in motility and virulence. Mol Microbiol. **77:**128-142.

183. **Pitzer, J. E., S. Z. Sultan, Y. Hayakawa, G. Hobbs, M. R. Miller, and M. A. Motaleb.** 2011. Analysis of the *Borrelia burgdorferi* cyclic-di-GMP-binding protein PlzA reveals a role in motility and virulence. Infect Immun. **79:**1815-1825.

184. **Butler, S. M., and A. Camilli.** 2005. Going against the grain: chemotaxis and infection in *Vibrio cholerae*. Nature Reviews Microbiology. **3:**611-620.

185. **Lertsethtakarn, P., K. M. Ottemann, and D. R. Hendrixson.** 2011. Motility and chemotaxis in *Campylobacter* and *Helicobacter*. Annu Rev Microbiol. **65:**389-410.

186. **Novak, E. A., S. Z. Sultan, and M. A. Motaleb.** 2014. The cyclic-di-GMP signaling pathway in the Lyme disease spirochete, *Borrelia burgdorferi*. Front Cell Infect Microbiol. **4:**56.

187. **Sampedro, I., R. E. Parales, T. Krell, and J. E. Hill.** 2015. *Pseudomonas* chemotaxis. FEMS Microbiol Rev. **39:**17-46.

188. **Motaleb, M., J. Liu, and R. M. Wooten.** 2015. Spirochetal motility and chemotaxis in the natural enzootic cycle and development of Lyme disease. Curr Opin Microbiol. **28:**106-113.

189. **Sze, C. W., K. Zhang, T. Kariu, U. Pal, and C. Li.** 2012. *Borrelia burgdorferi* needs chemotaxis to establish infection in mammals and to accomplish its enzootic cycle. Infect Immun. **80:**2485-2492.

190. **Sultan, S. Z., P. Sekar, X. Zhao, A. Manne, J. Liu, R. M. Wooten, and M. A. Motaleb.** 2015. Motor rotation is essential for the formation of the periplasmic flagellar ribbon, cellular morphology, and *Borrelia burgdorferi* persistence within *Ixodes scapularis* tick and murine hosts. Infect Immun. **83:**1765-1777.

191. **Li, C., H. Xu, K. Zhang, and F. T. Liang.** 2010. Inactivation of a putative flagellar motor switch protein FliG1 prevents *Borrelia burgdorferi* from swimming in highly viscous media and blocks its infectivity. Mol Microbiol. **75:**1563-1576.

192. **Lambert, A., M. Picardeau, D. A. Haake, R. W. Sermswan, A. Srikram, B. Adler, and G. A. Murray.** 2012. FlaA proteins in *Leptospira interrogans* are essential for motility and virulence but are not required for formation of the flagellum sheath. Infect Immun. **80:**2019-2025.

193. **Guyard, C., S. J. Raffel, M. E. Schrumpf, E. Dahlstrom, D. Sturdevant, S. M. Ricklefs, C. Martens, S. F. Hayes, E. R. Fischer, and B. T. Hansen.** 2013. Periplasmic flagellar export apparatus protein, FliH, is involved in post-transcriptional regulation of FlaB, motility and virulence of the relapsing fever spirochete *Borrelia hermsii*. PLoS One. **8:**e72550.

194. **Lin, T., L. Gao, X. Zhao, J. Liu, and S. J. Norris.** 2015. Mutations in the *Borrelia burgdorferi* Flagellar Type III Secretion System Genes *fliH* and *fliI* Profoundly Affect Spirochete Flagellar Assembly, Morphology, Motility, Structure, and Cell Division. MBio. **6:**e00579-15.

195. **Armitage, J. P.** 1999. Bacterial tactic responses. Adv Microb Physiol. **41:**229-289.

196. **Bren, A., and M. Eisenbach.** 2000. How signals are heard during bacterial chemotaxis: protein-protein interactions in sensory signal propagation. J Bacteriol. **182:**6865-6873.

197. **He, K., and C. E. Bauer.** 2014. Chemosensory signaling systems that control bacterial survival. Trends Microbiol. **22:**389-398.

198. **Charon, N. W., S. F. Goldstein, M. Marko, C. Hsieh, L. L. Gebhardt, M. A. Motaleb, C. W. Wolgemuth, R. J. Limberger, and N. Rowe.** 2009. The flat-ribbon configuration of the periplasmic flagella of *Borrelia burgdorferi* and its relationship to motility and morphology. J Bacteriol. **191:**600-607.

199. **Kimsey, R. B., and A. Spielman.** 1990. Motility of Lyme disease spirochetes in fluids as viscous as the extracellular matrix. J Infect Dis. **162:**1205-1208.

200. **Porter, S. L., G. H. Wadhams, and J. P. Armitage.** 2011. Signal processing in complex chemotaxis pathways. Nature Reviews Microbiology. **9:**153-165.

201. **Sarkar, M. K., K. Paul, and D. Blair.** 2010. Chemotaxis signaling protein CheY binds to the rotor protein FliN to control the direction of flagellar rotation in *Escherichia coli*. Proc Natl Acad Sci U. S. A. **107:**9370-9375.

202. **Park, S. Y., B. Lowder, A. M. Bilwes, D. F. Blair, and B. R. Crane.** 2006. Structure of FliM provides insight into assembly of the switch complex in the bacterial flagella motor. Proc Natl Acad Sci U. S. A. **103:**11886-11891.

203. **Sourjik, V., and N. S. Wingreen.** 2012. Responding to chemical gradients: bacterial chemotaxis. Curr Opin Cell Biol. **24:**262-268.

204. **Kristich, C. J., and G. W. Ordal.** 2002. *Bacillus subtilis* CheD is a chemoreceptor modification enzyme required for chemotaxis. J Biol Chem. **277:**25356-25362.

205. **Yuan, W., G. D. Glekas, G. M. Allen, H. E. Walukiewicz, C. V. Rao, and G. W. Ordal.** 2012. The Importance of the Interaction of CheD with CheC and the Chemoreceptors Compared to Its Enzymatic Activity during Chemotaxis in *Bacillus subtilis*. PLoS One. **7:**e50689.

206. **Chao, X., T. J. Muff, S. Park, S. Zhang, A. M. Pollard, G. W. Ordal, A. M. Bilwes, and B. R. Crane.** 2006. A receptor-modifying deamidase in complex with a signaling phosphatase reveals reciprocal regulation. Cell. **124:**561-571.

207. **Rao, C. V., G. D. Glekas, and G. W. Ordal.** 2008. The three adaptation systems of *Bacillus subtilis* chemotaxis. Trends Microbiol. **16:**480-487.

208. **Motaleb, M. A., S. Z. Sultan, M. R. Miller, C. Li, and N. W. Charon.** 2011. CheY3 of *Borrelia burgdorferi* is the key response regulator essential for chemotaxis and forms a long-lived phosphorylated intermediate. J Bacteriol. **193:**3332-3341.

209. **Novak, E. A., P. Sekar, H. Xu, K. Moon, A. Manne, R. M. Wooten, and M. A. Motaleb.** 2016. The *Borrelia burgdorferi* CheY3 Response Regulator is Essential for Chemotaxis and Completion of its Natural Infection Cycle. Cell Microbiol. In press.

210. **Li, C., R. G. Bakker, M. A. Motaleb, M. L. Sartakova, F. C. Cabello, and N. W. Charon.** 2002. Asymmetrical flagellar rotation in *Borrelia burgdorferi* nonchemotactic mutants. Proc Natl Acad Sci U. S. A. **99:**6169-6174.

211. **Li, C., A. Motaleb, M. Sal, S. F. Goldstein, and N. W. Charon.** 2000. Spirochete periplasmic flagella and motility. J Mol Microbiol Biotechnol. **2:**345-354.

212. **Schneider, W. R., and R. N. Doetsch.** 1974. Effect of viscosity on bacterial motility. J Bacteriol. **117:**696-701.

213. **Shoesmith, J.** 1960. The measurement of bacterial motility. J Gen Microbiol. **22:**528-535.

214. **Goldstein, S. F., and N. W. Charon.** 1988. Motility of the spirochete *Leptospira*. Cell Motil Cytoskeleton. **9:**101-110.

215. **Klitorinos, A., P. Noble, R. Siboo, and E. Chan.** 1993. Viscosity-dependent locomotion of oral spirochetes. Oral Microbiol Immunol. **8:**242-244.

216. **Nakamura, S., Y. Adachi, T. Goto, and Y. Magariyama.** 2006. Improvement in Motion Efficiency of the Spirochete *Brachyspira pilosicoli* in Viscous Environments. Biophys J. **90:**3019-3026.

217. **Micali, G., and R. G. Endres.** 2016. Bacterial chemotaxis: information processing, thermodynamics, and behavior. Curr Opin Microbiol. **30:**8-15.

218. **Bi, S., and L. Lai.** 2015. Bacterial chemoreceptors and chemoeffectors. Cellular and Molecular Life Sciences. **72:**691-708.

219. **Silversmith, R. E., and R. B. Bourret.** 1999. Throwing the switch in bacterial chemotaxis. Trends Microbiol. **7:**16-22.

220. **Glekas, G. D., M. J. Plutz, H. E. Walukiewicz, G. M. Allen, C. V. Rao, and G. W. Ordal.** 2012. Elucidation of the multiple roles of CheD in *Bacillus subtilis* chemotaxis. Mol Microbiol. **86:**743-756.

221. **Motaleb, M. A., M. R. Miller, C. Li, and N. W. Charon.** 2007. Phosphorylation Assays of Chemotaxis Two-Component System Proteins in *Borrelia burgdorferi*. Meth Enzymol. **422:**438-447.

222. **Motaleb, M. A., M. R. Miller, C. Li, R. G. Bakker, S. F. Goldstein, R. E. Silversmith, R. B. Bourret, and N. W. Charon.** 2005. CheX is a phosphorylated CheY phosphatase essential for *Borrelia burgdorferi* chemotaxis. J Bacteriol. **187:**7963-7969.

223. **Pazy, Y., M. A. Motaleb, M. T. Guarnieri, N. W. Charon, R. Zhao, and R. E. Silversmith.** 2010. Identical phosphatase mechanisms achieved through distinct modes of binding phosphoprotein substrate. Proc Natl Acad Sci U. S. A. **107:**1924-1929.

224. **Bono, J. L., A. F. Elias, J. J. Kupko 3rd, B. Stevenson, K. Tilly, and P. Rosa.** 2000. Efficient targeted mutagenesis in *Borrelia burgdorferi*. J Bacteriol. **182:**2445-2452.

225. **Elias, A. F., P. E. Stewart, D. Grimm, M. J. Caimano, C. H. Eggers, K. Tilly, J. L. Bono, D. R. Akins, J. D. Radolf, T. G. Schwan, and P. Rosa.** 2002. Clonal polymorphism of *Borrelia burgdorferi* strain B31 MI: implications for mutagenesis in an infectious strain background. Infect Immun. **70:**2139-2150.

226. **Jewett, M. W., K. A. Lawrence, A. Bestor, R. Byram, F. Gherardini, and P. A. Rosa.** 2009. GuaA and GuaB are essential for *Borrelia burgdorferi* survival in the tick-mouse infection cycle. J Bacteriol. **191:**6231-6241.

227. **Motaleb, M. A., M. R. Miller, R. G. Bakker, C. Li, and N. W. Charon.** 2007. Isolation and Characterization of Chemotaxis Mutants of the Lyme Disease Spirochete *Borrelia burgdorferi* Using Allelic Exchange Mutagenesis, Flow Cytometry, and Cell Tracking. Meth Enzymol. **422:**419-437.

228. **Stewart, P. E., and P. A. Rosa.** 2008. Transposon mutagenesis of the Lyme disease agent *Borrelia burgdorferi*, p. 85-95. *In* Anonymous Bacterial Pathogenesis. Springer.

229. **Bertani, G.** 1951. Studies on lysogenesis. I. The mode of phage liberation by lysogenic *Escherichia coli*. J Bacteriol. **62:**293-300.

230. **Zhang, X., X. Yang, M. Kumar, and U. Pal.** 2009. BB0323 function is essential for *Borrelia burgdorferi* virulence and persistence through tick-rodent transmission cycle. J Infect Dis. **200:**1318-1330.

231. **Li, X., U. Pal, N. Ramamoorthi, X. Liu, D. C. Desrosiers, C. Eggers, J. F. Anderson, J. D. Radolf, and E. Fikrig.** 2007. The Lyme disease agent *Borrelia burgdorferi* requires BB0690, a Dps homologue, to persist within ticks. Mol Microbiol. **63:**694-710.

232. **Simm, R., U. Remminghorst, I. Ahmad, K. Zakikhany, and U. Romling.** 2009. A role for the EAL-like protein STM1344 in regulation of CsgD expression and motility in *Salmonella enterica* serovar Typhimurium. J Bacteriol. **191:**3928-3937.

233. **Livak, K. J., and T. D. Schmittgen.** 2001. Analysis of relative gene expression data using real-time quantitative PCR and the $2^{-\Delta\Delta CT}$ method. Methods. **25:**402-408.

234. **Smith, J. G., J. A. Latiolais, G. P. Guanga, S. Citineni, R. E. Silversmith, and R. B. Bourret.** 2003. Investigation of the role of electrostatic charge in activation of the *Escherichia coli* response regulator CheY. J Bacteriol. **185:**6385-6391.

235. **Toker, A. S., and R. M. Macnab.** 1997. Distinct regions of bacterial flagellar switch protein FliM interact with FliG, FliN and CheY. J Mol Biol. **273:**623-634.

236. **Silversmith, R. E., J. L. Appleby, and R. B. Bourret.** 1997. Catalytic mechanism of phosphorylation and dephosphorylation of CheY: kinetic characterization of imidazole phosphates as phosphodonors and the role of acid catalysis. Biochemistry (N.Y.). **36:**14965-14974.

237. **Stewart, P. E., A. Bestor, J. N. Cullen, and P. A. Rosa.** 2008. A tightly regulated surface protein of *Borrelia burgdorferi* is not essential to the mouse-tick infectious cycle. Infect Immun. **76:**1970-1978.

238. **Jewett, M. W., K. Lawrence, A. C. Bestor, K. Tilly, D. Grimm, P. Shaw, M. VanRaden, F. Gherardini, and P. A. Rosa.** 2007. The critical role of the linear plasmid lp36 in the infectious cycle of *Borrelia burgdorferi*. Mol Microbiol. **64:**1358-1374.

239. **Simpson, W. J., W. Burgdorfer, M. E. Schrumpf, R. H. Karstens, and T. G. Schwan.** 1991. Antibody to a 39-kilodalton *Borrelia burgdorferi* antigen (P39) as a marker for infection in experimentally and naturally inoculated animals. J Clin Microbiol. **29:**236-243.

240. **Grimm, D., A. F. Elias, K. Tilly, and P. A. Rosa.** 2003. Plasmid stability during *in vitro* propagation of *Borrelia burgdorferi* assessed at a clonal level. Infect Immun. **71:**3138-3145.

241. **Yang, X. F., U. Pal, S. M. Alani, E. Fikrig, and M. V. Norgard.** 2004. Essential role for OspA/B in the life cycle of the Lyme disease spirochete. J Exp Med. **199:**641-648.

242. **Mulay, V. B., M. J. Caimano, R. Iyer, S. Dunham-Ems, D. Liveris, M. M. Petzke, I. Schwartz, and J. D. Radolf.** 2009. *Borrelia burgdorferi bba74* is expressed exclusively during tick feeding and is regulated by both arthropod- and mammalian host-specific signals. J Bacteriol. **191:**2783-2794.

243. **Patton, T. G., G. Dietrich, M. C. Dolan, J. Piesman, J. A. Carroll, and R. D. Gilmore Jr.** 2011. Functional analysis of the *Borrelia burgdorferi bba64* gene product in murine infection via tick infestation. PLoS One. **6:**e19536.

244. **Park, S., X. Chao, G. Gonzalez-Bonet, B. D. Beel, A. M. Bilwes, and B. R. Crane.** 2004. Structure and function of an unusual family of protein phosphatases: the bacterial chemotaxis proteins CheC and CheX. Mol Cell. **16:**563-574.

245. **Walukiewicz, H. E., P. Tohidifar, G. W. Ordal, and C. V. Rao.** 2014. Interactions among the three adaptation systems of *Bacillus subtilis* chemotaxis as revealed by an *in vitro* receptor-kinase assay. Mol Microbiol. **93:**1104-1118.

246. **Lux, R., J. N. Miller, N. H. Park, and W. Shi.** 2001. Motility and chemotaxis in tissue penetration of oral epithelial cell layers by *Treponema denticola*. Infect Immun. **69:**6276-6283.

247. **Sowa, Y., and R. M. Berry.** 2008. Bacterial flagellar motor. Q Rev Biophys. **41:**103-132.

248. **Chaban, B., H. V. Hughes, and M. Beeby.** 2015. The flagellum in bacterial pathogens: for motility and a whole lot more. Semin Cell Dev Biol. **46:**91-103.

249. **Minamino, T., and K. Imada.** 2015. The bacterial flagellar motor and its structural diversity. Trends Microbiol. **23:**267-274.

250. **Kojima, S.** 2015. Dynamism and regulation of the stator, the energy conversion complex of the bacterial flagellar motor. Curr Opin Microbiol. **28:**66-71.

251. **Kudryashev, M., M. Cyrklaff, W. Baumeister, M. M. Simon, R. Wallich, and F. Frischknecht.** 2009. Comparative cryo-electron tomography of pathogenic Lyme disease spirochetes. Mol Microbiol. **71:**1415-1434.

252. **Wolgemuth, C. W.** 2015. Flagellar motility of the pathogenic spirochetes. Semin Cell Dev Biol. **46:**104-112.

253. **Liu, J., J. K. Howell, S. D. Bradley, Y. Zheng, Z. H. Zhou, and S. J. Norris.** 2010. Cellular architecture of *Treponema pallidum*: novel flagellum, periplasmic cone, and cell envelope as revealed by cryo electron tomography. J Mol Biol. **403:**546-561.

254. **Raddi, G., D. R. Morado, J. Yan, D. A. Haake, X. F. Yang, and J. Liu.** 2012. Three-dimensional structures of pathogenic and saprophytic *Leptospira* species revealed by cryo-electron tomography. J Bacteriol. **194:**1299-1306.

255. **Murphy, G. E., J. R. Leadbetter, and G. J. Jensen.** 2006. *In situ* structure of the complete *Treponema primitia* flagellar motor. Nature. **442:**1062-1064.

256. **Suaste-Olmos, F., C. Domenzain, J. C. Mireles-Rodriguez, S. Poggio, A. Osorio, G. Dreyfus, and L. Camarena.** 2010. The flagellar protein FliL is essential for swimming in *Rhodobacter sphaeroides*. J Bacteriol. **192:**6230-6239.

257. **Kudryashev, M., M. Cyrklaff, R. Wallich, W. Baumeister, and F. Frischknecht.** 2010. Distinct in situ structures of the *Borrelia* flagellar motor. J Struct Biol. **169:**54-61.

258. **Jenal, U., J. White, and L. Shapiro.** 1994. *Caulobacter* flagellar function, but not assembly, requires FliL, a non-polarly localized membrane protein present in all cell types. J Mol Biol. **243:**227-244.

259. **Belas, R., and R. Suvanasuthi.** 2005. The ability of *Proteus mirabilis* to sense surfaces and regulate virulence gene expression involves FliL, a flagellar basal body protein. J Bacteriol. **187:**6789-6803.

260. **Attmannspacher, U., B. E. Scharf, and R. M. Harshey.** 2008. FliL is essential for swarming: motor rotation in absence of FliL fractures the flagellar rod in swarmer cells of *Salmonella enterica*. Mol Microbiol. **68:**328-341.

261. **Zhu, S., A. Kumar, S. Kojima, and M. Homma.** 2015. FliL associates with the stator to support torque generation of the sodium-driven polar flagellar motor of *Vibrio*. Mol Microbiol. **98:**101-110.

262. **Caimano, M. J., S. Dunham-Ems, A. M. Allard, M. B. Cassera, M. Kenedy, and J. D. Radolf.** 2015. Cyclic di-GMP modulates gene expression in Lyme disease spirochetes at the tick-mammal interface to promote spirochete survival during the blood meal and tick-to-mammal transmission. Infect Immun. **83:**3043-3060.

263. **Iyer, R., M. J. Caimano, A. Luthra, D. Axline, A. Corona, D. A. Iacobas, J. D. Radolf, and I. Schwartz.** 2015. Stage-specific global alterations in the transcriptomes of Lyme disease spirochetes during tick feeding and following mammalian host adaptation. Mol Microbiol. **95:**509-538.

264. **Elias, A. F., J. L. Bono, J. J. Kupko 3rd, P. E. Stewart, J. G. Krum, and P. A. Rosa.** 2003. New antibiotic resistance cassettes suitable for genetic studies in *Borrelia burgdorferi*. J Mol Microbiol Biotechnol. **6:**29-40.

265. **Moon, K., G. Hobbs, and M. A. Motaleb.** 2016. *Borrelia burgdorferi* CheD promotes various functions in chemotaxis and pathogenic life cycle of the spirochete. Infect Immun. **84:**1743-1752.

266. **Liu, J., T. Lin, D. J. Botkin, E. McCrum, H. Winkler, and S. J. Norris.** 2009. Intact flagellar motor of *Borrelia burgdorferi* revealed by cryo-electron tomography: evidence for stator ring curvature and rotor/C-ring assembly flexion. J Bacteriol. **191:**5026-5036.

267. **Kremer, J. R., D. N. Mastronarde, and J. R. McIntosh.** 1996. Computer visualization of three-dimensional image data using IMOD. J Struct Biol. **116:**71-76.

268. **Hu, B., D. R. Morado, W. Margolin, J. R. Rohde, O. Arizmendi, W. L. Picking, W. D. Picking, and J. Liu.** 2015. Visualization of the type III secretion sorting platform of *Shigella flexneri*. Proc Natl Acad Sci U. S. A. **112:**1047-1052.

269. **Pettersen, E. F., T. D. Goddard, C. C. Huang, G. S. Couch, D. M. Greenblatt, E. C. Meng, and T. E. Ferrin.** 2004. UCSF Chimera—a visualization system for exploratory research and analysis. J Comput Chem. **25:**1605-1612.

270. **Ge, Y., I. G. Old, I. Saint Girons, and N. W. Charon.** 1997. Molecular characterization of a large *Borrelia burgdorferi* motility operon which is initiated by a consensus sigma70 promoter. J Bacteriol. **179:**2289-2299.

271. **Ge, Y., and N. W. Charon.** 1997. Identification of a large motility operon in *Borrelia burgdorferi* by semi-random PCR chromosome walking. Gene. **189:**195-201.

272. **Miller, C. L., S. Karna, and J. Seshu.** 2013. *Borrelia* host adaptation Regulator (BadR) regulates *rpoS* to modulate host adaptation and virulence factors in *Borrelia burgdorferi*. Mol Microbiol. **88:**105-124.

273. **Pappas, C. J., R. Iyer, M. M. Petzke, M. J. Caimano, J. D. Radolf, and I. Schwartz.** 2011. *Borrelia burgdorferi* requires glycerol for maximum fitness during the tick phase of the enzootic cycle. PLoS Pathog. **7:**e1002102.

274. **Rogers, E. A., D. Terekhova, H. Zhang, K. M. Hovis, I. Schwartz, and R. T. Marconi.** 2009. Rrp1, a cyclic-di-GMP-producing response regulator, is an important regulator of *Borrelia burgdorferi* core cellular functions. Mol Microbiol. **71:**1551-1573.

275. **Dresser, A. R., P. Hardy, and G. Chaconas.** 2009. Investigation of the genes involved in antigenic switching at the *vlsE* locus in *Borrelia burgdorferi*: an essential role for the RuvAB branch migrase. PLoS Pathog. **5:**e1000680.

276. **Hyde, J. A., D. K. Shaw, R. Smith III, J. P. Trzeciakowski, and J. T. Skare.** 2009. The BosR regulatory protein of *Borrelia burgdorferi* interfaces with the RpoS regulatory pathway and modulates both the oxidative stress response and pathogenic properties of the Lyme disease spirochete. Mol Microbiol. **74:**1344-1355.

277. **Brisson, D., D. Drecktrah, C. H. Eggers, and D. S. Samuels.** 2012. Genetics of *Borrelia burgdorferi*. Annu Rev Genet. **46:**515-536.

278. **Sonnhammer, E. L., G. Von Heijne, and A. Krogh.** 1998. A hidden Markov model for predicting transmembrane helices in protein sequences., p. 175-182. *In* Anonymous Ismb.

279. **Krogh, A., B. Larsson, G. Von Heijne, and E. L. Sonnhammer.** 2001. Predicting transmembrane protein topology with a hidden Markov model: application to complete genomes. J Mol Biol. **305:**567-580.

280. **Partridge, J. D., V. Nieto, and R. M. Harshey.** 2015. A new player at the flagellar motor: FliL controls both motor output and bias. MBio. **6:**e02367-14.

281. **Blair, D. F.** 2003. Flagellar movement driven by proton translocation. FEBS Lett. **545:**86-95.

282. **Leake, M. C., J. H. Chandler, G. H. Wadhams, F. Bai, R. M. Berry, and J. P. Armitage.** 2006. Stoichiometry and turnover in single, functioning membrane protein complexes. Nature. **443:**355-358.

283. **Kojima, S., and D. F. Blair.** 2004. Solubilization and purification of the MotA/MotB complex of *Escherichia coli*. Biochemistry (N.Y.). **43:**26-34.

284. **Fukuoka, H., T. Wada, S. Kojima, A. Ishijima, and M. Homma.** 2009. Sodium-dependent dynamic assembly of membrane complexes in sodium-driven flagellar motors. Mol Microbiol. **71:**825-835.

285. **Paulick, A., A. Koerdt, J. Lassak, S. Huntley, I. Wilms, F. Narberhaus, and K. M. Thormann.** 2009. Two different stator systems drive a single polar flagellum in *Shewanella oneidensis* MR-1. Mol Microbiol. **71:**836-850.

286. **Cooley, R. A., and G. M. Kohls.** 1945. The genus *Ixodes* in North America. National Institute of Health Bulletin. **184.** U.S. Government Printing Office, Washington, D.C., 246 p.

287. **Dunham-Ems, S. M., M. J. Caimano, U. Pal, C. W. Wolgemuth, C. H. Eggers, A. Balic, and J. D. Radolf.** 2009. Live imaging reveals a biphasic mode of dissemination of *Borrelia burgdorferi* within ticks. J Clin Invest. **119:**3652-3665.

288. **Ribeiro, J. M., T. N. Mather, J. Piesman, and A. Spielman.** 1987. Dissemination and salivary delivery of Lyme disease spirochetes in vector ticks (Acari: Ixodidae). J Med Entomol. **24:**201-205.

289. **Lin, T., L. Gao, C. Zhang, E. Odeh, M. B. Jacobs, L. Coutte, G. Chaconas, M. T. Philipp, and S. J. Norris.** 2012. Analysis of an ordered, comprehensive STM mutant library in infectious *Borrelia burgdorferi*: insights into the genes required for mouse infectivity. PLoS One. **7:**e47532.

290. **Kasumba, I. N., A. Bestor, K. Tilly, and P. A. Rosa.** 2016. Virulence of the Lyme disease spirochete before and after the tick bloodmeal: a quantitative assessment. Parasites & Vectors. **9:**1.

291. **Rajagopala, S. V., B. Titz, J. Goll, J. R. Parrish, K. Wohlbold, M. T. McKevitt, T. Palzkill, H. Mori, R. L. Finley, and P. Uetz.** 2007. The protein network of bacterial motility. Molecular Systems Biology. **3:**128.

292. **Cerveny, L., A. Straskova, V. Dankova, A. Hartlova, M. Ceckova, F. Staud, and J. Stulik.** 2013. Tetratricopeptide repeat motifs in the world of bacterial pathogens: role in virulence mechanisms. Infect Immun. **81:**629-635.

293. **D'Andrea, L. D., and L. Regan.** 2003. TPR proteins: the versatile helix. Trends Biochem Sci. **28:**655-662.

Appendix

Copyright © 2012, Rights Managed by Nature Publishing Group, Fig.1.4

NATURE PUBLISHING GROUP LICENSE
TERMS AND CONDITIONS

Jun 23, 2016

This Agreement between Ki Hwan Moon ("You") and Nature Publishing Group ("Nature Publishing Group") consists of your license details and the terms and conditions provided by Nature Publishing Group and Copyright Clearance Center.

License Number	3894880194808
License date	Jun 23, 2016
Licensed Content Publisher	Nature Publishing Group
Licensed Content Publication	Nature Reviews Microbiology
Licensed Content Title	Of ticks, mice and men: understanding the dual-host lifestyle of Lyme disease spirochaetes
Licensed Content Author	Justin D. Radolf, Melissa J. Caimano, Brian Stevenson and Linden T. Hu
Licensed Content Date	Feb 1, 2012
Licensed Content Volume Number	10
Licensed Content Issue Number	2
Type of Use	reuse in a dissertation / thesis
Requestor type	academic/educational
Format	print and electronic
Portion	figures/tables/illustrations
Number of figures/tables/illustrations	1
High-res required	no
Figures	Figure 1
Author of this NPG article	no
Your reference number	
Title of your thesis / dissertation	MOTILITY AND CHEMOTAXIS IN THE LYME DISEASE SPIROCHETE BORRELIA BURGDORFERI: ROLE IN PATHOGENESIS
Expected completion date	Aug 2016
Estimated size (number of pages)	150
Requestor Location	Ki Hwan Moon 421 Brighton Park Dr. Apt.7 GREENVILLE, NC 27834 United States Attn: Ki Hwan Moon
Billing Type	Invoice
Billing Address	Ki Hwan Moon 421 Brighton Park Dr. Apt.7 GREENVILLE, NC 27834 United States Attn: Ki Hwan Moon
Total	0.00 USD

NATURE PUBLISHING GROUP LICENSE
TERMS AND CONDITIONS

Jul 05, 2016

This Agreement between Ki Hwan Moon ("You") and Nature Publishing Group ("Nature Publishing Group") consists of your license details and the terms and conditions provided by Nature Publishing Group and Copyright Clearance Center.

License Number	3902511024595
License date	Jul 05, 2016
Licensed Content Publisher	Nature Publishing Group
Licensed Content Publication	Nature Reviews Microbiology
Licensed Content Title	The burgeoning molecular genetics of the Lyme disease spirochaete
Licensed Content Author	Patricia A. Rosa, Kit Tilly and Philip E. Stewart
Licensed Content Date	Feb 1, 2005
Licensed Content Volume Number	3
Licensed Content Issue Number	2
Type of Use	reuse in a dissertation / thesis
Requestor type	academic/educational
Format	print and electronic
Portion	figures/tables/illustrations
Number of figures/tables/illustrations	1
High-res required	no
Figures	Box 2 | The phylum Spirochaetes
Author of this NPG article	no
Your reference number	
Title of your thesis / dissertation	MOTILITY AND CHEMOTAXIS IN THE LYME DISEASE SPIROCHETE BORRELIA BURGDORFERI: ROLE IN PATHOGENESIS
Expected completion date	Aug 2016
Estimated size (number of pages)	150
Requestor Location	Ki Hwan Moon 421 Brighton Park Dr. Apt.7 GREENVILLE, NC 27834 United States Attn: Ki Hwan Moon
Billing Type	Invoice
Billing Address	Ki Hwan Moon 421 Brighton Park Dr. Apt.7 GREENVILLE, NC 27834 United States Attn: Ki Hwan Moon
Total	0.00 USD

Copyright © 1999, American Society for Microbiology, Fig.1.6

Copyright © 2005 Elsevier Inc., Fig.1.8

ELSEVIER LICENSE
TERMS AND CONDITIONS

Jul 05, 2016

This Agreement between Ki Hwan Moon ("You") and Elsevier ("Elsevier") consists of your license details and the terms and conditions provided by Elsevier and Copyright Clearance Center.

License Number	3902511446579
License date	Jul 05, 2016
Licensed Content Publisher	Elsevier
Licensed Content Publication	Plasmid
Licensed Content Title	The plasmids of Borrelia burgdorferi: essential genetic elements of a pathogen
Licensed Content Author	Philip E. Stewart,Rebecca Byram,Dorothee Grimm,Kit Tilly,Patricia A. Rosa
Licensed Content Date	January 2005
Licensed Content Volume Number	53
Licensed Content Issue Number	1
Licensed Content Pages	13
Start Page	1
End Page	13
Type of Use	reuse in a thesis/dissertation
Intended publisher of new work	other
Portion	figures/tables/illustrations
Number of figures/tables/illustrations	1
Format	both print and electronic
Are you the author of this Elsevier article?	No
Will you be translating?	No
Order reference number	
Original figure numbers	Fig. 2. The segmented genome of B. burgdorferi
Title of your thesis/dissertation	MOTILITY AND CHEMOTAXIS IN THE LYME DISEASE SPIROCHETE BORRELIA BURGDORFERI: ROLE IN PATHOGENESIS
Expected completion date	Aug 2016
Estimated size (number of pages)	150
Elsevier VAT number	GB 494 6272 12
Requestor Location	Ki Hwan Moon 421 Brighton Park Dr. Apt.7 GREENVILLE, NC 27834 United States Attn: Ki Hwan Moon
Total	0.00 USD

Copyright © 2011, Rights Managed by American Chemical Society, Figs.1.9, 1.10

(Request) Copy right permission

DH

Darla Henderson <D_Henderson@acs.org>
Today 12:06 PM

Dear Kihwan,

Thank you for your inquiry. I confirm you have permission to reuse two figures from the ACS article here http://pubs.acs.org/doi/full/10.1021/bi500059y in the thesis you are preparing to meet the degree-granting requirements of East Carolina University. ACS asks that you:

- Cite the ACS article as the source of the figures;
- Note modifications (if any) from the original figures; and
- Include a link from your thesis to the ACS article, link here: http://pubs.acs.org/doi/full/10.1021/bi500059y

With kind regards,
Darla

Darla Henderson, PhD.
Assistant Director, Open Access Programs
Publications Division
American Chemical Society
1155 16th Street NW
Washington, D.C. 20036
V 828.245.3702

The ACS Vision: *Improving people's lives through the transforming power of chemistry*

ACS Chemistry for Life
American Chemical Society

NATURE PUBLISHING GROUP LICENSE
TERMS AND CONDITIONS

Jul 05, 2016

This Agreement between Ki Hwan Moon ("You") and Nature Publishing Group ("Nature Publishing Group") consists of your license details and the terms and conditions provided by Nature Publishing Group and Copyright Clearance Center.

License Number	3902520310477
License date	Jul 05, 2016
Licensed Content Publisher	Nature Publishing Group
Licensed Content Publication	Nature Reviews Microbiology
Licensed Content Title	Signal processing in complex chemotaxis pathways
Licensed Content Author	Steven L. Porter, George H. Wadhams and Judith P. Armitage
Licensed Content Date	Mar 1, 2011
Licensed Content Volume Number	9
Licensed Content Issue Number	3
Type of Use	reuse in a dissertation / thesis
Requestor type	academic/educational
Format	print and electronic
Portion	figures/tables/illustrations
Number of figures/tables/illustrations	1
High-res required	no
Figures	Figure 1 | The Escherichia coli chemotaxis pathway
Author of this NPG article	no
Your reference number	
Title of your thesis / dissertation	MOTILITY AND CHEMOTAXIS IN THE LYME DISEASE SPIROCHETE BORRELIA BURGDORFERI: ROLE IN PATHOGENESIS
Expected completion date	Aug 2016
Estimated size (number of pages)	150
Requestor Location	Ki Hwan Moon 421 Brighton Park Dr. Apt.7 GREENVILLE, NC 27834 United States Attn: Ki Hwan Moon
Billing Type	Invoice
Billing Address	Ki Hwan Moon 421 Brighton Park Dr. Apt.7 GREENVILLE, NC 27834 United States Attn: Ki Hwan Moon
Total	0.00 USD

Copyright © 2012, Annual Reviews, Fig.1.7, and 1.11

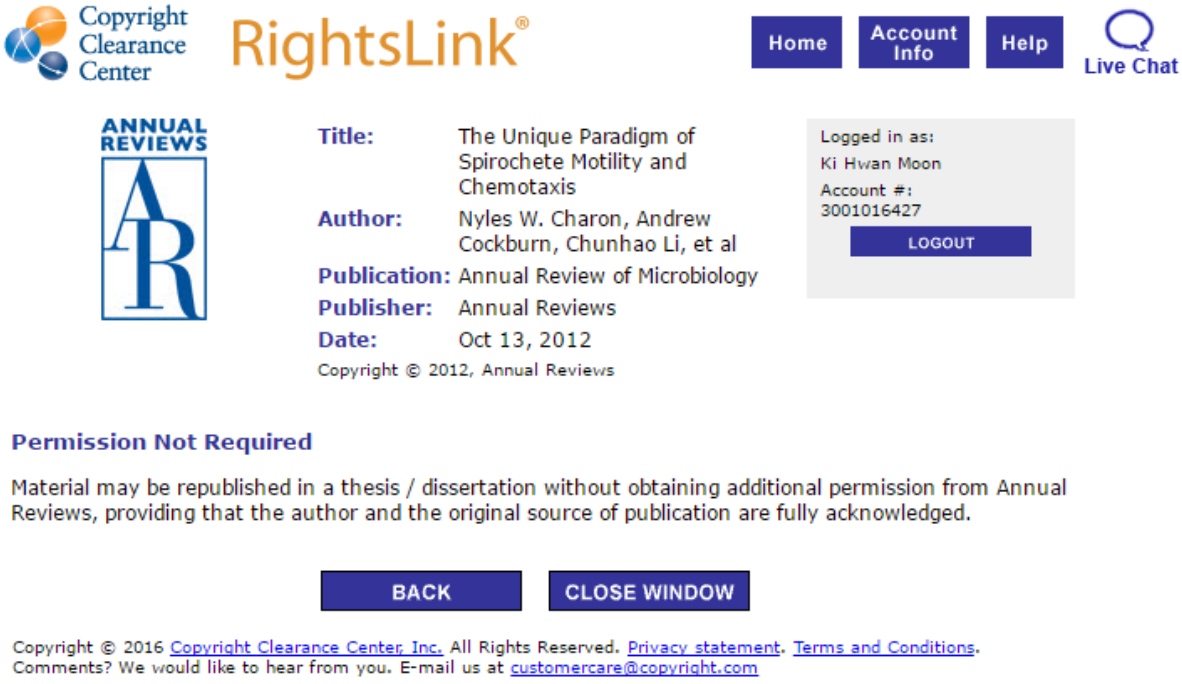

Copyright © 2016, American Society for Microbiology, Chapter 2.

Copyright © 2016, John Wiley & Sons Inc., Chapter 3.

Copyright Clearance Center RightsLink®

Home | Account Info | Help | Live Chat

Title: Spirochetes flagellar collar protein FlbB has astounding effects in orientation of periplasmic flagella, bacterial shape, motility, and assembly of motors in Borrelia burgdorferi

Author: Ki Hwan Moon,Xiaowei Zhao,Akarsh Manne,Juyu Wang,Zhou Yu,Jun Liu,Md A. Motaleb

Publication: Molecular Microbiology

Publisher: John Wiley and Sons

Date: Aug 9, 2016

Logged in as:
Ki Hwan Moon
Account #:
3001016427
LOGOUT

Review Order

Please review the order details and the associated terms and conditions.

No royalties will be charged for this reuse request although you are required to obtain a license and comply with the license terms and conditions. To obtain the license, click the Accept button below.

Licensed Content Publisher	John Wiley and Sons
Licensed Content Publication	Molecular Microbiology
Licensed Content Title	Spirochetes flagellar collar protein FlbB has astounding effects in orientation of periplasmic flagella, bacterial shape, motility, and assembly of motors in Borrelia burgdorferi
Licensed Content Author	Ki Hwan Moon,Xiaowei Zhao,Akarsh Manne,Juyu Wang,Zhou Yu,Jun Liu,Md A. Motaleb
Licensed Content Date	Aug 9, 2016
Licensed Content Pages	1
Type of use	Dissertation/Thesis
Requestor type	Author of this Wiley article
Format	Print and electronic
Portion	Full article
Will you be translating?	No
Title of your thesis / dissertation	MOTILITY AND CHEMOTAXIS IN THE LYME DISEASE SPIROCHETE BORRELIA BURGDORFERI: ROLE IN PATHOGENESIS
Expected completion date	Aug 2016
Expected size (number of pages)	150
Requestor Location	Ki Hwan Moon 421 Brighton Park Dr. Apt.7 GREENVILLE, NC 27834 United States Attn: Ki Hwan Moon
Publisher Tax ID	EU826007151
Total	0.00 USD

Edit Order Details

Edit Requestor Location This location may be used to determine your tax liability.

☑ I agree to these terms and conditions.

☐ I understand this license is for reuse only and that no content is provided.

Customer Code (if supplied) APPLY

BACK | DECLINE | ACCEPT

Please click accept only once.

East Carolina University

...mal Care and Use Commitee
212 Ed Warren Life Sciences Building
East Carolina University
Greenville, NC 27834

252-744-2436 office
252-744-2355 fax

February 24, 2014

MD Motaleb, Ph.D.
Department of Micro/Immuno
Brody 5E-106
ECU Brody School of Medicine

Dear Dr. Motaleb:

Your Animal Use Protocol entitled, "Virulence of Motility and Chemotaxis of *Borrelia Burgdorferi* Using a Mouse Model of Lyme Disease" (AUP #K151b) was reviewed by this institution's Animal Care and Use Committee on 2/24/14. The following action was taken by the Committee:

"Approved as submitted"

Please contact Dale Aycock at 744-2997 prior to hazard use

A copy is enclosed for your laboratory files. Please be reminded that all animal procedures must be conducted as described in the approved Animal Use Protocol. Modifications of these procedures cannot be performed without prior approval of the ACUC. The Animal Welfare Act and Public Health Service Guidelines require the ACUC to suspend activities not in accordance with approved procedures and report such activities to the responsible University Official (Vice Chancellor for Health Sciences or Vice Chancellor for Academic Affairs) and appropriate federal Agencies. **Please ensure that all personnel associated with this protocol have access to this approved copy of the AUP and are familiar with its contents.**

Sincerely yours,

SB McRae

Susan McRae, Ph.D.
Chair, Animal Care and Use Committee

SM/jd

Enclosure

East Carolina University

Animal Care and Use Commitee
212 Ed Warren Life Sciences Building
East Carolina University
Greenville, NC 27834

252-744-2436 office
252-744-2355 fax

July 15, 2015

MD Motaleb, Ph.D.
Department of Micro/Immuno
Biotechnology Building
ECU Brody School of Medicine

Dear Dr. Motaleb:

The Amendment to your Animal Use Protocol entitled, "Virulence of Motility and Chemotaxis Mutants of *Borrelia Burgdorferi* Using a Tick-Mouse Model of Lyme Disease", (AUP #K152b) was reviewed by this institution's Animal Care and Use Committee on 7/15/15. The following action was taken by the Committee:

"Approved as amended"

****Please contact Dale Aycock prior to any hazard use**

A copy of the Amendment is enclosed for your laboratory files. Please be reminded that all animal procedures must be conducted as described in the approved Animal Use Protocol. Modifications of these procedures cannot be performed without prior approval of the ACUC. The Animal Welfare Act and Public Health Service Guidelines require the ACUC to suspend activities not in accordance with approved procedures and report such activities to the responsible University Official (Vice Chancellor for Health Sciences or Vice Chancellor for Academic Affairs) and appropriate federal Agencies. **Please ensure that all personnel associated with this protocol have access to this approved copy of the AUP/Amendment and are familiar with its contents.**

Sincerely yours,

SB McRae

Susan McRae, Ph.D.
Chair, Animal Care and Use Committee

SM/jd

enclosure

East Carolina University

Animal Care and Use Committee
212 Ed Warren Life Sciences Building
East Carolina University
Greenville, NC 27834

252-744-2436 office
252-744-2355 fax

MEMORANDUM

TO: Ki Hwan Moon
Department of Micro/Immuno

FROM: Dorcas O'Rourke, D.V.M.
University Veterinarian

SUBJECT: Certificate of Training
Training Date 10/6/11

DATE: November 4, 2011

This letter is provided to certify that you have completed training in humane methods of animal experimentation, proper handling of selected species of research animals, and methods for reporting deficiencies in animal care and treatment. The training was provided in accordance with U.S. Department of Agriculture (9 CFR 2.32) regulations and the Public Health Service Policy.

This training included information on ECU animal care organizational structure, regulatory requirements, IACUC procedures, program for veterinary and animal care, occupational health and safety program, and methods for reporting concerns. Information on biology and care, proper restraint and procedures, and allergies and zoonoses were also provided.

We suggest that you retain this letter in your training file for future reference.